



HAL
open science

Relationships between microstructural aspects and mechanical properties in polymer based nanocomposites

L. Chazeau, Catherine Gauthier, Gérard Vigier, Jean-Yves Cavaillé

► To cite this version:

L. Chazeau, Catherine Gauthier, Gérard Vigier, Jean-Yves Cavaillé. Relationships between microstructural aspects and mechanical properties in polymer based nanocomposites. Handbook of organic-inorganic hybrid materials and nanocomposites, 2,, 2003. hal-02917761

HAL Id: hal-02917761

<https://hal.science/hal-02917761>

Submitted on 19 Aug 2020

HAL is a multi-disciplinary open access archive for the deposit and dissemination of scientific research documents, whether they are published or not. The documents may come from teaching and research institutions in France or abroad, or from public or private research centers.

L'archive ouverte pluridisciplinaire **HAL**, est destinée au dépôt et à la diffusion de documents scientifiques de niveau recherche, publiés ou non, émanant des établissements d'enseignement et de recherche français ou étrangers, des laboratoires publics ou privés.

Please cite as :

Chazeau, L., Gauthier, C., Vigier, G., & Cavaillé, J. Y. (2003). Relationships between microstructural aspects and mechanical properties of polymer-based nanocomposites. *Handbook of organic-inorganic hybrid materials and nanocomposites*, 2, 63-111.

**Relationships between microstructural aspects and
mechanical properties in polymer based
nanocomposites**

L. Chazeau, C. Gauthier, G. Vigier, J.Y. Cavaillé*

Groupe d'Etudes de Metallurgie Physique et Physique des Matériaux , INSA de Lyon, Bât
Blaise Pascal, 20 Av. Albert Einstein, 69621 Villeurbanne Cedex, France

* corresponding author: Tel. +33 (0)4 72-43-88-03, Fax: +33 (0)4 72-43-88-03,e-mail: [jean-
yves.cavaille@insa-lyon.fr](mailto:jean-
yves.cavaille@insa-lyon.fr)

INTRODUCTION	4
I. MECHANICAL BEHAVIOR OF POLYMERS.....	6
I-1. LINEAR BEHAVIOR.....	6
<i>I-1-1. Case of thermoplastics.....</i>	<i>7</i>
<i>I-1-2. Case of cross-linked polymers</i>	<i>8</i>
<i>I-1-3. Case of semi-crystalline polymers</i>	<i>8</i>
I-2. NON LINEAR MECHANICAL PROPERTIES OF POLYMERS	9
<i>I-2-1. Case of thermoplastics.....</i>	<i>9</i>
<i>I-2-2. Case of crosslinked polymers.....</i>	<i>11</i>
<i>I-2-3. Case of semi-crystalline polymers</i>	<i>12</i>
II NANOFILLERS	13
II-1. QUASI SPHERICAL NANOFILLERS (ASPECT RATIO CLOSE TO 1).....	13
<i>II-1-1. Carbon black</i>	<i>13</i>
<i>II-1-2. Amorphous silica</i>	<i>15</i>
II-2. PLATELET LIKE NANOFILLERS	17
II-3. ROD LIKE FILLERS	19
<i>II-3-1. Cellulose whiskers</i>	<i>19</i>
<i>II-3-2. Emerging field : single and multiwalled carbon nanotubes</i>	<i>20</i>
III PROCESSING AND MICROSTRUCTURE OF NANOCOMPOSITES.....	21
III-1. PROCESSING NANOSIZED FILLER REINFORCED POLYMERS.....	21
III -2 CHARACTERIZATION OF NANOCOMPOSITES	25
<i>III-2-1 Wide angle X-ray scattering (WAXS).....</i>	<i>26</i>
<i>III-2-2 Small angle X-ray and neutron scattering (SAXS, SANS).....</i>	<i>28</i>
<i>III-2-3 Electron microscopy.....</i>	<i>33</i>
<i>III-2-4 Atomic force microscopy.....</i>	<i>34</i>
IV LINEAR MECHANICAL BEHAVIOR	36
IV-1 MODEL SYSTEMS	36
<i>IV-1-1. Effect of the modulus contrast</i>	<i>37</i>
<i>IV-1-2. Effect of volume fraction</i>	<i>37</i>
<i>IV-1-3. Effect of the dispersion</i>	<i>38</i>
<i>IV-1-4. Effect of the shape factor</i>	<i>39</i>
IV-2 MODELING OF THE LINEAR BEHAVIOR	40
<i>IV-2-1. Bounds calculation</i>	<i>41</i>
<i>IV-2-2. Models for spherical fillers</i>	<i>42</i>
<i>IV-2-3. Models for high aspect ratio fillers</i>	<i>45</i>
<i>IV-2-4. Theory and nanocomposites in the rubbery state</i>	<i>47</i>

<i>Conclusion</i>	52
IV-3 INDUSTRIAL MATERIALS	53
<i>IV-3-1. Nanosized filled Rubbers</i>	53
<i>IV-3-2. Mica-type silicates filled layers</i>	53
V NON LINEAR BEHAVIOR IN THE GLASSY STATE	59
V-1 EXPERIMENTAL BEHAVIOR.....	59
V-2 MODELING OF THE PLASTIC BEHAVIOR	60
V-3 INDUSTRIAL MATERIALS	63
VI NON-LINEAR BEHAVIOR OF FILLED ELASTOMER.....	66
VI-1 SMALL DEFORMATION RANGE, THE PAYNE EFFECT	66
<i>VI-1-1. Experimental features</i>	66
<i>VI-1-2. Modeling of the Payne effect</i>	70
VI-2. THE MULLINS EFFECT AND THE ULTIMATE BEHAVIOR	72
<i>VI-2-1. The Mullins effect</i>	72
<i>VI-2-2. Ultimate behavior</i>	74
GENERAL CONCLUSION	76

Introduction

Since a very long time, human beings (and even some birds and mammal species) are used to combine different materials in order to improve at least one mechanical behavior of what they intend to build. For example, the combination of mud with straw (swallow nest, brick, etc.) leads to a better resistance to the crack propagation. Life itself requires such combination, as wood for example must be considered as composite materials in which, very roughly speaking, cellulose fibers reinforce lignin which plays the role of a matrix. Equivalent analysis may be done about insects, as for instance, beetles are armored with an exoskeleton consisting of a protein matrix riddled with layers of chitin fibers. Lots of similar examples have been quoted in various works devoted to the study of bio-mimetism (see for example ref. [1]).

In this later case, it is the stiffness which is improved, mainly in the axis of cellulose fibers (mechanical properties appear to be strongly anisotropic). Thus, it is clear that if the fillers are stiffer than the matrix, then the stiffness is increased. Since the last world war, following the fast industrial development of polymers (and more especially thermosets) a special attention has been paid to glass fiber polymer composites, but also to polymeric materials filled by various inorganic fillers (which are generally speaking stiffer than the polymer matrix).

As an other example of combination of materials which exhibit drastically different properties, the case of stiff but brittle polymers (with a modulus of few GPa at room temperature) like polystyrene (PS) or poly(methyl methacrylate) (PMMA) is also very interesting. Soft domains are introduced (such as rubber particles, having few MPa modulus) in order to improve their toughness. They belong to the large class of high impact (HI) reinforced polymers like HIPS and have been largely studied by some authors like Dikie [2-4], who considered this class of materials as "polymer-polymer" composites. In the following, except for special demonstration, we will only consider polymers reinforced by stiff fillers, restricting "Composite materials" to the case where the fillers improve the modulus of the matrix.

Among the large number of parameters which have to be considered, the average length / diameter ratio of reinforcing elements, known as "aspect ratio" is one of the most important. Roughly speaking, two groups of composite materials are considered, (i) the case where the fillers are long fibers (which means that the length is comparable to the sample dimensions, i.e. the aspect ratio becomes infinity) and (ii) the case where in contrast, filler dimensions are negligible compared to the sample dimensions. In the latter case, the aspect ratio may change

from 1 (for spheres, for instance) to values as high as 1000 (so-called short fiber composites). In this presentation, we will focus on this second class of materials.

On the other hand, the size of fillers may be also an important parameter, though for classical composite materials, the mechanical properties do not deeply depend on this size. In fact, it must be chosen mainly in agreement with the object or structure dimensions, which has to be processed. Indeed, with fillers having a too large size, surface defects as well as bulk heterogeneities may appear. Thus, classical fillers or fibers have average dimensions or diameters in the order of 10 μm or more, which for fibers leads to length of few mm's. The point is that if typical filler dimensions are strongly decreased down to few nanometers, then several features may change. It is worthy to notice that researchers have only recently investigated in a systematic way how the physical properties can be affected by the small size of domains. It is usual to call these materials "nanocomposites materials". However, it must be pointed out that people have processed such materials for a long time, especially in the automotive industry where tires are mostly made of carbon black filled rubber, with the typical size of carbon black particles in the nanometer range.

What can be considered as specific features in nanocomposite materials? The first one, is the huge interfacial area which reaches 100 to 1000 m^2/g of fillers. As interfacial properties are an important parameter for the macroscopic behavior of composite materials, it may become the dominant parameter in nanocomposites. As an example, if we consider that, from the filler surface towards the matrix, the molecular mobility of polymer chain segment may vary over a few nanometers (this has to be compared with the macromolecule gyration radius), then it means that an important matrix fraction has physical properties modified by the presence of the fillers. Moreover, decreasing the particle size at constant volume fraction decreases the average distance between particle surface, down to value comparable with the macromolecule coils. This can favor the short distance filler-filler interaction. The consequence may also be that fillers can be connected by macromolecules and form a flexible network. In this case, the rheological behavior of the mixture during the process (for instance injection process at high temperature) should be drastically modified, as well as the long time creep behavior.

As for all scientific approaches, it is extremely important to try to model the behavior of composite materials, in order to predict it when, either the filler content changes, or the thermo-mechanical conditions are modified, etc. A large class of modeling methods, known as "homogenisation technique" [5] or "self consistent modeling" has been relevant for classical composites, but often underestimate the modulus of nanocomposites. In fact, these models, at least in their former developments, ignore direct interactions between fillers, and thus may be inefficient when these interactions rule the mechanical response of the

composite. Moreover, they cannot simply account for the percolation of rigid fillers within a soft matrix. From this remark, a new question arises: what is the role of the fillers dispersion and how can we account for it ?

In order to propose a consistent overview of the various questions concerning the mechanical behavior of polymeric nanocomposites (which means that at least the matrix is polymeric), we will first recall the main features of the thermo-mechanics of polymers, then focus on the fillers generally used (nanofillers) and on the main techniques used to process these materials and to characterize their morphology. We will continue by describing the linear viscoelastic behavior of model materials, then we will discuss the main modeling approaches and their recent development and give some industrial examples. At last, we will focus on non linear mechanical properties, including the plastic behavior (glassy polymer state) and the filled rubber behavior (Payne and Mullins effects).

I . Mechanical behavior of polymers

I-1. Linear behavior

Polymers submitted to a mechanical solicitation show a viscoelastic response. The deformation presents an instantaneous elastic component and a viscous component (time dependent). Many static or dynamic experimental techniques are used to characterize this behavior. At low stress, the material behavior is linear, i.e. the compliance (or modulus) is independent of the applied stress level. At higher stress level, it becomes dependent on the stress (at given time or strain rate) and the behavior is then non-linear. In all cases, the response results from mechanisms so called relaxation processes acting at the molecular level [6].

The study at low stress levels can be performed either by dynamic tests (i.e. in sine wave condition) that lead to complex modulus or compliance, or static tests such as micro-creep (where in fact the behavior corresponds to the transitory response to a stress step). Both types of tests lead to equivalent information since the complex compliance is the Fourier transform of the time dependent compliance (Figures I-1 and I-2).

The relaxational processes involved in the mechanical behavior of polymers are thermo-mechanically activated. This means that an increase of temperature is equivalent to a decrease of frequency or strain rate. This means also that an increase of the stress decreases the time necessary to observe these relaxation processes. Therefore, the polymer response to a mechanical test under given experimental conditions strongly depends on these conditions.

The deformation of a polymer leads to the observation of three components, as evidenced in a creep experiment (figure I.1) :

- an elastic component (ϵ_{el})
- an anelastic (or viscoplastic) component which can give rise to a recovery (ϵ_{an})
- a plastic component (ϵ_{pl}), non-recoverable below the glass transition temperature.

Figure I-1

I-1-1. Case of thermoplastics

Figure I.2 displays the typical linear behavior of a glassy polymer (poly(methyl methacrylate) or PMMA) studied in dynamic torsion as a function of temperature, at constant frequency.

Figure I-2

At low temperature, the material is in the glassy state, i.e. out of equilibrium, and can display secondary relaxations such as the β one, generally associated to local molecular motions of few segments of the main chain. In this temperature range, the stiffness is mainly due to the intermolecular Van der Waals bonds. The resulting shear modulus is always of the order of 1 GPa.

At higher temperature (T_α) a strong decay of the modulus is observed during the so-called main or α relaxation. This relaxation is associated to the glass transition of the material. It can be analyzed as the result of hierarchically correlated motions of segments of polymer chains.

Above T_α , the thermal agitation makes the Van der Waals bonds negligible. The entropic forces become predominant. If the polymer chains are short, the material flows. However if the length of macromolecules is larger than a critical length, a “rubbery plateau” is observed. This critical length corresponds to the length above which chain entanglements can occur. The modulus in the rubbery plateau is proportional to the entanglement density. The width of the plateau depends on the molar weight, which controls the time necessary for the disentanglement. At given $T \gg T_\alpha$, the typical time for disentanglement is given by [7]:

$$\tau_D \approx \kappa(T) \overline{DP}^{3.4} \quad (\text{E-I-1})$$

Where \overline{DP} is the average degree of polymerisation, $\kappa(T)$ is a function of temperature and τ_D is the typical time for disentanglement.

I-1-2. Case of cross-linked polymers

For chemically cross-linked polymers (as elastomers for example), the behavior in the glassy state is close to that observed for linear polymers. The only significant difference lies in the rubbery plateau where no flow can occur (case of natural rubber in Figure I-3).

Figure I-3

An elastomer is constituted of long polymer chains linked to each other by crosslinking nodes. The mechanical response of an elastomer is directly deduced from the modeled behavior of one polymer chain, free from interactions with the other chains. The simplest model is the Gaussian one, which models the chain as an assembly of independent segments free of rotation. The elasticity of the chain is entropic by nature and is deduced from a statistical description of its possible conformations. The behavior of a network of such chains can be done with the assumption that the macroscopic deformation of the material is proportional to that of each chain. The theoretical description is based on a 3 chain unit and, under simple shear, this leads to the known formula available for low amplitude deformation [8]

$$G=NkT \quad (E-I-2)$$

where G is the shear modulus, T the temperature and N the crosslink density (N).

The shear modulus appears to be proportional to the temperature (as shown in Figure I-4) and to the crosslink density. The main differences between elastomers and thermosets (epoxy, unsaturated polyesters...) are

- the temperature of the main relaxation : roughly speaking, it is well below room temperature for elastomers, and above for thermosets,
- the modulus in the rubbery plateau since the crosslink density is much higher in thermosets than in elastomers.

Figure I-4

I-1-3. Case of semi-crystalline polymers

The typical viscoelastic behavior of a semi-crystalline polymer (Nylon 6) is also presented on Figure I-3. Semi-crystalline polymers consist in sequences of crystalline and amorphous lamellae. In most cases, the lamella thickness is about 2-30 nm depending on the crystallization conditions (the other dimensions are of the order of a few microns). These lamellae are often organized in larger structures evidenced by the observation of spherulites.

Their size depends on the crystallization conditions (cooling kinetic) but is often in the range $1\mu\text{m}$ - $10\mu\text{m}$. In many respects, a semi-crystalline polymer is a nanocomposite, the crystallites acting both as filler and as crosslinking nodes. The filler/matrix (crystallite/amorphous part) interactions are due on the one hand to the tie molecules (molecules shared by an amorphous part and its two adjacent crystallites), and to the other hand to Van Der Waals bonds between amorphous and crystalline parts. The elastic modulus of the crystallites is only slightly higher than the modulus of the amorphous parts below their T_{α} . Consequently, in this temperature range, the elastic modulus of a semi-crystalline polymer is close to that of an amorphous polymer. Moreover, a simple mechanical modeling can take into account the increase of modulus due to crystallites (acting as fillers) by considering the material as a composite.

At increasing temperature, two successive decreases of the modulus are observed, the first is associated to the main relaxation of the amorphous phase (T_{α}), the second to the melting of the crystallites (T_m). Between T_{α} and T_m , the modulus of a semi-crystalline polymer is strongly dependent on the crystallinity (amount, dimension, texture of the crystalline phases). Though the large number of experimental data, its precise modeling is difficult, for four main reasons:

- The modulus of the amorphous part is never well known
- The ratio between the moduli of amorphous and crystallite phase is very large (about a factor 10^3)
- Their microstructure is complex and must be considered at different scales: crystallite, spherulite.
- The anisotropic characteristics (modulus..) of crystallites

Further works are required to develop and validate composite models for the calculation of the elastic properties of semi-crystalline polymers.

I-2. Non linear mechanical properties of polymers

I-2-1. Case of thermoplastics

As recalled previously, when the applied stress is large enough, the response of the polymer becomes non-linear i.e. dependent on the stress level. Moreover, different temperature range may be considered.

For mechanical tests carried out below the secondary relaxation temperature T_{β} (measured at about 1Hz), practically no molecular motions can occur. Thus, thermoplastics are often very

brittle, as illustrated by the brittleness of polystyrene (PS) and poly(methyl methacrylate) (PMMA) at room temperature. Conversely, at room temperature, polycarbonate (PC) does not exhibit this brittleness because its secondary relaxation is observed at very low temperature, well below room temperature.

The classical stress-strain curve obtained for a glassy polymer, when the mechanical test is performed in the temperature range above T_{β} and below T_{α} , and within the classical strain rate range (10^{-1} - 10^{-4} s $^{-1}$), is presented on Figure I-5. Similarly to Figure I-1, it is possible to separate the three components of the macroscopic strain, from the recovery of the deformation applied during a standard mechanical test (plane strain compression test in the case of experiments displayed by Figure I-5) [9]. At the maximum stress (σ_y), the plastic deformation is nearly equal to zero; the anelastic deformation occurs even if the stress is very low and increases beyond σ_y , up to the stress plateau (σ_p) where a stationary value is reached. During such a mechanical test, the polymer stores a great amount of energy, compared to other materials (ceramics, metals). This energy can be restored when the stress is removed, by the recovery of the elastic and anelastic part of the deformation. The anelastic deformation induces small change in the intermolecular bonds, leading to both a slight increase of density and a very strong increase of the molecular mobility [10] (this behavior shows that the free volume theory cannot work at least below the main relaxation temperature). Conversely, the microstructural modifications induced by the plastic component of the strain do not change deeply the density and the molecular mobility. The physical modeling of such a behavior has been studied for wholly amorphous polymers by several authors [11-19].

It can be added that the increase of molecular mobility, related to the increase of anelastic deformation, leads often to deformation instabilities: the strain first induces a softening of the material, i.e. already deformed domains become easier to deform, leading to the observation of shear bands and / or of necking phenomena.

Figure I-5

At last, for temperature above T_{α} , macromolecules of thermoplastics flow under the action of stress. The study of this non linear mechanical behavior is part of the rheology, and is not under the scope of this review.

I-2-2. Case of crosslinked polymers

In the case of chemically cross-linked polymers (thermosets, elastomers) tested below T_{α} , the behavior is not really different from that observed for linear polymers. The modulus still results mainly from the Van der Waals bonds, and the presence of cross-linking nodes does not deeply modify the elastic modulus. The only significant difference lies in the hardening observed for stresses higher than σ_{pl} . This phenomenon is partly due to the chain stretching in the strain direction. In the case of thermosets, the chain length between cross-links is much smaller than the distance between entanglements in linear or branched polymers; therefore, hardening occurs more rapidly and more strongly.

The stress-strain behavior of unfilled elastomers tested at room temperature (i.e. above T_{α}) is shown on Figure I-6. In the deformation range below 0.5, a quasi-linear behavior is observed in agreement with equation E-I-2. That means that, in this range, the deformation remains well below the maximum extensibility of the chains (large deformation is possible because the chain length in between nodes is large). At higher level of strain, a strain-hardening is observed (prior to break) : the behavior becomes non linear and equation E-I-2 is no longer valid. This simplest description can be refined at two levels : (i) at the level of the chain description by considering its maximal extensibility (the Gaussian description is replaced by the Langevin equation), and (ii) at the level of the network description, by using a 8 chain models or a random distributed chain model [20]. These improvements allow a better description of the stress strain curve in the large deformation range, but the determination of the supplementary parameters is not totally univocal when one try a modeling of all the experimental data obtained from different load paths.

An alternative way to these modeling is to adopt a phenomenological descriptions (such as the Mooney-Rivlin or Ogden equations [22,23], with adjustable parameters the number of which depends on the accuracy needed for the fit of the experimental curves.

Note that a theoretical estimation of the strain at break is given by \sqrt{Nc} , Nc is the number of Kuhn segments of a lattice chain. However large deviation from this law has been reported in the literature [24]. Nevertheless it appears that crosslinking allows to increase the elastic modulus but induces a decrease of the strain at break : a compromise has to be found, and can be largely improved by filler incorporation.

Figure I-6

I-2-3. Case of semi-crystalline polymers

The case of semi-crystalline polymers used below the main relaxation temperature (T_α) is more complicated. As already suggested, in semi-crystalline polymers, the crystallites can be regarded as both filler and crosslinking nodes. By studying polymer which can be obtained either in wholly amorphous state or with various crystallinity rates (such as Poly(Ethylene-Terephthalate)), it can be observed that the yield stress (σ_s) and the flow stress (σ_p) increase and the hardening occurs for lower deformation as the crystallinity increases. Their hardening is explained by the presence of crystallites acting as supplementary crosslinks. Moreover, large deformations lead to the destruction of crystallites and their transformation into a fibrillar structure [25].

This phenomenon is still more pronounced as the mechanical tests are achieved above the main relaxation temperature. Although the numerous studies on the plastic deformation of semi-crystalline polymers between T_α and T_m [26-29], the description of the mechanisms involved in plastic deformation is still quantitative. During deformation, the lamellar structure is progressively transformed into a fibrillar structure. The morphological evolution depends on the mechanical test (tensile, compression, shear tests). In the simple case of a tensile test, the interlamellar amorphous parts are firstly deformed and the deformation is elastic and homogeneous. Then, the plastic deformation occurs inside the crystallites when shear stress exceeds a critical value. This deformation firstly occurs in crystalline lamellae located in the diagonal areas and the equatorial zone of spherulites. The polar parts of spherulites are lastly deformed because they are parallel to the stress axis. Because of the lack of plastic shear, a fragmentation occurs, as the stress in these areas becomes too large. The necking phenomenon, observed during the test, is induced by this fragmentation. Depending on the polymer nature, this necking is more or less important (very important in polyethylene but less in polyamide). Beyond the necking, all the lamellae are fragmented in small blocks, which are rearranged in microfibrils [30]. These microfibrils are themselves organised in fibrils connected by tie macromolecules and separated by many cavities (Figure I.7). At larger deformation, the plastic deformation of this structure occurs by gliding of fibrils.

Figure I.7

To conclude this section, polymers have complex mechanical behaviors depending strongly (i) on their microstructure and (ii) on the conditions (temperature, frequency, strain rate...) of solicitation. This must be taken into account to understand the mechanical properties of polymer matrix nanocomposites.

II Nanofillers

The use of particulate materials (fillers) for enhancement of polymer properties dates back to the earliest years of the polymer industry. Initially used as extending agents to reduce the cost of polymer-based products, fillers were soon recognized to be an integral component in many applications involving polymers, particularly in reinforcement. As explained in the introduction, this review focuses on mechanical behavior of polymers reinforced with stiff fillers. In this context, various parameters seem to be of importance to characterize the nanofillers i.e. (i) geometrical factors as the shape, the size and the aspect ratio, (ii) intrinsic properties such as modulus and flexibility and (iii) surface characteristics such as the specific surface area and eventual surface treatments. Since the reinforcement efficiency of inorganic fillers is strongly related to their aspect ratio, we will present several types of nanofillers, starting from the lower to the higher aspect ratio values. The scope of this part includes the production, the structure and properties of carbon black, amorphous silica, nano clays, cellulose whiskers and carbon nanotubes.

II-1. Quasi spherical nanofillers (aspect ratio close to 1)

II-1-1. Carbon black

Chemically, carbon black is a form of elemental carbon consisting of 90 to 99 percent carbon. It is obtained by uncompleted combustion or thermal decomposition of hydrocarbons. Carbon black is a material that has been known since antiquity. But it only found its widespread application when it was discovered that, when mixed into rubber it improves its mechanical properties [31]. Several processes can be used, leading to different products such as lampblacks, channel, thermal or furnace blacks. Furnace blacks are made in a furnace by partial combustion of hydrocarbons. Channel blacks are produced by impingement of natural gas flames on channel irons. Thermal blacks are manufactured by thermal decomposition of natural gas. Lampblacks are made by burning hydrocarbons in open, shallow pans. Nowadays, the blacks with smaller particle size are produced by the oil furnace process from liquid, aromatic hydrocarbons. In this process, carbon blacks are produced in a refractory lined reactor where a flame is produced from air and natural gas. As the carbon black feedstock is atomized into the flame, the carbon black formation reaction takes place. Downstream from this reaction zone, water is sprayed into the reactor to stop the carbon black formation reaction. At this point, the main properties of the black are determined. Different

grades of carbon blacks, with varying aggregate sizes and structures, can be produced by altering the reactor geometry, the reactive flows of air, gas and feedstock or the position of the water quench. Subsequent processing involves additional cooling (using heat exchanger) separation from the gas stream and densification (fluffy form) or process into a pelleted form.

In the furnace, primary carbon black particles coalesce to form larger units known as primary aggregates (Figure II-1-1). These clusters are the ultimate dispersible units of carbon black. The extent of primary particle aggregation is controlled in the reactor and is called structure. This parameter characterizes the empty space between randomly packed aggregates and agglomerates. Thus, the most used parameters to describe carbon black morphology are (i) the specific surface area (the total exposed surface per mass unit) and (ii) the complex shape of the aggregate.

Figure II-1-1

The specific surface directly impacts the amount of interfacial contact area with the polymer. Undoubtedly, it is a geometrical characteristic that could be calculated but its measurement involves molecular adsorption i.e. is influenced by the carbon black surface energy and activity. Thus, measurements of the specific surface area become a physicochemical characteristic as well as a geometrical one. Depending on the grade of black, the average diameter of the primary particles ranges from about 12 to about 75 nm. The corresponding surface areas, per gram of carbon black, range from 25 m² for the coarser particle size grades to an excess of 500 m² for the finest particle size grade.

Grades in which the particles are allowed to cluster into relatively large, complex aggregates are known as high structure grades. Grades where the extent of aggregation is minimized are known as low structure grades. The description of morphology in terms of particle size and structure for commercial carbon black dates back to the electron microscope studies of Ladd and co-authors in the earlier 1940's [32]. In the following twenty-five years, electron microscope was primarily restricted to quantitative measurements on particle size, and structure was assessed by oil absorption, followed later by DBP absorption test. Nowadays, the use of automated image analysis method has provided pattern recognition capabilities and carbon blacks are now classified in different specific shape categories, based on nine categories ranging from spheroidal to fibrous configurations (ASTM Standard - D1765).

At equal structure level, finer particle size (higher surface area) grades are more difficult to disperse due to the greater number of contacts between aggregates: they result in higher viscosity in the final product. Higher structure blacks are easier to disperse than low structure

blacks of the same surface area because their larger, bulkier aggregates cannot pack together as tightly.

Furnace blacks contain small quantities of chemisorbed oxygen on their surfaces, that form functional groups which include phenols and carboxylic acids, among others. Some grades of black are treated in an oxidative process to increase the amount of functional groups adsorbed on their surfaces. The various polar acidic oxygenated groups present at the surface of the black allow interactions with polymer. It is generally agreed that interaction between carbon black and non-polar elastomer is physical (i.e. Van der Waals interactions) in nature.

II-1-2. Amorphous silica

Silica, or silicon dioxide, SiO_2 , in its pure form is colorless to white. Silica is widely and abundantly distributed throughout the earth, both in the pure state and in silicates, (e.g., in quartz, agate, amethyst, chalcedony, flint, jasper, onyx, rock crystal, opal, sand, sandstone, clay, granite and many other rocks). Silica occurs in several forms and in two varieties, i.e. amorphous and crystalline. In crystalline forms, the structures are characterized by tetrahedral configuration of atoms within the crystals, whereas in the amorphous forms, the sub-units show no regular lattice pattern. All types of amorphous silica can be converted to crystalline forms when heated to a sufficiently high temperature. Amorphous silica is usually prepared by vapor-phase hydrolysis or precipitation. Three forms of synthetic amorphous silica are classified according to their method of preparation: silica gel (silica G), precipitated silica (silica P) and fumed silica (silica F).

Fumed silica is derived from vapor-phase hydrolysis of a silicon-bearing halide, such as silicon tetrachloride. It is the byproduct of a high-temperature process when elemental silicon is produced by reacting coke and silica sand (crystalline) in an electric arc furnace. At the high temperatures of the flame, primary particles of SiO_2 are formed but are not stable; they are fused together to form space-filling aggregates. Leaving the flame, at lower temperatures, the silica aggregates stick together by physico-chemical forces building up large micron-sized agglomerates and finally fluffy flocks [33]. Fumed silica offers primary particles with diameters from 5 to 40 nm, as well as a low density of silanols (around $2.5/\text{nm}^2$), and very few impurities. Fumed silica are generally used as common rheological fillers in solvent-based polyurethanes adhesives.

Precipitated silica is produced by chemical reactions; the process stages include precipitation, filtration, drying and milling. The process can be described as follows: sulfuric acid and

sodium silicate solutions are added simultaneously with agitation to water. The resulting white precipitate is filtered, washed and dried in the manufacturing process. During the precipitation stage, product properties may be varied through changes in composition and ratio of reactants, reaction time, temperature and concentration. The important characteristics that result from the precipitation process include physical properties such as particle morphology and structure (oil absorption and compressibility), and chemical properties such as pH, silanol group density and optical properties. For precipitated silica, the reaction mixture is held in the alkaline pH region, and offers limited aggregates of primary particles. For silica gel, the reaction mixture is held in the acidic pH region, leading to a three-dimensional network of particles with low characteristic sizes (3 nm), and a high specific surface area ($>350 \text{ m}^2/\text{g}$).

Precipitated silica can be used in a variety of functions, including reinforcing elastomers to improve modulus, elongation, tear strength and abrasion resistance (see part IV-3-1). The manufacturing process results in the formation of distinct agglomerates based on primary particles. These agglomerates range in size from 50 to 100 microns. They can be milled by various methods to reduce their size down to the range of 2 to 15 microns. Precipitated silica contains mainly aggregates in which the radial distribution function appears to be fairly uniform throughout the aggregate (Figure II-1-2)

Figure II-1-2

The specific gravity of precipitated silica is approximately 2.1. This is a chemical property of silicon dioxide manufactured by this type of process. Generally, precipitated silica can adsorb two to three times its weight depending on the density of the liquid being absorbed (DBP Dibutyl Phthalate or DOP dioctylphthalate). Particle size and surface characteristics determine how much DBP or DOP silica can absorb. This characteristic is directly linked with its morphology.

Precipitated silica contains both physically and chemically bound moisture. The physically bound moisture is driven off of heating to 105 degrees centigrade for two hours to determine Loss on Drying (LOD), which is usually in the range of 5 percent. Chemically bound moisture, in the form of surface silanol groups, is removed by igniting the dried silica for two hours at 1000 degrees centigrade. Loss on Ignition (LOI) is also in the range of 5 percent.

Due to surface silanol groups, silica particles have higher tendency interacting among themselves via hydrogen bonds than with non-polar matrix. To improve the interactions

between silica particles and the polymeric matrix, surface treatment is often achieved using organofunctional silanes. With such a surface treatment, the surface tension of the filler is affected. By the way, it is possible to control wetting, rheology and dispersion of fillers in the matrix. On the other hand, filler/polymer interactions can be enhanced through coupling mechanisms, leading to improved properties at moderate to high deformation. The chemistry involves reaction of the silane groups with water, which generates first silanol hydrolysis, then grafting to the filler surface and condensation to polysiloxane. The silane also reacts through its organic group with the polymer matrix under many possible mechanisms including radical reactions with unsaturated resins, condensation and addition reactions with urethanes and epoxies. One of the most commonly used coupling agent is the triethoxysilyl propyl tetrasulfane, TPTS.

To sum up, carbon blacks and precipitated silica are the most common fillers used for reinforcing polymers and more precisely elastomers. Both consists of aggregates of spherical particles (diameter from 10 nm) fused together. The aggregated nature of reinforcing fillers manifests itself primarily in its ability to occlude rubber and to shield occluded rubber from deformation. This point will be further commented in part VI .

II-2. Platelet like nanofillers

Clays are hydrous alumino silicates with a layered structure. They have been used as fillers in polymer systems because of their low cost. But until recently, clay particles could only be dispersed on the microscale. Because of its suitable charge density, montmorillonite, discovered in 1847 in France (Montmorillon) by Damour et Salvétat [34], is nowadays the most widely used clay as a nanofiller. Its development started in the early 1990s, when the treatment with amino acids was found to allow the dispersion of montmorillonite clay at an individual scale (1 nm-thick silicate layers) in polyamide 6. Nowadays, both natural clays and synthetic layered silicates have been successfully used in the synthesis of polymer nanocomposites (mica, fluoro mica, vermiculite, hectorite, fluororhectorite, saponite,...) [35]. They belong with montmorillonite to the structural family known as the 2:1 phyllosilicate. Their crystalline structure consists of a two dimensional lamina obtained by blending two tetrahedral silica layer with metal atoms (i.e. Mg for talc and Al for mica) to form a corresponding octahedral metal oxide layer. Montmorillonite chemical structure is $(\text{OH})_4\text{Si}_8(\text{Al}_{4-x}\text{Mg}_x)\text{O}_{20}$. Its idealized structure, proposed by Hoffman, Endell and Wilm [36], is presented on Figure II-2-1.

Figure II-2-1

The platelet thickness is around 1 nm while the lateral dimensions range from 0.1 to several μm . Each platelet is separated from the next by a van der Waals gap called gallery or interlayer. An increasing interest is observed in the literature for synthetic clay, particularly for fluorohectorite [37] that displays a crystallographic structure similar to montmorillonite. It is prepared by heating talcum in the presence of Na_2SiF_6 for several hours at high temperature in an electric furnace. Montmorillonite, and other layered silicate clays, are naturally hydrophilic. The stacks of clay platelets are held tightly together by electrostatic forces and they are poorly suited to mixing and interacting with most polymer matrices. Thus, making a composite out of untreated clay would not be a very effective use of material, because most of the clay would be stuck inside, unable to interact with the matrix. For these reasons, the clay must be treated before it can be used to make a nanocomposite.

A popular and relatively easy method of modifying the clay surface, making it more compatible with an organic matrix, is ion exchanging. The galleries are normally occupied by cations that counterbalance the excess negative charge generated by the isomorphous substitution of the atoms forming the crystal (i.e. Mg^{2+} or Fe^{2+} replacing Al^{3+} in montmorillonite, Li^+ replacing Mg^{2+} in hectorite) and are usually alkaline and hydrated alkaline-earth metal cations. Dispersion of the silicate particles in the polymeric matrix is improved by replacing the metal cations with ions bearing an aliphatic chain so as to compatibilise the silicate and enhance its interaction with the polymer by enlarging the interlayers. Under proper conditions, the gallery spaces can be filled with monomer, oligomer, or polymer. This increases the distance between platelets, swelling the clay. Clay platelets swollen with polymer are said to be intercalated. If the clay swells so much that it is no longer organized into stacks, it is said to be exfoliated. Nanocomposites can then be made from the intercalated or exfoliated clay as described in part IV-3. The effective dispersion state of nano clay in a polymer can be evaluated by X rays diffraction (See part III-2-1).

The aspect ratio and the dispersion can reach very high values in delaminated composites (aspect ratio ranging from 100 to 1000). Completely exfoliated clay has a surface area of about $700\text{m}^2/\text{g}$. The anisotropy of modulus is a key factor of montmorillonite: the longitudinal modulus is about 150 GPa, and the Poisson ratio is assumed to be close to 0.2, i.e. that close to that of mica crystal. On microscope observation, the clay platelet displays curvature indicating a certain amount of flexibility (see figure II-2-2). Note that the dark lines in a TEM image of a polymer-clay nanocomposite are not the result of absorption of electrons, but

rather of interference of electron waves that are diffracted by the clay platelets. They should therefore not be interpreted as the cross sections of the clay layers [38].

Figure II-2-2

II-3. Rod like fillers

During the past few years, there has been an important development of new large aspect ratio nanofibers. These new materials combine the advantages of a large interface area (more than 100 m²/g) with a much lower percolation threshold than spherical particles. Just as for the other nanoscopic fillers (spherical, platelets) , the size of these fibers makes possible the processing of small thickness composites and a possible transparency of the final product. Moreover, their very large aspect ratio and their mechanical properties provide them with a great industrial potential for the reinforcement of polymer matrices.

II-3-1. Cellulose whiskers

Many cellulosic products, such as wood shavings, have long been used as filler in polymer, in order to decrease their cost without degrading their mechanical properties. For twenty years, cellulose fibers such as wood fibers, or cotton have been increasingly studied for their potential as reinforcement agents in composites. They combine good mechanical properties, i.e. a strength and a modulus of the same order of those of mineral fillers, with the advantages of cellulose which is biodegradable and renewable [39]. Nowadays, cellulose fibers are used as fillers in the majority of resin composites [40]; their use in rubber composites has also been reported [41,42].

It is worthy to notice that a large part of agricultural waste contains "cellulose micro-fibrils" easily extracted. This is the case of sugar beat after the sugar extraction, as well as most of the citry fruits after their juice extraction. Such micro-fibrils have typical diameter ranging between 5 to 10 nm, with length of several μm and they consist in the alternation of mono-crystals linked to their neighbors by disordered segments. The hydrolysis of these segments allows the extraction of quasi-perfect mono-crystals in the nano-size range. Thus rod shaped quasi-perfect crystals with high aspect ratio can be extracted from the biomass: their are so called "cellulose whiskers". Among the various way to obtain such whiskers, the most perfect were obtained from sea animals, namely tunicates, after a treatment described by Sassi [43]. The final aqueous suspension of whiskers does not sediment or flocculate due to the electrostatic repulsion between the surface sulfate groups grafted during the sulfuric acid

treatment. The whisker average dimensions, determined by transmission electron microscopy, are 1 μm length and 15 nm diameter (see Figure II-3-1). They have a tensile modulus (120 GPa) much higher than the usual modulus of polymers (around 3 GPa below the glass transition temperature T_g) and can form hydrogen bonds with their neighbors thanks to the numerous hydroxyl groups on their surface. Processing a bucky paper (tensile modulus around 15 GPa) can assess this last point. Whiskers were firstly studied by Favier [44,45] who was interested in their reinforcing effect in a poly(Styrene-Butyl Acrylate) matrix. Several others matrices have also been evaluated (Poly(Propylene), Poly(Vinyl Chloride), epoxy resins).

Figure II-3-1

II-3-2. Emerging field : single and multiwalled carbon nanotubes

Carbon nanotubes, long and thin cylinders of carbon, were discovered in 1991 by the electron microscopist Iijima who was studying the arc-evaporation synthesis of fullerenes [46]. He found that the central core of the cathodic deposit contained a variety of closed graphitic structures including nanoparticles and nanotubes, of a type which had never been observed. Carbon nanotubes can be seen as a sheet of graphite (a hexagonal lattice of carbon) rolled into a cylinder (see Figure II-3-2). Just a nanometre across, the cylinder can be tens of microns long, and each end is "capped" with half of a fullerene molecule. Nanotubes can have either a unique cylindrical wall (SWNTs) or multiple walls (MWNTs). A short time later Iijima's discovery, Ebbesen showed how nanotubes could be produced in bulk quantities by varying the arc-evaporation conditions [47]. A major event in the development of carbon nanotubes was the synthesis in 1993 of single-layer nanotubes. The standard arc-evaporation method produces only multilayered tubes. It was found that addition of metals such as cobalt to the graphite electrodes resulted in extremely fine tube with single-layer walls. An alternative method of preparing single-walled nanotubes involved the laser-vaporisation of a carbon target in a furnace at 1200 °C, and resulted in a high yield of single-walled tubes with unusually uniform diameters. These highly uniform tubes had a greater tendency to form aligned bundles (often called "ropes") than those prepared using arc-evaporation. The ropes are between 10 and 20 nm across and up to 100 μm long. When examined in a transmission electron microscope, each rope is found to consist of a bundle of single-wall carbon nanotubes aligned along a single direction. X-ray diffraction, which views many ropes at once, also shows that the diameters of the single-wall nanotubes have a narrow distribution. This relatively efficient way to produce bundles of ordered single-wall nanotubes opened new opportunities for quantitative experimental studies on carbon nanotubes.

Figure II-3-2

These intriguing structures have sparked much excitement in the recent years and a large amount of research has been dedicated to their understanding. Currently, the physical properties are still discussed. Many theoretical studies have predicted the properties of single-wall nanotubes. Structural properties depends on the diameter, length, and chirality, or twist of the nanotubes. Their predicted mechanical characteristics are remarkable (Young's Modulus ~ 1 Tpa [48-49], maximum tensile strength ~ 30 GPa [50]). They have excellent thermal conductivity, they are chemically inert and, depending on the details of their atomic arrangement (chirality), they behave as metals or semiconductors.

On the basis of early predictions of fantastic mechanical properties, carbon nanotubes have attracted a great deal of attention in the structural materials community. There is a growing interest in the use of nanotubes as reinforcing fillers in polymer composites. To be useful in real applications, nanotube/polymer composites will have to exhibit improved physical properties relative to traditional carbon fiber composites. A key factor is the strength of the nanotube/polymer interface. Thus, there is a real need of ongoing work focused on understanding the nature of nanotube/polymer matrix interactions and how this information can be integrated with larger scale micromechanical and continuum modeling techniques.

One can also mention related products such as carbon nanofibers that are produced by chemical vapour deposition process. These nanofibers (Pyrograf TM supplied by Applied Sciences Inc) have circular cross-sections with diameters around 200 nm and a high aspect ratio. Kilogram quantities are available from the manufacturer, enabling composite development at an industrial scale. A Transmission Electron Microscopy image of these fibers is reported in Figure II-3-3. The high aspect ratio is confirmed and a bamboo like structure can be seen [51].

Figure II-3-3

III Processing and microstructure of nanocomposites

III-1. Processing nanosized filler reinforced polymers

In the field of composite materials, it is often assumed that an increase of the developed interface allows an optimum mechanical stress transfer between the filler and the matrix.

However, it is also reported that the presence of a certain amount of aggregates leads to an increase of the elastic properties [52]. On the other hand, the presence of large agglomerates is known to have a dramatic effect on the ultimate properties of the composite and a uniform dispersion of fillers in the matrix is needed to obtain homogeneous properties at a mesoscopic level. This suggests that an optimum dispersion (uniform and without large aggregates) is needed in order to reach the best mechanical behavior.

Generally, fillers are added when the polymer is in a viscous state (melt or in solvent). This incorporation leads to an increase of viscosity directly related to the amount of fillers as described by the Einstein's law (for spherical particles) [53]. In the case of nano-fillers, a high increase of viscosity is observed even at low amount of filler due to the high interfacial surface and the interactions between particles. Due to this large viscosity, the bubbles necessarily introduced during the process are difficult to remove. The problem appears even more difficult in the case of high aspect ratio fillers, since the viscosity increases also with this parameter.

Different routes have been explored, in the literature, to process nanosized filler reinforced polymers.

1. Nanofillers can be incorporated directly in the polymer melt. This route is for example used for silica or carbon blacks particles filled elastomers. In this case, the viscosity problem is generally solved thanks to mechanical shear as discussed in the following. Use can also be made of additives (processing aids, plasticisers...)
2. Another way is to disperse the fillers in the monomer or prepolymer and then to achieve the polymerization step. For example, the polymerization of nylon in the presence of nanoclay platelets has been firstly performed in the early 90's [54]. In this case, the issue is to control the polymerization or the curing process, which might be modified by the filler. The in situ polymerization has been also developed to produce organic –inorganic hybrids in which the polymerization of the matrix and the formation of the silica fillers occur in the same time[55].
3. A third route consists in using a solvent in which fillers and polymer are first dispersed separately and then mixed together. The solvent can be either polar or non polar depending on the polymer chemistry. The main problem is to obtain a stable suspension of the fillers in the chosen solvent: this stabilization depends on the chemical groups on the filler surface. In some cases, the functionalization of the surface of the filler can be an efficient way to solve the problem: for instance, in the case of hydrophilic fillers such as cellulose whiskers, sulfate

groups are grafted on the surface in order to create electrostatic repulsion in between individualized fillers. In other cases, the stabilization can be achieved by grafting long polymeric chains (steric stabilisation). In the case of silica particles, the surface treatments are based on silane chemistry, and provide chemical bond between filler and matrix. For nanolayered silicates, use is made of ammonium salts in order to exfoliate the stacks of platelets [56]. For carbon blacks, the modification of the surface properties is usually due to an oxidation treatment [57]. The surface treatment of the fillers can be also used in the two other routes (incorporation in the polymer melt or in the monomer). This, however, modifies the surface chemistry and therefore influences the filler matrix interface.

The stabilization of the filler suspension can also be improved by the use of surfactant molecules, either ionic for electrostatic repulsion, or non ionic for steric stabilization. In the case of a polypropylene matrix, cellulose whiskers have been stabilized thanks to surfactants, and incorporated in an organic solvent of polypropylene [58]. The use of surfactants may also have consequences on the final properties of the composite as they can be either localized in the interface or as clusters in the matrix.

4. Another way to process nanocomposite materials is based on the mixture of various aqueous suspensions (colloids). It is well known that emulsion polymerization provides in a simple way polymer colloidal suspension, and is a flexible tool to produce structured particles by two or more steps of polymerization (having for instance a soft core and the stiff shell, with a more or less important composition gradient) [59]. In fact, in colloids, the typical size of particles in suspension is in the range of ten to hundred nanometers. A mixture of an aqueous suspension of nanofillers with a colloidal suspension of film forming polymer leads, after water evaporation, to a nanocomposite films, like for instance in the case of cellulose whisker-P(S-BuA) matrix composite (cf. Figure III-1-1).

Figure III-1-1

In other cases, the fillers can be a colloidal suspension of polymer below its glass transition temperature (for instance polystyrene particles in a P(S-BuA) matrix). When both colloids are film forming, a co-continuous material can be expected, providing the fraction of each component is large enough. In Figure III-1-2, a schematic representation is given. The white domains have low T_g , and therefore can be film forming at room temperature. If particles, stiff (hatched) and soft (white) are mixed together, and if they are randomly dispersed, then they have a certain probability to form aggregates. On the contrary, if the particles are

structured, with a stiff core and a soft shell, then after the shell coalescence, the material should consist in a soft matrix with regularly dispersed stiff spherical domains, without contact between each other.

Figure. III-1-2

Such systems have been processed by Cavaillé et al.[60] and more recently by Rios et al [61,62]. It must be pointed out that the synthesis of such core-shell particles is often difficult, as it requires that the structure remains unchanged during the polymerization which occurs well above T_g of the soft shell. In order to avoid that the soft phase minimizes its interfacial area with the core particle, one way consists in slightly crosslinking the soft polymer during its polymerization (this has been obtained in this particular case by the copolymerization of N-isobutoxy methyl acrylamide or IBMA, with BuA during the second polymerization step). The use of structured particles appears to be very efficient to reduce problems of aggregation during the processing of nanocomposites. It can be developed in the case of mineral particles leading to encapsulated fillers.

The aggregation of particles in the solution or in the melt polymer can also be reduced thanks to mechanical shear. The classical industrial processing techniques like extrusion or melt compounding (Brabender) are well known in the case of microsized fillers. Such techniques have also been effective in the case of nanosized fillers like silica or carbon blacks in an elastomeric matrix. They have been used with success in the case of nano layered silicates. However, it seems that they are not appropriate in the case of nanofibers such as cellulose whiskers. In this case, sonication appears to be one of the most efficient tools to disperse aggregates. But, the practical conditions of this technique (time, power) have to be controlled in order to avoid degradation of the fillers (decrease of their length due to break).

A second issue in the processing of nanosized filled polymers is the stability of the filler dispersion. This deals with a kinetical aspect in respect with the time necessary to process the nanocomposite. For instance, in the case of the latex route, the dispersion of the fillers should be stable during film forming, especially during the evaporation of water, to avoid a gradient in the thickness of the sample. For example, two dispersions of carbon nanofibers (PYROGRAF III fibers supplied from Applied Sciences, Inc., USA) were prepared from a latex of styrene-butadiene (SB) with (A) and without (B) the addition of the 1 wt% of the non-ionic surfactant TRITON X-100 [51]. Photographs taken 1 h after the mixing are shown in Figure III-1-3. While the fibers in sample A stay well dispersed in the latex, the fibers in

sample B agglomerate and form a thick swimming layer on the latex. In the case of curing, the stability has to be ensured during the whole time of the chemical reaction. The viscosity can play an important role in maintaining the suspension of fillers and avoiding flocculation. Therefore, the optimum viscosity is a compromise between a low value to ensure dispersibility and a high value to maintain stability. Freeze-drying can be used to by pass this problem, as evidenced in the case of cellulose whiskers [44].

Figure III-1-3

Thanks to these different techniques, a great number of nanocomposites can be processed, with a polymeric matrix either thermoplastic or thermosets, amorphous or semi-crystalline. For instance, the incorporation of layered silicate in polymers has been actively studied in the last decade. The work was begun in the 1980's by researchers at Toyota's [66]. Montmorillonite clay was exchanged with a quaternary ammonium ion, allowing the clay to mix with ϵ -caprolactam. The caprolactam was then polymerized through ring-opening to form nylon-6. Many other matrices have been evaluated since, including polyamides, epoxy resins, polystyrene, polyurethanes, low molecular weight waxes, polypropylene, poly(N-vinylcarbazole), and more. Reports on clay chemical modification and nanocomposite elaboration may be found in the literature (see for instance review papers [63-65,67-69]).

Although an optimized process can a priori lead to a good dispersion, it is however always necessary to carefully investigate the state of aggregation of the fillers, and their possible orientation in the matrix. Moreover, in the case of semi-crystalline matrix, the possible modification of the crystallinity (amount, nature, dimension, texture of the crystalline phases) by the filler presence must be evaluated. These aspects will be discussed in the following part.

III -2 Characterization of nanocomposites

Due to the size of the fillers, the investigation of nanocomposite morphology needs techniques that can provide details up to a subnanometer size scale. But, as discussed in part II, the fillers can gather in clusters, aggregates or more complex superstructure (fractal superstructure for example). Therefore, a wide range of microscopy or scattering techniques can be relevant, with observation domains ranging from subnanometer to millimeter. Table 1 presents the different characterization techniques and their corresponding size range. The following part will give an overview of these different techniques and illustrate their application in the field of nanocomposites. It is worthy to notice that the two groups of techniques, namely (i) microscopies and (ii) scattering techniques lead to different

information. Microscopies give direct local observation and a lot of observations have to be performed to get average conclusion, while scattering experiments provide average characterization on a large volume, but require the use of various models and hypothesis.

Characterization techniques	Size range
Wide angle X-ray scattering (WAXS)	0.01nm - 3 nm
Small angle X-ray or neutron scattering (SAXS, SANS)	1nm - 200nm
Transmission electron microscopy (TEM)	0.15nm - 1000nm
Scanning electron microscopy (SEM)	1nm - 1mm
Atomic force microscopy (AFM)	0.2nm - 0.2mm
Optical microscopy (OM)	300nm - 1mm
Light scattering (LS)	300nm - 0.2mm

Table 1: characterization techniques and their size range.

III-2-1 Wide angle X-ray scattering (WAXS)

The wide angle X-ray scattering measurements are concerned mainly with the determination of crystal structure via the Bragg law:

$$n \lambda = 2 D \sin(\theta) \quad (\text{E-III-1})$$

where D is the distance between crystallographic planes, λ is the wavelength of the X-rays ($\lambda = 0.154 \text{ nm}$ for copper anode), n (integer) is the order of reflection and 2θ is the angle between the diffracted and incoming X-ray waves.

The width of diffraction peak depends on spacing variations and the number of planes involved in the scattering units. When the distance variations can be neglected, the thickness of the diffraction units can be evaluated as follows (Debye-Scherrer relationship) [70]:

$$d = (0.9 \lambda) / (\Delta (2\theta) \cos \theta_0) \quad (\text{E-III-2})$$

Where d is the thickness of the diffraction units, λ is the wavelength of the incident beam, $\Delta (2\theta)$ is the full width at half maximum of the diffraction peak (in radians) and θ_0 is the position peak.

This is true for peaks corresponding to crystalline plans close to the main lamella plane, so that d corresponds to the thickness of the crystalline lamella. Generally it is not easy to separate the effect due to spacing variations from the effects due to the number of planes

involved in the scattering unit; it makes necessary to observe several peaks ((1,0,0), (2,0,0) for example).

In the case of semi-crystalline polymers, the degree of crystallinity can be estimated from the ratio of sharp (due to crystallites) to diffuse (due to amorphous part) diffracted intensity.

The wide angle X-ray scattering measurements can be relevant in two different issues : (i) to investigate the modification of the crystallinity of the matrix due to the presence of the fillers, (ii) to characterize the repartition of the fillers when they are crystalline[71] or wholly crystalline (i.e. cellulose whiskers).

As already evoked, the fillers, and specially nanofillers, can modify the crystalline morphology of the polymer: the nature of crystalline phases, the degree of crystallinity, the size of crystallite and the degree of perfection and orientation of crystallites. WAXS experiments can provide pertinent information on different aspects. The nature of crystalline phases can be deduced from the position of diffraction peaks according to the Bragg's law. For instance, it has been reported that montmorillonite promotes the formation of the γ phase in polyamide-6 (against α -phase in the pure matrix). Similar observations can be made in polypropylene which also contains two types of crystalline phases (α and β) [72]. Thanks to equation (E-III-2), the width of diffraction peaks gives information about the crystallite size and the degree of disorder within the crystal. At last the degree of orientation of crystallites can be computed from the study of the textures determined with a specific goniometer, a simpler method can consist in determining the angular spread of a chosen reflection. Let us remark that the depth of X-ray penetration is typically 0.1mm. Therefore, by controlled abrasion of the sample surface, it is possible to obtain the WAXS pattern as a function of the depth; this can be useful to determine “ core-skin ” effects.

Furthermore, in the specific case of layered silicate based nanocomposites, WAXS appears to be a very convenient technique to analyze the efficiency of the surface treatment and the exfoliation level. Consecutive silica layers lead to the observation of the (1,0,0) reflection and the spacing between these layers can be determined from the Bragg's law. The surface treatment, used to modify the clay/polymer interactions generally swells the clay. The WAXS patterns of non-treated, slightly swollen (by methyl octadecyl bis-2-hydroxyethyl ammonium methylsulfate) and highly swollen (by dimethyl dioctadecyl ammonium chloride) montmorillonites are shown in Figure III-2-1 [73].

Figure III-2-1

Non treated clay exhibits a peak at $2\theta=7^\circ$ ($\lambda=0.154\text{nm}$), it corresponds to a spacing layer equal to 1.26nm. For swollen montmorillonite, the (1,0,0) peaks are shifted toward smaller angles: the spacing is increased and equal to 1.96 nm and 36.8nm for slightly swollen and highly swollen montmorillonite, respectively. As far as highly swollen is concerned, the peaks located at 4.8° and 7.4° can be seen as harmonics of the peak at 2.4° , revealing an extremely narrow variation of spacing. Based on equation E-III-2, the number of layers involved in the scattering for non treated montmorillonite leads to d equal to 4nm . This corresponds to about 6 sheets.

When clay is incorporated into the polymer, exfoliation or intercalation can be studied by WAXS. Actually, the exfoliation leads to the evanescence of (1,0,0) peak, while intercalation shifts this peak toward smaller angles. Figure III-2-2 displays the WAXS pattern of slightly swollen montmorillonite in PA-6 (curve A in Figure III-2-2)[73]. The lack of the (1,0,0) peak indicates that single sheets of montmorillonite are dispersed in the polymer matrix. On the contrary, intercalation is observed for highly swollen montmorillonite in PA-6: the (1,0,0) peak is located at an angle slightly lower than before the incorporation of the filler into the polymer (curve B in Figure III-2-2).

Figure III-2-2

III-2-2 Small angle X-ray and neutron scattering (SAXS, SANS)

Small angle scattering is the common name given to small angle neutron (SANS), X-ray (SAXS) or light scattering (LS). The radiation is elastically scattered by a sample and the scattering pattern can be analyzed to provide information on the size, shape, orientation of nanoparticles and/or distance between nanoparticles in the polymer matrix.

Figure III-2-3

A typical SAXS set up is schematically presented in Figure III-2-3. The source can be either synchrotron sources or rotating anode X-ray generators. The block collimation leads generally to a point collimation (note that slit collimation is sometimes used for SAXS). As the scattering laws depend on the collimation mode, following relationships will be given only for point collimation. The experiments provide, after some corrections [74], a plot of the scattered intensity I (Neutron or X-ray intensity) as a function of the scattering vector q expressed as:

$$q = (4 \pi \sin \theta) / \lambda \quad (\text{E-III-3})$$

where λ is the wavelength of the radiation, and 2θ is the angle between the scattered and transmitted waves.

The intensity due to the particles is given by :

$$I(q) = N_p V_p (\Delta\rho)^2 P(q) S(q) \quad (\text{E-III-4})$$

Where N_p is the number of particles, V_p the volume of one particle, $(\Delta\rho)^2$ is the contrast term, $P(q)$ is the shape factor and $S(q)$ is the interparticle structure factor.

$(\Delta\rho)^2$ is the square of the difference in neutron scattering length, while for X-rays, $(\Delta\rho)^2$ represents the square of the difference in electronic concentration (between particle and matrix). According to the value of $(\Delta\rho)^2$, SAXS or SANS can give a more or less high contrast. It may be also noticed that in SANS experiments, hydrogen and deuterium have a very different scattering length. This can be useful to optimise the contrast between the particles and polymer by selectively deuterating the one or the other.

General treatment

The integral Q of the intensity over the reciprocal space, named "invariant", is directly related to the volume of the particles in the polymer matrix:

$$Q = \int_0^{\infty} I(q) q^2 dq \quad (\text{E-III-5})$$

The asymptotic behavior of the intensity at large q provides information about the particle/matrix interface. In the case of a sharp interface, the asymptotic behavior is given by the following equation known as Porod law:

$$\lim_{q \rightarrow \infty} I(q) \propto \frac{S}{q^4} \quad (\text{E-III-6})$$

where S is the total interface.

This equation is valid for single particles and for densely packed systems as well. As it is possible to relate the volume of particles in the polymer matrix (V) to the invariant Q , the ratio S/V can be determined from the asymptotic behavior and the invariant :

$$\frac{S}{V} = \pi \lim_{q \rightarrow \infty} I(q)q^4 / Q \quad (\text{E-III-7})$$

Thus, knowing V, it is possible to obtain the value of S, without using additional data. In the same way the ratio V/S leads to a length which can be related to the particle dimension if the shape is known. When the interface is not sharp, a deviation from the Porod law is observed, indicating the presence of transition layers. The thickness of these layers can be determined in some cases [75].

Quantitative information can be also deduced from the comparison of experimental data with theoretical expressions in different specific cases. Let's first consider the case of dilute systems.

Dilute systems

For dilute systems (distances between particles are large compared to the dimensions of particles), S(q) is equal to 1, and the patterns are simple to interpret. The theoretical expression of P(q) for particles with different shapes (assuming random orientations) are reported in Table II [76].

Shape of the particle	Dimensions	Expression for P(q)
Sphere	radius R	$P(q) = \left[3 \frac{\sin qR - qR \cos qR}{(qR)^3} \right]^2 = \Phi^2(qR)$
Ellipsoid of revolution	axes 2a, 2va	$P(q) = \int_0^{\frac{\pi}{2}} \Phi^2(qa \sqrt{\cos^2 \theta + v^2 \sin^2 \theta} \cos \theta d\theta)$
Cylinders of revolution	diameter 2R height 2H	$P(q) = \int_0^{\frac{\pi}{2}} \frac{\sin^2(qr \cos \theta)}{q^2 \cos^2 \theta} * \frac{4J_1^2(qR \sin \theta)}{q^2 \sin^2 \theta} \sin \theta d\theta$ <i>J₁ is the one-order Bessel function</i>
Rods I _c (q) is related to the cross-section (A)	length L circular cross section (radius R ₀)	$P(q) = L \frac{\pi}{q} I_c(q) \text{ and } I_c(q) = A^2 \left[2 \frac{J_1(qR_0)}{qR_0} \right]^2$ <i>J₁ is the one-order Bessel function</i>
Flat particles (discs, lamellae) I _t (q) is related to the	Thickness T	$P(q) = A \frac{2\pi}{q^2} I_t(q) \text{ with } I_t(q) = T^2 \left[\frac{\sin qT/2}{qT/2} \right]^2$

thickness		
-----------	--	--

Table II: formulae of the form factor $P(q)$ for dilute systems of randomly oriented particles.

In the case of rods, particles are elongated in one direction with a constant cross-section (A) of arbitrary shape. The cross section, with maximum dimension d , should be small in comparison to the thickness T . On the opposite, flat particles display a constant thickness (T) extremely small compared to the two others dimensions ; they can be either stiff or slightly bent.

The calculated scattering intensity is plotted in Figure III-2-4 in the case of a sphere. The presence of the oscillations, observed at large q , is due to the unique value of the radius. In case of distributed radius, even in the case of a very narrow distribution, these oscillations vanish.

Figure III-2-4

Most of the times, the shape of particles is a priori known and the curves $I(q)=f(q)$ can be fitted by the previous equations. When the particle dimensions are distributed, both the shape of the particles and the size distribution influence the scattering. In this case, if the shape is assumed, the distribution can be deduced [77,78].

Guinier approximation

A convenient way to analyze the central part of the scattering curve is based on the approximation proposed by Guinier. The expressions of the scattered intensity for particles of various shapes are given in Table III. They introduced R_g , the giration radius of the particle, which is defined by analogy with the radius of inertia in mechanics. It is therefore related to the dimensions of the particle, as reported in Table III.

In practice the Guinier plot [$\ln(Iq) = f(q^2)$] is drawn, and from the slope of the obtained straight line it is possible to determine R_g . The Guinier plot is easy to use and works well in the majority of cases, for spherical or very anisotropic particles. In the case of polydisperse particles the radius determined from a Guinier plot is in fact a ratio of moments of the size distribution [79]:

$$R_g^2 = 3 \langle R^8 \rangle / \langle R^6 \rangle. \quad (E-III-8)$$

Particle shape	Scattered intensity	Giration radius
Spherical particles radius R	$I(q) \propto e^{-q^2 R_g^2 / 3}$	$R_g = \sqrt{3/5} R$
rod-like particles	$Ic(q) \propto e^{-q^2 R_g^2 / 2}$	$R_g = R_0 / \sqrt{2}$
flat particles	$Ih(q) \propto e^{-q^2 R_g^2}$	$R_g = T / \sqrt{12}$

Table III: Guinier approximation of scattered intensity of dilute particles.

An example of a Guinier plot in the case of montmorillonite lamellae in PA6 is given in Figure III-2-5. The thickness of montmorillonite lamellae calculated from the slope is about 0.6-0.7nm. This value is in fair agreement with the theoretical value.

Figure III-2-5

Non dilute systems (interparticle interference)

In this case the interparticle structure factor $S(q)$ is not negligible. Up to now no exact analytical expression for $S(q)$ exists and then just an estimation of the distance d between particles can be given. Generally speaking, the interparticle interference leads to the observation of a maximum. For nearly spherical particles, by considering that these particles constitute a regular lattice, it is possible to estimate d from the Bragg's law. For anisotropic particles, the same assumption can be made, but the intensity must be corrected by the Lorentz factor. In the case of lamellae, the intensity must be multiplied by q^2 before using Bragg's law.

Orientation

In the case of anisotropic nanofillers, an orientation of these fillers in the matrix, due to the process, is often observed. This phenomenon leads to the observation of a SAXS pattern depending on the direction of the wave vector. Figure III-2-6 displays an illustration of the orientation of Montmorillonite layers in PA-6 matrix elaborated through an extrusion-injection route. The maximum corresponds to the characteristic length (distance between layers : 3.6 nm). The intensity varies as a function of the incident beam direction compared to the different faces of the sample. It is highest for direction 1 (beam perpendicular to the smallest lateral faces, corresponding to the thickness of the injected plate). It reveals that most of the sheets are parallel to the largest surface of the specimen. The signal to noise ratio is still satisfactory when the beam is parallel to the direction 2: a few sheets are perpendicular to the largest surface of the specimen. Orientations 3 and 4 do not give an intense correlation peak.

This example illustrates the possibility to study the preferential orientations of anisotropic fillers by small angle scattering.

Figure III-2-6

Complex particles

As explained in part II, nanofillers in polymers are difficult to disperse and leads to the formation of clusters, aggregates and agglomerates with characteristic size ranging from nanometre to micron scale. The characterization of these different dimensions when they are in the range of the observation window can be performed by small angle scattering technique. When fillers have a fractal structure, it is possible to determine the fractal dimension from the asymptotic behavior of the scattering. The article of P.W. Schmidt [80] presents a complete review about this aspect.

III-2-3 Electron microscopy

Electron microscopy can be divided in two main techniques (i) scanning electron microscopy (SEM) and (ii) transmission electron microscopy (TEM).

Classical SEM microscopes are useful to characterize the dispersion of fillers with size in the range of 100 nm, like for instance carbon nanofibers in a rubbery matrix [51]. Recent improvements of scanning electron microscope make it suitable to observe nanocomposites. The use of a Schottky based emission field allows reaching a resolution of about 2nm. Moreover, they have been optimized to work at low voltage that allows observation of samples with low electrical conduction (like polymer) without metal coating. Although only few observations have been carried out until now, this technique will certainly be extensively used in the next future. In recent developments, new microscopes allow to work within low gas pressure, up to 10 bar ("environmental conditions") which in turn, allow normal voltage and no metal coating. In such devices, electrical charges are continuously removed because of the presence of ionised atoms of the environmental gas.

The transmission electron microscopy is a powerful technique to study structures at and below the nanometer scale. The electron microscopes are analog to light microscopes, but the specimens are illuminated by an electron beam and the conventional glass lenses are replaced by magnetic lenses. The very high resolution of TEM is due to the short wavelength of the electrons which is directly connected to the accelerating voltage. Typical instruments use now

accelerating voltages from 200-400kV. However, polymeric matrices are very sensitive to electron irradiation and degrades quickly under the beam (radiation damage causes destruction of crystalline order, chain scission, creation of radicals...). For this reason, a low voltage (below 100kV) is sometimes required.

As the sample thickness has to be around 100 nm, for nanocomposite, their preparation constitutes a major difficulty for TEM observations. In the case of thick or bulk specimens, ultra-microtomy is generally used and carried out below the glass transition temperature of the polymer. In the case of solution or suspension polymers, simpler methods can provide a thin specimen. For instance, the fluid can be spread over the support film on the TEM grid.

If the objective aperture is centered on the optical axis, a bright field imaging is obtained. Thanks to the so called mass-thickness contrast, regions of the specimen which are thicker or with a higher density will scatter more strongly the electron beam and will appear darker in the image. Examples have already been presented in section II for silica particles prepared from a dry cast suspension (cf. Figure II-1-2) and silicate layers in a polymer matrix prepared by ultra-microtomy (cf. Figure II-2-2). When filler and matrix (for instance, cellulose in a polymer matrix) exhibit low electron density contrast, it can be improved by staining, i.e. the selective incorporation of electron dense atoms into the polymer matrix or into the fillers. For instance, classical staining agents are osmium tetroxide and silver nitrate [82]. In the case of crystalline fillers, dark field imaging can be used; the obtained images are much more contrasted than bright field image but are much weaker in intensity. The dark field image is formed from one spot in the diffraction pattern, and can provide information such as the crystal dimensions and the orientation corresponding to the selected diffracted entities.

On the other hand, electron microscopy can be used also as very local spectrometer. In fact, when a high energy electron beam crosses a specimen, X-rays characteristic of the atoms of the specimen are produced. Their analysis (intensity as a function of energy) allows the determination of the nature of the chemical elements and gives some quantitative information about their respective content. Moreover, in TEM, the loss energy spectrum of electrons (EELS) may be used to get local information about the surrounding of the analyzed atoms in term of their chemical bonds. In new devices, it is now possible to select electron of a given energy to make cartography of the chosen element.

III-2-4 Atomic force microscopy

Atomic force microscopy was invented in 1986 by Binnig, Quate and Gerber [83], and has been widely used since. The principal element of the set up is a cantilever, which moves in

response to the forces acting on its tip [84]. These forces are due to the interaction of this tip with the atomic layers of the surface sample. The tip scans along the sample and an optical detector measures the cantilever's displacement. The displacements in the three directions of space (horizontal scan (x,y) and adjustment of the vertical position (z)) are often carried out by a piezoelectric actuator. AFM can be performed following mainly two different modes.

In the "contact mode", while scanning, either a feedback loop keeps the interaction constant, by adjusting the height of the sample (z), or the height of the sample is kept constant, and the resulting interaction force is measured. Then it is possible to obtain an image, giving the relief of the surface with a resolution lower than one nanometer. In this mode the interaction forces are relatively important (at the molecular level), around 10nN. In the case of soft materials, this can lead to a damage of the surface.

In the "tapping mode", the oscillation of the cantilever is controlled at a fixed frequency slightly above its resonance frequency (about 300kHz), with large amplitude (about 50nm). When the cantilever is put closer to the surface, the tip comes periodically into contact and the oscillation amplitude decreases. This decrease depends on the interaction between the tip and the sample surface. While scanning the surface a feedback loop keeps this amplitude constant by moving the sample height. The tip is in contact with the surface only for a very small time so that the average force is 100 times lower than in the contact mode. This is very interesting for soft materials such as rubbers. But the main application of tapping mode is the phase imaging. Indeed, it is possible to measure the phase difference between the signal sent to piezoelectric crystal (in to order oscillate the cantilever) and the signal due to the oscillations of the cantilever. This phase difference is sensitive to the variation of viscoelastic properties, friction and adhesion properties. Figure III-2-7 displays an image carried out on an rubber with silica fillers with this technique: the silica fillers appear clearly at the surface.

Figure III-2-7

However many phenomena can disturb the image (mechanical coupling between fillers and matrix for example) and the filler size, deduced from this technique, can be misleading. Other modes exist, such as "Force Mode" or "Lateral Force Mode", but are less used. Last developments allow direct measurements of local electrical and dielectric behavior as well as thermal behavior.

To conclude, many experimental techniques are available to perform the characterization of nanofillers and of their dispersion in a composite. A complete characterization of the nanocomposite (i.e. the use of several techniques) needs to take into account all the scales

characteristic of the microstructure to obtain the pertinent parameters necessary for the understanding of the mechanical behavior.

IV Linear mechanical behavior

In order to estimate the weight of specific parameters in the behavior of nanocomposites, it can be useful to work, as a first approach, with model systems. The first part presents model nanocomposites in which both interfacial properties and dispersion are controlled as well as possible. From experimental data, a discussion of theoretical modeling is proposed and, once some clear conclusions can be deduced, the analysis of more general cases is carried out.

IV-1 Model systems

Let's start with model systems obtained by a latex route (as described in part III) from Poly(styrene) (PS) and Poly(Butyl Acrylate) (PbuA) latexes (with typical particle diameter around 100 nm and volume fraction of PS in the range [30-50 vol. %]) [61,62].

Figure IV-1-1 presents the storage shear modulus of films made from (a) a mixture of PS and PBuA latexes and (b) a PS core - PBuA shell structured latex. Looking at the micrographies obtained by electron microscopy on these two systems (Figure IV-1-2), it is clearly visible that for the simple mixture, the random dispersion allows the formation of large aggregates of PS. This is much less probable for the two step polymerized system.

Figure IV-1-1

Figure IV-1-2

The comparison between the mechanical behaviors on these two systems is very instructive. The behavior of both "as obtained" materials (i.e. just after complete water evaporation at 40°C) shows a plateau (glassy state, see above part I). At about T_g of P(BuA) (-50°C), a large drop of modulus appears, by a factor of about 2 decades, followed by a continuous decrease (at least for Figure IV-1-1a).

After a heat treatment at temperature higher than T_g of PS, the behaviors of both materials diverge. The film obtained from blend (i.e. containing randomly dispersed PS particles) exhibits a much higher modulus. Moreover, the temperature dependence of this modulus, up

to T_g of PS, is very close to that of the PS at the same temperatures. On the other hand, for the film containing PS domains regularly localized (i.e. obtained from core-shell particles), the modulus measured in the rubbery domain keeps a low value and exhibits a decrease with increasing temperature.

It is noteworthy that the use of PS particles allows direct conclusions that are more difficult to reach with classical fillers. The fact that at relatively low temperature (about 140°C) PS becomes soft enough to coalesce should lead, after the heat treatment, to the formation of cluster. Even, a rigid continuous network could form if PS particles were already in contact, or furthermore were forming a continuous skeleton before the heat treatment. In other words, the heat treatment temperature is high enough to allow the coalescence of two particles in contact (i.e. suppression of their boundaries), but is too low to allow the complete coalescence of particles (formation of one unique particle of PS) and the diffusion of the particles that were not in contact (the initial repartition of the PS particles is conserved) .

Thus, it seems from these preliminary results that interactions between hard particles embedded in a soft matrix play the main role. This corresponds to a very large class of materials, as most of polymers are in fact filled by particles much stiffer than the matrix. For example, this is the case of most of polypropylene, polyamide, etc. based compounds which contain various fillers like calcium carbonate, kaolin, etc. However, to go further, it is of interest to check the effect of various parameters, like the modulus contrast between the different phases, the volume fraction, and the shape factor of the reinforcing particles.

IV-1-1. Effect of the modulus contrast

In the case of the examples presented previously (mixture of latexes), no reinforcement is observed in the glassy state, since both phases have a comparable modulus. This is different with rigid particles such as silica, whose modulus is more than ten times higher than that of a glassy polymer. In that case, the modulus of the nanocomposite in the glassy state is increased by 100% for 45 vol. % of silica particles (100 nm diameter). In fact, as it will be shown later (cf. part IV-2), the reinforcement provided by rigid fillers is much more significant when the polymer matrix is in the rubbery state, or alternately in the temperature range in between the glass transition temperature and the melting temperature of a semi-crystalline polymer matrix.

IV-1-2. Effect of volume fraction

Figure IV-1-3 exhibits the mechanical behavior of simple blend materials for various concentration of PS particles. Two main features must be pointed out. In both cases, before

and after heat treatment (3h at 140°C), for 30 vol.% PS, only a very weak reinforcement appears. The effect of the heat treatment becomes significant at increasing volume fraction above 30%.

Figure IV-1-3

To sum up, for "low volume fractions" (below 30 vol.% PS for the mixture of latexes) or when PS domains are embedded, i.e. are not allowed to form clusters, the reinforcing effect exists but remains very weak. On the contrary, when the interactions between particles are favored (for higher contents, above 30 vol. % PS for the mixture of latexes) the reinforcing effect starts to increase more rapidly and the heat treatments play a major role. This means that the dispersion state may have an influence on the mechanical behavior.

IV-1-3. Effect of the dispersion

The influence of the dispersion state of the particles within the matrix has already been exhibited in Figure IV-1-1 where the formation of a continuous network of reinforcing particles is shown to play a key role. But the situation is in fact more complicated as illustrated by the following experiments. Poly(Methyl Methacrylate) filled with silica particles (aggregates size around 150 nm) have been elaborated through three different ways : an industrial route (involving extrusion and injection), a solvent technique requiring the use of acetone and finally high energy ball-milling. The dispersion state was strongly influenced by the process, as illustrated on TEM micrographs for 10 vol. % of silica (Figure IV-1-4: a, b, c). The industrial route was found to give the best dispersion. However, given the viscosity increase due to the nanofiller presence, the maximum fraction of silica in PMMA obtained with this technique was 10 wt. %. The maximum amount of incorporated silica is 30 wt. % with the solvent route and 50 wt. % in the case of ball-milling. The presence of agglomerates is observed for these techniques, the worst dispersion corresponding to ball-milling (cf. Figure IV-1-4). The storage modulus in the rubbery plateau appears to be very sensitive to the dispersion state (Figure IV-1-5) : at a given volume fraction, the worse the dispersion state or the larger the agglomerates, the higher the modulus.

Figure IV-1-4

Figure IV-1-5

Up to this point, and recalling that the fraction at which a random distribution of spheres percolates is about 25%, one hypothesis may be that the stiffness of the composite material increases much more rapidly with the volume fraction of rigid fillers once they are able to form a continuous network. An easy way to check this hypothesis consists in increasing the shape factor of the reinforcing fillers, as the critical volume fraction at which the percolation occurs, decreases rapidly.

IV-1-4. Effect of the shape factor

In Figure IV-1-6, X_c is the critical volume fraction (called the percolation threshold) needed to reach the geometrical percolation of the whiskers. To define rigorously this percolation, one can imagine a network (cubic, hexagonal), whose nodes or links can be filled with two type of objects with a probability p and $(1-p)$. It is then possible to calculate the probability p_c , called percolation threshold, and its associated volume fraction ϕ_c , above which the network can be crossed from one side to the opposite side of the volume, through a continuous path. As described in the literature [7,85,86], this percolation threshold depends on the aspect ratio of the objects studied and on their orientation distribution. Moreover, it can be shown that the percolation threshold calculated for a non-uniform length distribution is lower than that calculated for a uniform length distribution having the same average length [45,87,88]. Figure IV-1-6 exhibits the strong variation of the percolation threshold versus the shape factor. Thus it appears that with rigid rods randomly dispersed (in position and orientation), a shape factor of 100 should lead to their percolation at a volume fraction of about 1%.

Figure IV-1-6

In other words, if the percolation plays an important role, we should find a large reinforcement for small fractions of high aspect ratio particles, especially if they form a rigid network inside the polymeric matrix. This can be seen in the following examples. As mentioned in section II, it is relatively easy to obtain cellulose whiskers which have an extremely high crystallinity degree, with an average diameter around 15 nm, very high tensile modulus, in the order of 150 GPa and a shape factor around 100 [89-91].

Following a protocol close to that described above for mixture of latexes (see Part III), it is possible to obtain nanocomposites of, for instance, p(BuA-S) reinforced by various fraction of these whiskers. Figure IV-1-7 exhibits the behavior of such materials. It is clear that the

reinforcement is much higher than expected for all types of short fibers composites: with only 1% of whiskers, a slight effect appears, while with 6%, a reinforcement by almost a 3 decade factor occurs. On the other hand, Figure IV-1-7b shows that the effect remains more or less unchanged up to the degradation temperature of cellulose, while the matrix alone began to flow and then to degrade. Such behavior suggests that the formation of a rigid network must be at the origin of the reinforcement.

Figure IV-1-7

Figure IV-1-8

Figure IV-1-8 exhibits the reinforcement versus the amount of cellulose whiskers below (a) and above T_g (b). Apart from the measurements performed on composite films obtained by water evaporation (Film (E)), another set of samples was processed (Film (XP)): the same aqueous suspension was freeze dried. This allows the extraction of water, but avoids that whiskers become in contact and form hydrogen bonds with their close neighbors. After this step, the resulting mixture was extruded and then hot pressed to obtain the desired samples. It is clear in Fig IV-1-8b that the reinforcement is much lower (by a factor of about 500) than for evaporated samples. On the other hand, the authors [91] checked that whiskers are locally parallel to each others (from X-ray diffraction data), which according to Figure IV-1-6c leads to no percolation in the range below 10% of whiskers.

As a conclusion, it is clear that for the latter systems, the occurrence of fillers percolation involving strong interactions (continuity of the rigid phase) increases drastically the stiffness of the composite. On the contrary, when the percolation can be avoided, the reinforcement occurs simply by stress transfer from the matrix to the fillers. In fact, this situation is rather similar with the case of spherical fillers like polystyrene. With films cast below T_g of PS and heat treated above T_g , then the reinforcing effect (Figure IV-1-1a) is much higher than for films where the PS nodules are encapsulated (Figure IV-1-1b).

In order to better understand these mechanisms of reinforcement, it is of interest to compare experimental data with simple models. This is presented in the next section of this chapter.

IV-2 Modeling of the linear behavior

As illustrated by the previous experimental results, the elastic modulus of a filled polymer is affected by (i) the elastic properties of its constitutive phases (i.e., modulus and Poisson ratio),

(ii) the volume fraction of fillers (iii) the morphology (i.e., shape, aspect ratio, and distribution of the fillers into the polymeric matrix) and (iv) the interactions between fillers. Various models are proposed in the literature to understand the complex interplay between these parameters and to display a prediction of the elastic modulus of polymer composites. Different authors propose a more or less exhaustive review [92-95]. In the case of nanocomposites, the comparison of theoretical values to experimental results can help for the definition of the key parameters in the reinforcement observed. In particular, the question of the possible effect of the nanoscopic size of the filler can be evaluated.

This paragraph will be firstly devoted to the presentation of the mechanical models and their account for the influence of simple parameters such as the aspect ratio and the filler fraction, in the prediction of the composite modulus. A comparison with experimental results will be proposed and discussed. Then, new approaches will be presented to account for the discrepancy generally observed between the models and the experimental modulus of nanocomposites above their glass transition temperature. Note that visco-elasticity will not be discussed. Indeed, it is generally admitted that elastic calculations can be extended to the description of the visco-elasticity of filled polymers through the correspondence principle[96-98].

A random distribution of the constituent phases in a filled system demands a statistical approach to describe the material structure. However, this requires knowledge of the distribution of the individual phases. To simplify the task of describing the mechanical properties of the composites one can consider an averaging process on a representative element volume (REV). The size of this REV must be small compared to that of the sample but large compared to the size of the heterogeneity (this is a serious limitation in the case of a percolated structure). Under these conditions, the material can be idealized as being effectively homogeneous. From the information about the properties of each phase and the interfacial geometry, one can predict the effective properties of the individual phases. The average properties of the material are defined as the ratio of the average stress and strain on the REV. Then the exact solution of the stress and strain field must be calculated. To do so, ideal geometry models have been proposed with more or less strong approximations, as discussed further.

IV-2-1. Bounds calculation

An estimation of the reinforcement effect of particles can be performed without any assumption on the geometry of the dispersion of the fillers. It only follows from the theorem

of minimum potential energy and from the theory of minimum complementary energy. Assuming either a uniform state of strain or uniform state of stress across all the different materials of the composite, one can estimate the well-known Reuss and Voigt bounds.

Using Eshelby's work [99], Hashin and Shtrikman proposed more restricted boundaries [100]. From the elasticity theory, Eshelby determined the local stress and strain fields in an ellipsoidal inclusion immersed in an infinite medium (so-called reference medium) submitted to a macroscopic stress and strain field. Generally speaking, the composite can be seen like an assembly of phases, each phase having the same average mechanical state as that of the inclusion with the same modulus immersed in an infinite homogeneous medium, submitted to an homogeneous deformation. The latter is determined from the property that the balanced summation of the average deformation of each phase is equal to the macroscopic deformation applied. The estimation of an infinite medium infinitely rigid or infinitely soft leads back to the Reuss and Voigt boundaries. The choice of the rigid phase and the soft phase as the infinite homogeneous medium gives the known Hashin-Shtrikman bounds. They allow an estimation of the expected reinforcement provided by the fillers. However, they are still far apart, especially when the contrast between the matrix and the filler modulus is important.

Instead of bounds, one can estimate the composite modulus from the exact strain stress field in the REV. We will first examine the models for spherical fillers

IV-2-2. Models for spherical fillers

The simplest case is to deal with low volume fraction of particles within the matrix ("dilute case"). The analytical calculation of the stress and strain fields of a spherical inclusion, representing the filler particle, in an infinite homogeneous matrix leads to the formula:

$$G_c = G_m \left[1 - \frac{15(1-\nu_m) \left[1 - G_f / G_m \right] \phi}{7 - 5\nu_m + 2(4 - 5\nu_m) G_f / G_m} \right] \quad (\text{E-IV-1})$$

where the subscript *c*, *m* and *f* refer for the composite, the matrix and the filler respectively. *G* is the shear modulus, *ν* is the Poisson coefficient, *φ* is the filler volume fraction .

In the case of a perfectly rigid inclusion in an incompressible material, this leads to the well known formula :

$$G_c = G_m (1 + 2.5\phi) \quad (\text{E-IV-2})$$

This is equivalent to the Einstein equation [53] for the viscosity of dilute infinitely rigid spheres in an incompressible fluid ($\nu_m=0.5$). In this specific case, the similarity comes from

the analogy between the mathematics governing linear elasticity behavior and that of Newtonian viscous fluid.

The description of high filler content in a matrix (non dilute systems) is more complex. Hashin introduced a composite sphere model consisting of gradation sizes of spherical particles embedded in a continuous matrix phase (cf. Figure IV-2-1a) [101]. He found an exact solution for the bulk modulus. But the calculation for the shear modulus lead only to lower and upper bounds for large filler concentration (the solutions for the dilute case being identical to equation E-IV-2).

Figure IV-2-1

Given the lack of solution for this specific geometry, Kerner [102] proposed a 3 phase model (cf. Fig IV-2-1b) in which one spherical inclusion is embedded in a spherical matrix (respecting the filler concentration) embedded in an equivalent homogenous medium whose properties are those of the composite material. The solution of this model for the bulk modulus being equal to that of the composite sphere model of Hashin, it is assumed that the solution for the shear modulus corresponds to the exact solution for the previous model. This solution was given by Christensen and Lo [103] who criticised the derivation of Kerner. A good correlation was shown between the model and experimental shear modulus of a composite of micron size glass spheres in an epoxy matrix (Figure IV-2-2).

Figure IV-2-2

In the case of spherical spheres in an incompressible medium, Batchelor and Green [104], and then Chen and Acrivos [105], used fluid mechanics to obtain the equation:

$$G_c = G_m(1 + 2.5\phi + 5\phi^2) \quad (\text{E-IV-3})$$

This is an extension of the Einstein equation [53] with the introduction of a term for the inter particle interaction. Note that Guth [106] derived a similar equation where this term is equal to $14.1\phi^2$. The prediction of these equations is close to that of the Christensen and Low formula [103] for low filler concentration. In the case of more concentrated suspension, Frankel and Acrivos [107] proposed an equation valid in the vicinity of the maximum packing fraction of the fillers. They also used the analogy with fluid mechanics. The suspension is described as a cubic packing of spheres and the shearing flow of the matrix in between two

spheres is idealized to be locally that of a simple shearing flow. It is found for the shear modulus, for concentration close to the maximum possible concentration ϕ_{\max} :

$$G_c = G_m \frac{3}{16 \left[1 - \left(\frac{\phi}{\phi_{\max}} \right)^{\frac{1}{3}} \right]} \quad (\text{E-IV-4})$$

where ϕ_{\max} is $\pi/6$ for cubical packing of spheres.

Let's recall that this result is only given for an incompressible matrix and infinitely rigid filler and therefore does not apply for rigid particles in a glassy matrix (where $\nu \approx 0.35$).

Among other models, the self-consistent scheme was first developed by Hershey [108] and Kroner [109] for the modeling of the behavior of polycrystalline materials. It was extended to multiphase media by Hill [110] and Budiansky [111]. Each phase of the composite is alternately viewed as being lumped as a single ellipsoidal inclusion in an infinite matrix of the unknown effective properties. This approach only gives an implicit expression for the calculation of the effective modulus of the composite. One can use an iterative method, taking the initial value found from the Eshelby's method. By definition, this method is not totally satisfactory since it assumes that the inclusion is embedded in a more rigid medium than the real one. Mori and Tanaka [112] proposed a similar calculation but took the matrix as the Equivalent Homogeneous Medium (EHM). This leads back to the low bound of Hashin Shtrikman. This estimation is correct as far as the inclusion are in sufficiently low interaction, i.e. for concentration below that associated to the percolation threshold.

All the methods presented above allow the description of the modulus of polymer composite filled with micron sized spherical filler from very low concentration up to high concentration when the particles are well dispersed. The 3-phase model seems the most appropriate for the large concentrations (up to 40 vol.%). It is then valid either with glassy matrix or rubbery matrix. In the latter case, it is equivalent to the Batchelor equation [104] (for low concentration).

Figure IV-2-3

The figure IV-2-3a presents a comparison between the composite modulus of PA6 filled with nanoscopic silica in the glassy domain and the 3-phase prediction [113]. A good agreement is observed, at least in the filler concentration range studied. This suggests that there is no specific effect of the size of the filler, for spherical particles in a glassy state. This was confirmed in the case of silica filled PMMA tested in the glassy domain. On the contrary,

above T_g (Figure IV-2-3b), a large discrepancy appears between experimental data and calculated curves. These results will be discussed later, as well as the possible mechanisms involved in such discrepancy (interfacial effects, filler matrix or filler-filler interactions).

IV-2-3. Models for high aspect ratio fillers

An aspect ratio different from one leads to consider two cases: oriented filler or filler with no preferential orientation. In the case of unidirectional filler, the calculation of the composite modulus is done through an extension of the previous models. For infinite fibers, Hashin and Rosen [114] proposed a composite cylinder model, which is the 2D counterpart of the 3D composite sphere model. This gives the longitudinal modulus E_{11} , the plane strain bulk modulus K_{23} , the Poisson coefficient ν_{12} and the shear modulus G_{12} in the longitudinal direction. The shear modulus G_{23} is calculated with the same assumption than previously (composite sphere model), by using a 2 dimensional 3-phase model.

When fibers are not infinite, the calculation can also be performed through the Eshelby calculation on an ellipsoidal inclusion in an infinite homogenous medium taken as the matrix. The solution of the problem can be expressed as a function of the aspect ratio of the ellipsoid as well as the properties of the 2 phases. In the case of $\xi=b/a \ll 1$ (a and b being the two ellipsoid axes), the solution is equal to the previous solutions for infinitely long fiber (calculation with Hashin and Rosen, or Christensen models). The general solution for the modulus in the direction of the longest axis shows the strong dependence of the reinforcement effect A on the modulus ratio E_f/E_m and the aspect ratio of the fiber ξ , as shown in Fig IV-2-4 [115]. Reinforcement effect A is defined as:

$$E_c = E_m(1 + A\phi) \quad (\text{E-IV-5})$$

Fig IV-2-4

It is noteworthy that for E_f/E_m equal to 100, the reinforcement effect for fiber with an aspect ratio of 100 is similar to that for infinite length fiber, so that the end effects can be neglected. Moreover, the higher the aspect ratio, the more important is the effect of the contrast in between the fiber and the matrix modulus.

The calculation for isotropic or transversely isotropic composite is made through an average calculation over all the equally possible orientation, of the unidirectional case. For instance, Tandon and Weng [116] used a combination of the Eshelby's calculation and the Mori Tanaka average stress theory. Another way is to use the laminate's theory which allows to express the

isotropic modulus as a function of the parallel and perpendicular moduli calculated for a unidirectional fiber ply. Tsai and Pagano [117] found:

$$E_{2D} = 0.375 E_{//} + 0.625 E_{\perp} \quad (\text{E-IV-6})$$

Halpin and Kardos [118] used the same equation for a transversely isotropic composite, with the approximation that the material is made of four plies with fibers oriented in directions of $0^\circ, -45^\circ, 45^\circ, 90^\circ$, respectively. The laminate theory can also be used to calculate the isotropic 3D modulus, one finds:

$$E_{3D} = 0.184 E_{//} + 0.816 E_{\perp} \quad (\text{E-IV-7})$$

The modulus of the unidirectional ply can be calculated from the Halpin-Tsai formula [119]. This is an empirical model. Its advantage is to give simple analytical prediction of all elastic constants over a broad range of volume fractions, making easy a 3D calculation. It writes:

$$\frac{M_c}{M_m} = \frac{1 + \zeta \eta \phi}{1 - \eta \phi} \quad (\text{E-IV-8})$$

where η writes:

$$\eta = \frac{\frac{M_f}{M_m} - 1}{\frac{M_f}{M_m} + \zeta} \quad (\text{E-IV-9})$$

where ϕ is the volume fraction of filler, ζ is a factor that depends on the shape of the filler particle and on the type of modulus M to be calculated.

ζ can be fitted to experimental results. Ashton et al [120] found that the equations can also be used to predict fiber reinforcement. They advised to calculate the longitudinal modulus E_{11} with $\zeta=2a/b$, and the in plane moduli E_{22} or E_{33} with $\zeta=2$, G_{23} with $\zeta=1/(3-4\nu_m)$, G_{12} or G_{31} with $\zeta=1$ and $\nu_{31} = \nu_{12}$.

Figure IV-2-5

As shown in figure IV-1-6a, the prediction by Halpin-Kardos of the modulus of whisker filled P(S-Abu) matrix in the glassy state is satisfactory. The transversely isotropic assumption is probably excessive. In the materials presented, the whiskers are not totally in the plan. This can explain the slight overestimation observed.

In another study [121], some materials were prepared from PVC latex with a freeze drying step followed by the extrusion (XP) rather than a simple evaporation. As explained previously, the extrusion process avoids the formation of a rigid whisker network by preventing as much as possible, hydrogen bonds between whiskers. Moreover, a plasticiser (DOP) was added in order to decrease the viscosity of the batch containing up to 12% of whiskers (which allows to process at low enough temperature to prevent chemical degradation); plasticised PVC will be referred to as pPVC in the following. The discrepancy between the Halpin Kardos prediction is higher with whisker filled pPVC than with whisker/P(S-Abu) composites (cf. Fig IV-2-5). This is probably due to a better isotropy of the filler. Indeed, a comparison with the 3D equation is better, but still overestimates the composite modulus. Like in the previous example of Figure IV-2-3a, the nanoscopic size does not lead to an abnormally high modulus.

The modulus of platelet filled composite can be predicted with Tandon and Weng's model. In that case, the Eshelby's calculation is performed with flattened ellipsoid. Van Es [38] noticed that the Halpin Tsai equation and Tandon and Weng's model for unidirectional platelet coincides if ζ is equal to $2a/4b$ for G_{12} , $2a/3b$ for E_{11} or E_{22} , and $\zeta=b/a$ for G_{13} and G_{23} , $\zeta=2$ for E_{33} , 1 and 2 being the in plane directions of the platelet and 3 the transverse direction. The average calculation leads to the modulus prediction for transversely isotropic and isotropic composite. As will be discussed later (see part IV-3-2), the model correctly describes the modulus of nano-clay filled composites in the glassy state.

Therefore, as far as the filler concentration is well below the maximum packing fraction, and the matrix is in the glassy state, the classical mechanical models correctly describe the nanocomposite modulus, whatever the filler geometry. The nanoscopic size of the filler does not lead to a more important reinforcement than classical micron size filler.

IV-2-4. Models for nanocomposites in the rubbery state

Things are totally different when the matrix is in the rubbery state. For example, in the case of silica filled PA6, the 3-phase model, which gives an accurate description of the behavior in the glassy state, is no more efficient to fit experimental data at 430K (above the glass transition temperature) (cf. Fig IV-2-3b). In particular, for a given volume fraction, the particle diameter appears to have a strong influence (see results at 6 wt. % for particle diameters of 12 and 50 nm in Fig IV-2-3b). Nevertheless, a direct interpretation of the results from the particle size seems difficult due to the difference in the filler dispersion: the TEM study of both samples indicates that the largest particles were well dispersed while the

smallest were aggregated. Besides, the dispersion is a key parameter as shown by the important influence of the process on the modulus measured with nanoscopic silica filled PMMA (Figure IV-1-5). For this second system also (silica- PMMA) , the classical 3-phase model leads to an underestimation of the modulus in the rubbery plateau, the description becomes worse when the particles are more aggregated.

Moreover, the disagreement between experiment and theory appears well below the theoretical percolation concentration of spheres. This suggests that the large reinforcement measured with the nanoscopic silica filler might come from the presence of occluded volume of matrix inside filler aggregates. The presence of immobilized matrix in an interphase cannot be excluded either, as discussed in part VI. Such effect of occluded or less mobile matrix cannot be observed in the glassy domain since the assumed decrease of macromolecular mobility near the filler surface is probably close to that observed in the glassy state.

An important discrepancy between theory and experiments is also observed with large aspect ratio nanofiller. The Halpin-Kardos model largely underestimates the modulus of whisker filled p(S-BuA) latex made by dry-casting. As discussed previously (cf. part IV-1), this is due to the formation of a rigid filler network which is not accounted by the models. The same phenomenon explains the large underestimation of the heat treated PS filled P(BuA) latex, in which the formation of a rigid PS network occurs in the material. An abundant literature indicates that the models fail also to describe nano-clay filled composites above T_g, as discussed later in part V.

From all these observations, influence of assumed phenomena such as occluded volume, immobilized matrix phase or mechanical percolation, should be taken into account in the models for a correct description of the experimental nanocomposite modulus in the rubbery plateau.

Agglomerates and occluded volume

Many models have been specifically developed for filled elastomer with carbon blacks. In the Guth equation [106], the occluded volume is accounted by an increase of the effective volume of filler [122]. Another way is to consider that the filler aggregates leads to a larger effective filler aspect ratio, which increases the reinforcement effect. Broodnyan [123] proposed a simple expression, equivalent to Einstein formula at low filler fraction, which takes into account the filler aspect ratio ξ :

$$G_c = G_m \exp\left(\frac{2.5\phi + 0.407(\xi - 1)^{1.508}\phi}{1 - \frac{\phi}{\phi_m}}\right) \quad (\text{E-IV-10})$$

with $1 < \xi < 15$. ϕ_m is the maximum packing fraction, which also depends on the aggregate and agglomerate geometry.

Like the effective filler fraction, both ϕ_m and ξ are mostly used as adjustable parameters since experimental data do not allow their precise determination. Note that the increase of the filler concentration is often related to a shell of immobilized matrix on the filler surface. This point will be discussed in part VI. The presence of aggregates and agglomerates means that there are local heterogeneity of concentration in the representative elementary volume. To account for this, Shaterzadeh [124] proposed to use a 3 phase self consistent scheme model in two successive steps. The behavior of the highly concentrated zone is firstly estimated with a filler concentration taken as the adjustable parameter. In the second step, these zones are considered as fillers in the matrix. This model gives satisfactory results in the case of micron sized fillers, but failed to describe the behavior of nanocomposites [125]. The occluded volume inside aggregates can also be accounted by a four phase self-consistent model [126]. The central inclusion is the occluded matrix embedded in a filler shell, surrounded itself by the matrix. The occluded volume is then estimated from the fit of the modulus in the rubbery domain. However, it leads to an overestimation of the reinforcement in the glassy domain, since it assumes that the filler-filler bonds have the same mechanical properties as the fillers [127]. The geometric simplicity of the Hashin model can be replaced with the idea of representative morphological motif [128]. This requires the definition of family of similar domains and a minimal description of their spatial distribution [5,129-131], a precise statistical description of the composite microstructure. The state of aggregation is taken into account without any assumption on the mobility of the matrix.

Interphase, immobilised layer

The existence of an interphase can be accounted by a Kerner type model in which the phase surrounding the matrix has the property of an homogenous interphase [132] (whose properties are in between the matrix and the filler properties). Papanicolaou [133] and then Sideredis [134] extended their model by taking into account the probable property gradient of the interphase. These models were developed for unidirectional fiber reinforced composite and can be extended to isotropic case. Their limitation, in the case of nanocomposite, is the total lack of information on the properties of the assumed interphase. Assumption can be made that the polymer in the interphase has a reduced mobility, i.e. exhibits vitreous properties, because of its closeness to the inorganic surface. For example, use can be made of a 4-phase model [5,135], the interphase modulus chosen equal to the one of the matrix in the glassy state. The volume fraction of interphase needed to fit the data is generally very important compared to the fraction of polymer matrix and no DSC measurements have revealed the presence of such

large values of interphase fraction [113] . Thus, without evident morphological proofs of the interphase existence, the interphase appears to be used to compensate for the deficiencies of the mechanical coupling approaches.

Thus, there is a need for approaches that are efficient to account for the possible formation of a more or less rigid filler structure in the composite, as discussed in the case of the materials presented previously.

New approaches accounting for filler network

A first attempt is called the percolation "model" and is derived from the phenomenological approach of Takayanagi [136,137]. The composite is described as a parallel mechanical coupling of a rigid phase, made of theoretical volume fraction of whisker network, and a soft one, made of the matrix reinforced with the whiskers out of the network. The modulus and the volume fraction of this phase can be chosen as that of the filler, as an adjustable parameter, or deduced from micro-structural observation. In the case of cellulose whisker filled P(S-BuA), the modulus of the rigid phase is deduced from the experimental value of a whisker sheet (see part II). Its volume fraction is calculated from the percolation theory [63,138]. In the case of random distributed objects, the volume fraction ψ of the percolated structure is given by :

$$\psi(\phi) = 0 \quad \text{for } \phi < \phi_c$$

And

$$\psi(\phi) = \psi(\phi) = \left(\frac{\phi - \phi_c}{1 - \phi_c} \right)^b \quad \text{for } \phi > \phi_c \quad (\text{E-IV-11})$$

As assumed by De Gennes [139], the dead branches do not participate actively to the stress transmission. An account only of the backbone of structure needs a b value close to 1.8.

This model is an important improvement of the description of P(S-BuA) composite, as shown in Figure IV-1-8b, but it overestimates the cellulose whisker filled pPVC composite behavior. Therefore the evaluation of the network modulus as a function of the mechanical properties of the link between the whiskers is necessary. This work, in progress, is now described.

The calculations are performed in two steps : (i) the generation of whisker network (definition of intersection nodes, of elements between nodes, and of the linking elements between two whiskers in contact, and (ii) the calculation of the mechanical properties of the network with a finite element code CASTEM 2000 (DMT-CEA software). In the first step, whiskers are generated, with random orientation (for isotropic network). Their number depends on the aspect ratio, the volume fraction of whiskers, and is limited by the calculation capacity of the computer. Due to the high aspect ratio of the fillers, a procedure to account for boundary

effects is adopted. Two whiskers are considered to intersect each other when the distance in between them is below their diameter. This leads to the definition of nodes and linking elements. When there is a path linking each face of the sample to the opposite side (i.e. percolation), there is a continuous whisker network that can be virtually (i.e. computerized) mechanically tested. The network is tested in tensile test and the apparent tensile modulus is deduced from the summation of the forces applied on the nodes of the displaced face. For whisker fraction equal or below 5%, the calculated value of the whisker network, with link beam modulus between 1.5 MPa and 15 GPa, is below the experimental tensile modulus of pPVC composite above T_g (at 60°C), as shown in figure IV-2-6. This suggests that, at this concentration, the network is too weak to have an influence on the modulus of the composite. This is confirmed by the reasonable agreement between experimental value and a mean field approach calculation for whisker content below 4%. Concerning P(S-ABu) composites, their mechanical properties are mainly due to the whisker network properties when the volume fraction is above 6%. For smaller fraction, the calculated modulus is lower than the experimental ones, even for high modulus of the links. Moreover, it must be noticed in Figure IV-1-8b that there is not a neat threshold for the mechanical properties. By contrast, the calculation necessarily leads to a steep increase of the modulus above 1% whisker concentration. Different assumptions are currently investigated to explain this disagreement: the percolation threshold might be lower than the simulated one since the calculation of the intersections does not take into account the possible inter-phase thickness. A slight orientation of the whiskers parallel to the surface of water evaporation exists in the P(S-BuA) composite, and the possibility of concentration heterogeneity is not excluded. However, the promising preliminary results suggest that the calculation presented here might be an alternative method to the classical models that are currently not efficient to describe the mechanical properties of such composites.

Figure IV-2-6

Another Discrete Element approach has been developed, to explicitly take into account both initial spherical morphology of PS and P(BuA) particles and nature of the contacts between them. A REV made of hundreds of spheres is chosen, with a given volume fraction of PS and P(BuA) particles. At each contact is associated a constitutive relation between forces and torques transmitted through the contact and the kinematic variables (displacement and rotation rate) defined at the particle center. By analogy with the work of Jagota [140] this relation involves normal, tangential, flexural and rotational viscous moduli. These moduli depend on the intrinsic viscosities of PS and P(BuA) and on the contact radii. Three types of

relationships are used, for PS/PS, PS/P(BuA) and P(BuA)/P(BuA) contacts. For PS/PS, the contact radius is temperature dependent, which allows to describe the beginning of the coalescence observed above 70°C. In the case of annealing treatment, the contact radius is assumed to be constant and of the same order than the particle radius. Moreover, the intrinsic viscosity of the P(BuA) matrix is chosen higher for P(BuA)/PS contacts than for P(BuA)/P(BuA), but the difference decreases at increasing temperature. The equilibrium equations of the particle assembly are solved, with homogeneous imposed kinematics conditions at the boundaries. The resulting forces are deduced and thus the effective viscosity in the temperature range [-10°C ; +100°C], i.e. above T_g and below T_f . The initial ratio for the PS and P(BuA) moduli is $5 \cdot 10^3$. In Figure IV-2-7a, it can be seen that the evolution of the effective shear modulus with temperature is qualitatively described for different volume fractions of reinforcing particles. In particular, the larger the volume fraction of PS, the more important is the decrease of the modulus with temperature. The beginning of the coalescence is also retrieved for PS concentrations larger than 30%. In Figure IV-2-7b the effect of the annealing treatment is shown. Experimental results at 50°C, before and after annealing are plotted. The numerical results illustrate the difference between the "geometrical percolation" (a skeleton of PS particles is formed with small contact radii) and the "mechanical percolation" (the same skeleton of PS particles is formed, but with large contact radii). The last one occurs at about 20-25 % of PS reinforcements.

Figure IV-2-7

Conclusion

All the approaches used to predict the composite behavior firstly try to account for the complexity of the composite microstructure. In the nanocomposite case, the models, which are no dimensional, show no particular effect of the nanoscopic size in the reinforcement measured below T_g . Conversely, above T_g , there is a strong discrepancy of experimental modulus with the theory which suggests that some effects negligible in the glassy state are no more negligible in the rubbery domain. In particular, the effect of mechanical interactions between fillers and/or between fillers and the matrix must be evaluated. One possible way is to use multi-scale approaches or finite element modeling including an as close as possible description of the microstructure. Obviously, such theoretical works have to be developed in parallel with the analysis of the mechanical properties at a local level.

This ongoing work is supported by the growing industrial interest for such materials. Actually, a broad range of potential applications may be envisioned, from sporting equipment

and stiffer automotive parts, yet at lower filler content. Packaging applications are also considered thanks to high barrier properties with insignificant loss of clarity, and improved safety in relation to enhanced flame retardance. Conversely to the model materials presented in the previous part, "industrial nanocomposites" are mainly based on rubbery, thermosets or semi-crystalline matrices. Typical viscoelastic behaviors of such systems are presented in the following.

IV-3 Industrial materials

IV-3-1. Nanosized filled Rubbers

Rubbers are largely used in industrial applications, mainly in shoes, joints, pipes and tires. For most applications, elastomers are reinforced by nano fillers, usually carbon blacks or silica particles. These nanocomposites have been firstly developed on an empirical basis in tire application. Their interest has been extended to many other applications, such as seals, because of a their very specific viscoelastic properties and wear resistance. The new interest of the rubber industry for silica particles as fillers (made possible by new surface chemical treatment of the silica) and the development of nanoscale characterization techniques, has lead these last years to a new interest of the scientist for these materials. However, the compatibility of hydrophilic silica (high tension surface) with the hydrophobic polymer matrix (low tension surface) is low. This compatibility can be enhanced by adding a bi-functional coupling agent. Using such coupling agents, an advantage of silica compared to carbon black is that it gives lower hysteresis loss, which for tyre applications leads to a lower rolling resistance and consequently fuel savings. Michelin introduced the silica reinforced "Green Tyre", which offers 30% less rolling resistance, and consequently 5% fuel savings. Thanks to their large industrial interest, the mechanical properties of filled elastomers have been abundantly studied, as shown by the impressive number of publications on the subject. The incorporation of small particle size fillers to crosslinked elastomeric matrix results in specific non-linear mechanical behaviors including high hysteresis, stress softening (Mullins effect) and strain dependent dynamic modulus effect (Payne effect). These non-linear effects will be discussed in part VI.

IV-3-2. Mica-type silicates filled layers

Due to their potentially high aspect ratio and unique intercalation / exfoliation characteristics mica-type silicates like montmorillonite have recently received a great deal of attention. As firstly reported on PA6-montmorillonite [54], with the addition of only 5 wt. % clay, the

following property improvements were observed : 170% higher tensile modulus, 40% higher tensile strength, 60% higher flexural strength, 13000% higher flexural modulus. Physical properties was also enhanced : decreased solvent uptake, increased thermal stability (heat distortion temperature increased from 65° to 152°C), improved barrier properties (40 % decrease in water permeability) and flame retardance [141]. The reported increase of modulus was particularly impressive when compared to that measured with composite reinforced with classical fillers. For example, only 3 or 4 wt% of the dispersed nanoclay is equivalent to 40 wt% of a standard mineral filler or 10-15 wt% of glass fiber in PA-6 composites to give comparable stiffness at a lower density. This first clay nanocomposite studied was also the first commercial clay nanocomposite used for under-the-hood components in automobile (timing belt covers). There is also a growing interest to use PA-6/nano-clays as a matrix for making both short and long glass fiber (GF) reinforced composites.

Now, let's focus on the way the microstructure can rule the mechanical properties of these nanocomposites.

The following results concern polyamide-6 / montmorillonite nanocomposites prepared by extrusion-injection route. The clay was supplied by Southern Clay products. Two different surface treatments were compared : the first one (methyl octadecyl bis 2-hydroxyethyl ammonium methylsulfate) leads to a slightly swollen montmorillonite (basal spacing $d_{001} = 18\text{\AA}$), the second one (dimethyl dioctadecyl ammonium chloride) leads to a highly swollen montmorillonite (basal spacing $d_{001} = 36\text{\AA}$). The following samples were obtained: PA2 (2.7wt %, intercalated, obtained from the highly swollen montmorillonite) , PA3 (3.4 wt %, delaminated, obtained from the slightly swollen montmorillonite). The sample processing conditions have been detailed elsewhere, as well as the corresponding nanocomposite morphology [73]. As presented in part III, due to the injection process, the montmorillonite sheets preferentially orient themselves around the injection axis. The platelet orientation and their surface nucleation effects seem to prevent the crystallization of the α -phase and promotes the crystallization of the γ -phase. The dynamic mechanical response of these nanocomposites is presented on Figure IV-3-1 [142].

Figure IV-3-1

Two different ranges of temperature can be considered : (i) when the amorphous part of the PA6 matrix is in the glassy state, i.e. when crystalline and amorphous polyamides have almost the same order of magnitude for the shear storage modulus (≈ 1 GPa) and (ii) when the

amorphous polyamide becomes rubbery (≈ 1 Mpa) whereas the properties of crystalline polyamide remain mainly unchanged. In agreement with the results observed in the case of model systems (parts IV-1 and IV-2), the reinforcement is more effective in the rubbery plateau of the amorphous part of the PA6 matrix. Although the results are higher in the case of the delaminated system, the interpretation is difficult since the volume fraction of incorporated filler is also different.

The influence of the delamination / exfoliation state can be further commented in the case of glassy epoxies matrices [143]. With 3 wt. % of montmorillonite, Korman reported an increase of 34 % in tensile modulus. The flexural modulus of both an intercalated and an exfoliated systems have been compared with a conventional composite (i.e. prepared with untreated clay) (see Figure IV-3-2). The flexural modulus increases substantially more for the two nanocomposites than for the conventional one at increasing clay content. Moreover, it appears that the difference between intercalated and exfoliated nanocomposites is small but significant (5% at 3.4 vol.%)

Figure IV-3-2

As discussed in parts IV-1 and IV-2, the properties of nanocomposites can be affected by two morphological parameters: the size and the aspect ratio of the reinforcing particles. Micromechanics of nanocomposites reinforced by platelet-shaped fillers were discussed by Brune et Bicerano [144]. They developed a model to predict the buckling of platelet in reinforced materials under compressive loading. The model was improved to account for the reduction of the reinforcement efficiency of clay platelets of high aspect ratio as the result of the incomplete exfoliation. They also showed that the deviation of the platelet orientation from perfect biaxial in-plane has a detrimental effect on the reinforcement efficiency. Van Es [38] also proposed a modeling of platelet reinforced composites derived from Mori-Tanaka formalism. A good agreement is obtained for volume fraction up to 4 wt %. Above this value, the calculation gives an overestimation of the experimental data. Van Es proposed that the low effectiveness of nanoclay at high loadings can be attributed either by the lower orientation of the platelets at a macroscopic scale (evidenced by TEM micrographs) or the high mobility of the confined polymer chains inside the clay galleries.

However, when the temperature increases above the glass transition of the amorphous phase of the nylon matrix, the relative increase of modulus is higher and the model developed by Van Es [38] is no more accurate. Moreover, as illustrated in part IV-2, geometrical percolation of the reinforcing elements is known to significantly improve the mechanical

response (modulus, stress) particularly when the amorphous phase is in the rubbery plateau. In the case of the montmorillonite-PA6 systems studied, the morphological characterization clearly indicates that percolation of the filler is not present but the reinforcement observed in the rubbery plateau is far from the one evaluated from classical mechanical approaches. It might be proposed that a network is formed with clay platelet (oriented in the injection direction) and crystalline lamellae (in a perpendicular direction) (Figure IV-3-3). Such a scheme has also been proposed by Kim et al. [145]. Above the main relaxation temperature of the amorphous phase, due to the decrease of its modulus, the contribution of the response of such a network is probably no more negligible.

Figure IV-3-3 .

On PA2 and PA3 samples, additional modulus measurements were performed in compression with various deformation axes (at room temperature) in order to study the influence of the montmorillonite orientation [142]. Figure IV-3-4 displays a schematic view of the deformation axis compared to the preferential orientation of the montmorillonite sheets. The values of modulus related to the deformation axis are presented in Figure IV-3-5. In the case of polyamide-6, the same modulus is obtained in the three direction that indicates an isotropic behavior. For the nanocomposites, the largest reinforcement is obtained when compressing the nanocomposites along a direction parallel to the injection axis.

In order to take into account the aspect ratio of silicate layers, use was made of the model proposed by Tandon and Weng [116] (cf. part IV-2). In the calculations, the aspect ratio is set equal to 0.015, the Young's modulus to 170 GPa and the Poisson's coefficient to 0.2. The comparison between calculated results and experimental data along all directions are reported on Figure IV-3-5. Satisfactory agreement is obtained for the exfoliated sample when compressing the nanocomposites along a direction parallel to the injection axis. In the other cases, the observed deviation is assumed to be linked to the definition of the representative elementary volume. Once again, it can be concluded that further works are required to develop and validate composites models for the calculation of the elastic properties of platelet reinforced composites

Figure IV-3-4

Figure IV-3-5

There is a general agreement on the reinforcing effect in modulus of nanosilicates layers when the polymeric matrix is in the rubbery state. The different parameters that have been evoked to explain this reinforcement are: (i) the degree of exfoliation, because it increases the interactions between fillers and matrix [146], (ii) the contribution of a constrained region where the polymer chains display a restricted mobility [147], (iii) the modification of the crystallinity due to the strong interactions between nylon and silicates layers [148], (iv) the increase of the effective volume fraction of the fillers in the nanocomposite due to the swollen of the clay [143]. Establishment of the structure-property relationships is complicated by the significant number of morphological and processing factors that impact both the inorganic filler and the polymer, such as heterogeneity of the nanoscale arrangement, orientation distribution of the layers, strength of polymer-inorganic interactions...

To give insights in these different interpretations, use can be made of dynamic mechanical analysis that provides information on both modulus and molecular mobility.

The addition of montmorillonite modifies the temperature of the main relaxation (α) (see figure IV-3-1b). A shift towards lower temperatures of the G'' peak is observed for all the nanocomposites ($T=60^\circ\text{C}$ for all the nanocomposites, about 5°C less than the temperature of pure PA6). The same decrease (around 5°C) was also observed on the glass temperature measured by DSC. This down shift of the glass temperature was assigned to the presence of the surfactant (plasticising effect). In the literature, it is also reported that the glass transition temperature of high performance epoxy layered nanocomposites decreases with organosilicate content. The reasons for this decrease may include thermal degradation of the surface modifiers and homopolymerisation of the epoxy between the silicate layers. A change of stoichiometry caused by a possible cation exchange of surface modifier for curing agent molecules as the latter diffuses between the silicate layers could also be an explanation. In an other PA6-montmorillonite system (with 2 wt% from Ube Industries), Gloaguen et al. observed that the position of the $\tan\delta$ peak temperature remains the same. However the area of the peak is strongly reduced. Although they analyzed the loss factor (which depends on the rubbery modulus), they concluded that this indicates the mobility reduction in the amorphous phase of the nylon in the presence of clay platelets, which are expected to be bond to the polymer matrix. The decrease of the loss peak is no more observed if the nanoclay is embedded in a polypropylene matrix[149].

Another way to assign the properties of polymer - layered silicate nanocomposites to the changed mobility of the polymer phase is to perform NMR studies that could yield information on the amount of mobilized and immobilized polymer. Van Es [38] investigated the polymer mobility in PA-6 - clay nanocomposites with 1-20 wt. % with proton NMR relaxation. He found that a part of the polymer phase in these nanocomposites appears as mobile as in low molecular weight liquid. The amount of polymer with high mobility rises if the amount of clay increase. At 20 % of clay, about 10% of polyamide-6 is as mobile as a liquid. Similar conclusions were reported by Manias et al. in the case of PS matrix [150]. They found that the mobility of polystyrene molecules in the confined space between clay layers differs greatly from the mobility of unconfined PS. PS in the center of clay galleries proved to be more mobile than the bulk PS while mobility of PS in direct contact with the clay surface was inhibited. The increase of mobility of the PS inside the clay galleries was confirmed by the results of self-diffusion coefficient measurement.

All these experimental features are not consistent with the general idea of reduced mobility related to the constrained dynamics of the polymer chains near the layered silicate surface. On the opposite, an increase of mobility can be observed, due to a plasticizing effect of the surfactant or a modification of the curing. However, these results show that further works are necessary before being able to give more general conclusions, at least on the interface properties

After discussion of the linear response of nanocomposites to a mechanical stress, the following parts will be devoted to the non linear behavior of these materials. As recalled above (part I), below their glass-rubber transition temperature, amorphous polymers present a non linear behavior in terms of plasticity when they are submitted to a stress of the order of roughly one tenth of their Young's modulus. This is also the case for semi-crystalline polymers, below T_{α} (where their behavior is similar to that of amorphous polymers), and between T_{α} and T_f (melting temperature of their crystalline phase). Above T_{α} , the viscoelastic response is governed by entropic forces and becomes non-linear at large deformation (hyper-elasticity) up to the plastic deformation of the crystallites. The influence of nano-fillers when the matrix is in the glassy state will be discussed first (part V). The specific non-linear behavior associated to filled elastomers will be presented in part VI. In the following sections, we will first give some experimental results on various materials, and present some modeling methods.

V Non linear behavior in the glassy state

For composite materials, the non linearity may have its origin either within the matrix itself, or may also be due to some damage occurring during the deformation of the composite (cavitations, decohesion, etc.).

V-1 Experimental behavior

As discussed in part IV, the introduction of nanofillers leads to an increase of the modulus that is often accompanied by an increase of the yield and plastic stress. However, the presence of fillers also leads, most of the times, to a increase of the brittleness of the composite.

As a first example [113], an attempt to determine the plastic behavior and fracture mechanisms of nylon - nanoscopic silica nanocomposites has been carried out using SAXS measurements on post-mortem samples. In these systems, two different states of dispersion were achieved in the same range of particle sizes (12 and 50 nm). The introduction of fillers leads to reinforcement of the modulus and of the yield stress (see Figure V-1-1). The stress-strain curves reveal that the strain at rupture decreases when the amount of filler increases and is much lower, at a given filler amount, in the case of an optimal dispersion of the filler than for aggregated structure. The damage was thought to evolve with decreasing filler size and worsened filler dispersion state from a single debonding process to a multiple debonding one (intra agglomerates) (see figure V-1-2).

Figure V-1-1

Figure V-1-2

The second example concerns the behavior of pPVC reinforced by cellulose whiskers presented in the previous part; pPVC can be considered, as a first approximation, as a slightly crosslinked amorphous polymer. The behavior of such material below T_g is given in Figure V-1-3. As expected, the slope at the origin of the stress – strain curve, i.e. the tensile modulus, increases with the amount of whiskers. More interesting, the yield stress increases with the whisker content as well as the slope after the yield point (hardening). The “peak” of the stress-strain curves (yield stress) decreases at increasing whisker content. In all cases, the elongation at break remains very high (more than 60% for amounts below 7 vol.%, and up to 40% for 12.4 vol.% of whiskers). These various points are now discussed.

Figure V-1-3

V-2 Modeling of the plastic behavior

In fact, very few attempts have been made to directly obtain the prediction of the plastic behavior of nanocomposites. Most of the time, the non-linear curves of the polymer matrix are considered as a set of successive linear segments. These segments correspond to the segments of the stress strain curve of the composite, calculated incrementally from an assumed relationship between their slope. Such a view has to be discussed carefully [151], as in a heterogeneous material, stress and strain are not constant within the material [152]. Several ways can be used [153], among which two simple methods recalled in Figure V-2-1. At first, segments can be simply taken tangent to the data curve and their slope leads directly to a value of an instantaneous modulus [110] (E_t in Figure V-2-1). Another way consists in considering the successive slope (i.e. E_s) of the secant straight line from the origin ($\sigma=0$, $\varepsilon=0$) for each value of the strain [154].

Note that the tangent modulus method cannot work for stress peak, as a negative modulus has no physical meaning. In that case, the peak must be neglected and the experimental curve (b, in Figure V-2-3) is, as a first approximation, fitted by only two tangent lines (a). It is then possible to build the σ - ε curves starting from $\sigma=0$ and $\varepsilon=0$. The use of a mechanical coupling model leads to the curve (d), which has to be compared with the experimental curve (c) of the nanocomposite. If experimental linear viscoelastic behavior is known for both the pure matrix and the composite, then, from classical dynamic mechanical analysis (DMA) or mechanical spectrometry (as function of either temperature or frequency), a coupling model is not necessary: to the slope corresponding to the pure matrix (i.e. a given value of the modulus E_V), it corresponds (at same frequency and temperature) a value of the composite modulus [155].

The fact that the stress is not homogeneous inside the matrix in the case of soft matrix reinforced by stiff particles can lead to the disappearance of the yield stress, as shown, for instance, by the stress-strain curve of whisker filled PVC (Figure V-1-3). Due to the presence of the whiskers, there are zones where stress concentration appears, i.e. the local plastic stress is reached for a lower applied stress. In order to account for this effect [156], it is possible to evaluate the stress versus the distance from the particle surface, using an empirical relationship as for instance (see Figure V-2-2):

$$\sigma = (K - 1)\sigma_m \exp\left(-\frac{x}{x_c}\right) + \sigma_m \quad (\text{Eq. V-2-1})$$

where x_c is close to the curvature radius of the particle surface, X , the distance from the surface, K , the stress concentration factor on the surface and σ_m is the stress applied on the materials (K is equal to 3 for a spherical particle).

Figure V-2-1

Figure V-2-2

Using on the one hand, the tangent modulus method, and on the second hand taking into account the stress concentration near the filler surface, it is possible to predict reasonably the mechanical behavior of pPVC reinforced with cellulose whiskers, as shown in Figure V-2-3. However, the calculation leads to curves above experimental data, but the yield stress and strain are correctly reproduced. At strain above 20%, the composites become progressively white, which is typical of the appearance of small holes (having a size close to the light wavelength, i.e. around 1 μm). These holes could occur where stress is the strongest, i.e. at the ends of the whiskers, or close to the contacts between whiskers. From this usual observation, it seems that the damage of the nanocomposite could be responsible for the lower stress (at given strain) than predicted by the modeling. Small angle neutron scattering (SANS) experiments confirmed that such damage appears around the yield stress [157].

Figure V-2-3

In the previous case, only weak interactions between fillers were evidenced, especially in the linear range. For materials where stronger interactions can be developed, as for example in evaporated latex / cellulose whiskers nanocomposite (see section IV), the question related to the network damage needs further developments. As a typical example of such materials, Figure V-2-4 exhibits the tensile behavior at increasing filler contents for cellulose whiskers / p(BuA-S). These specific experiments were performed at temperature above T_g (T_g+30 K), in order to get a typical rubbery behavior for the pure matrix. At increasing whisker content, the initial slope of the curve drastically increases. For whisker contents for which DMA evidenced the formation of a network, at a strain above 0.2, the stress starts to decrease and around 0.5 the composite is strongly damaged. Such a behavior does not occur for PVC materials described above, for which the formation of the network is avoided (Figure V-2-5).

Figure V-2-4

Figure V-2-5

From these two examples, it is clear that the stiffness of a filler network leads to the brittleness of the nanocomposite. This specific feature has to be taken into account even at temperature below T_g , as discussed in the following example. Figure V-2-6 exhibits the stress – strain behavior of silica reinforced p(BuA-S), with 45 wt. % of fillers (i.e. ≈ 25 vol. %). Two domains are clearly identified, (i) below $\varepsilon = 0.03$, where the behavior is nearly elastic, with a relatively high modulus (compared to the pure matrix), and (ii) above, where the slope is much lower. This behavior can also be characterized by the ratio of the initial modulus versus the yield stress, which is here rather high (around 80) compared to classical behavior of materials (generally speaking, the yield stress appears for strain between 0.05 to 0.1, and this ratio is around 10 to 20).

Figure V-2-6

In order to analyze this behavior two modeling attempts were performed combining the tangent linearisation and two mechanical coupling models that were validated to describe the linear response. The first one, based on a three phase mean field model, does not account for the modulus at low strain, but predicts rather well the stress for higher strain (curve c on Figure V-2-6). On the contrary, the second approach based on the numerical simulation presented in section IV-2 (discrete element approach) predicts a fairly good elastic behavior, but fails above strain of 0.03, as it leads to very high yield stress (curve d on Figure V-2-6). Two features must be recalled. First of all, none of these models take into account any damage effect; on the other hand, the mean field model does not account for the formation of a stiff filler network, while the numerical model was designed for that. It can be then suggested that silica particles form a continuous network linked by hydrogen bonds and responsible for the high initial stiffness of the composite. At high enough strain, this network starts to damage and interaction parameters in the numerical model should be modified, unless it leads to unrealistic stress. As soon as the network is fragmented, the mean field model becomes appropriate, and leads to relatively good stress level.

To sum up, the plastic behavior of the matrix is predominant, in the sense that a brittle matrix will lead to a brittle composite. Conversely, a ductile matrix may in some case leads to rather ductile nanocomposites, while it is known that classical composites are often very brittle at low contents of fillers. The topology of the fillers dispersed within the matrix is the second key parameter. Strong interactions between fillers above the percolation threshold lead to high elastic response at low deformation, but as the consequence of the network brittleness, the

yield stress may be rather small. At last, adhesion between fillers and matrix is another important parameter, as it rules the composite damage during its deformation. This process is responsible for the energy dissipation at the origin of the ductility and the toughness of the material.

In the case of semi-crystalline matrices, the analysis of the non-linear behavior is more complex, as it involves mechanisms proper to the crystalline phase (c.f. part I). Moreover these mechanisms may be influenced by the presence of nanofillers either because of the modification of the crystalline morphology, or because of a mechanical coupling effect (modification and heterogeneity of the stress strain fields in and around the spherulites, etc...). These aspects will be further discussed in the next part, considering the example of nanolayered silicates reinforced semi-crystalline matrices, which have been developed for industrial applications. The issues will be to understand the elementary mechanisms operating in their non linear behavior and to identify some general trends related to the nanostructure organisation.

V-3 Industrial materials

In contrast to the more conventional particulate-filled microcomposites, one of the goal of polymer nanocomposite research is to reach a good compromise between the strength and the toughness. Sumita et al. [158] early underlined the interest of replacing micrometric silica particles by nanoscopic counterparts. They observed an increase of both the yield stress and the stress at break, along with a limited decrease in the strain at rupture. Earlier papers also reported that the use of montmorillonite or hectorite type clays in polymeric matrix allows to achieve high specific modulus, high strength and high toughness in PA6/NC even at very low content (2 to 5 wt%).

How the clay particles achieve these feats is not well understood (these effects were only interpreted in terms of high surface to volume ratio of such thin silicate dispersions), but it is undoubtedly a key point for the industrial application of these fillers.

Concerning the strength, the improvement is generally more impressive in nylon matrix than in amorphous glassy polymers. For the samples PA2 and PA3 presented previously, it was found a 175% increase of yield stress under compression along the direction parallel to the injection axis. The increase was only of 15% with 10% of montmorillonite in glassy PMMA[159]. For glassy epoxy, several studies reported the absence of tensile strength improvement, even at increasing clay content, but a small positive effect on compressive strength (17% increase of compressive strength with 10% of clay in an glassy epoxy [160]).

Just like in the case of modulus, a total exfoliation of the clay is thought necessary to obtain the best strength, but the interfacial interactions clearly play a role in the strength improvement. When the interfacial adhesion is weak, like between polar layered silicate and non-polar matrix such as polypropylene, no significant improvement is observed. So, at the present time and in view of the different trends reported in the literature, a strong strength improvement is mainly observed in the case of PA6. Mechanisms responsible for this reinforcement have not been clearly identified yet. There is still a great need to define the exact role of the size and of the aspect ratio of the nano-fillers, and to precise the effects of the interfacial interactions between the silicate nano-layers and the polymer during the deformation process.

Improvements in properties at break are even more controversial. Gloaguen et al. [149] observed that PA6 nanocomposites reveals an extremely fragile tensile behavior at room temperature (with a strain at break as small as 5 to 7%). The ultimate properties of montmorillonite / PA6 composites described in part IV.3 were determined from tensile tests. When comparing intercalated and exfoliated samples (so-called PA2 and PA3 respectively), the largest failure stresses were obtained with exfoliated systems, whereas the intercalated systems lead to the largest failure strains (see Figure V-3-1). In addition, Varlot and col. indicate that any inhomogeneous dispersion of the layered silicate on a microscale can affect dramatically the mechanical performances [142]. In natural clay, such as montmorillonite, the presence of large aggregates may be difficult to avoid because of natural fluctuations of their chemical composition. That may be a reason to the growing interest in synthetic layered silicates such as fluorohectorite.

Figure V-3-1

Concerning fracture toughness, Harcup and Yee[162] observed a clear deterioration in fracture toughness of polyamide 6- clay nanocomposites: for 4 wt.% of well dispersed nano-clay, G_c decreases from 10 to 1 kJ/m². They reported that the decrease of toughness is less pronounced in a second sample with the same amount of clay, but containing microscale aggregates of pure silicate (G_c around 5 kJ/m²). In this second sample, plastic deformation is observed to concentrate within agglomerates of partially intercalated material. Moreover, these agglomerates appeared to break under the applied load. Other authors proposed that the intercalated morphology can give some property improvements that are unavailable to fully exfoliated systems : the aggregates are assumed to act as stress concentrators and with induce plastic deformation around them. Zerda and Lesser [163] studied a glassy epoxy with aliphatic diamine curing agents and observed that intercalated montmorillonite leads to an almost unchanged compressive behavior (with a slight decrease in ultimate strength and strain

to failure) (Figure V-3-2). However, improvements in toughness values of 100% over unmodified resin were demonstrated (Figure V-3-3). By investigating the surface roughness, the authors assumed that the creation of additional surface area during crack propagation is the primary mechanism for toughening in intercalated systems.

Figure V-3-2

Figure V-3-3

Kim et al investigated the micromechanical deformation processes of stacked silicate layers in a PA-12 matrix by electron microscopy during *in situ* tensile measurements [145]. The main event is microvoid formation inside the stacked silicate layers. During deformation, the separated bundles tilt perpendicular to the direction of the applied load. Depending on the orientation of the stacked layers, some amount of energy is dissipated by splitting, sliding or opening of the separated bundles (Figure V-3-4). As a result, the toughness of the nanocomposite is enhanced.

Figure V-3-4

In conclusion, polymer-clay nanocomposites display, even at low clay content, improved strength and modulus compared to both pure matrix and conventional composites. They also display a high heat distortion temperature under load (DTUL) and improved moisture resistance. In some glassy or semi-crystalline polymer layered silicate nanocomposites, these improvements are obtained without sacrificing too much toughness. Moreover, to improve the toughness without decreasing the modulus, an efficient means is to optimise the microstructure to dissipate a maximum of energy (by plastic deformation of the matrix, cavitation...). This optimisation should of course avoid microscale heterogeneities, which may act as detrimental defects. For this purpose, the recent trend is to prefer synthetic layered silicates versus natural ones like montmorillonite.

At this moment, a broad range of potential applications may be envisioned for these layered silicates filled nanocomposites. Their use in crosslinked rubbers has also been investigated. For instance, 7.5 vol. % of the exfoliated silicate layers improves the strength of elastomeric epoxy polymer matrix by more than 10-fold [164]. Wang and Pinnavaia observed similar benefit in polyurethane-clay systems : stress and strain at rupture were both increased relative to the pristine polymer [165]. By the way, the mechanical response of filled elastomers is known to display specific non-linear behaviors. These behaviors are strongly dependent on

microstructural parameters including the filler nature. They will be discussed in the following part in the case of silica and carbon black fillers.

VI Non-linear behavior of filled elastomer

The introduction of nanoscopic filler such as, for the most common, carbon blacks or silica particles, strongly modifies the viscoelastic behavior described in part I. In the small deformation range, instead of the quasi linearity observed in shear with unfilled elastomer, one observes a typical non-linear viscoelastic behavior, so called Payne effect. In the large deformation range, the stress is remarkably increased for a given strain solicitation, the hysteretic loss during deformation cycle is enhanced, a strong sensitivity to the first deformation, so-called Mullins effect, is revealed, and the ultimate properties such as wear resistance and rupture behavior are improved.

VI-1 Small deformation range, the Payne effect

VI-1-1. Experimental features

The non-linearity induced by the introduction of nanoscopic filler can be shown by two different mechanical experiments. In dynamic mechanical measurements, when submitted to successive sinusoidal deformations with increasing amplitude, the samples exhibit a decrease of their measured storage modulus, and the appearance of a maximum for the loss modulus at a deformation level around 0.1. Two plateaux are also visible, as shown in figure VI-1-1, with what will be hereafter called low amplitude modulus (LAM) and high amplitude modulus (HAM), respectively.

Figure VI-1-1

The non-linearity at low deformation - unrevealed in pure elastomer- is equivalently demonstrated in classical shear-stress measurements (cf. Figure VI-1-2). The apparent modulus measured as the slope of the stress strain curve decreases strongly when deformation is increased. The composite presents a pseudo-plastic behavior with a strong strain rate dependence of the material response. A decrease of the strain rate of measurement decreases the amplitude of the Payne effect, which quasi-vanishes at strain rate below 10^{-6} . An increase of temperature has the same influence since it strongly decreases the initial modulus and much less the terminal one [166].

Figure VI-1-2

It is noteworthy that the DMA measurements presented in Figure VI-1-1 represent “fully equilibrated material response”: the storage and loss moduli measured at each strain amplitude are steady state value that would remain constant indefinitely if the strain amplitude were sustained at a constant value. However, dynamic measurements performed at increasing strain amplitude do not give the same DMA curves when measurements are performed at decreasing amplitude. In other words, the material has the memory of the modulus reduction that occurs at high strain amplitude. This memory effect vanishes with time [167,168]. Indeed, a material submitted to a static offset, present, after a sufficient elapsed time, the same DMA curve than without static offset as shown in figure VI-1-3 [169]. The curves virtually superpose, even for deformation of 0.2, i.e. much higher than that at which the modulus decrease occurs.

Figure VI-1-3

The main features of the Payne effect described above are general to all filled elastomers. It depends essentially on the filler surface: the size of the filler and the chemical nature of its surface are therefore two main parameters [170]. Figure VI-4 presents the influence of the surface of filler (i.e. their size) on the modulus decrease in filled elastomer during the DMA experiment described above (HAM minus LAM). The so-called structure of filler, measured by DPB measurement, and which is characteristic of the complexity of the aggregates geometry, is a very minor parameter compared to their size.

The surface developed by the nanoscopic fillers makes preponderant the matrix-filler and filler-filler interactions which are key parameters for the filler dispersions during the composite processing. For this reason, all the interpretation of the non linear behavior of filled elastomers in studies which deal with a modification of these interactions via chemical treatment of the filler surface, or via the matrix chemistry, must be done taking into account a possible modification of the dispersion. Moreover, the nanoscopic filler can favour an important and uncontrolled adsorption of activator, accelerator and crosslinking agents that in turn can modify the crosslinking density of the matrix in the filler vicinity [171]. However, it is noteworthy that a chemical treatment of the nanoscopic fillers does not modify the general features of the Payne effect [172], though it may modify its intensity (i.e. LAM-HAM).

Figure VI-1-4

Two different types of mechanisms are proposed to explain the Payne effect. Indeed, though the very abundant literature, the debate is still on-going. The existence of two different pictures of this phenomenon is directly related to the nanoscopic size of the filler for which it is impossible to neglect either filler-filler interaction (with or without the involvement of the matrix), or the filler-matrix interaction.

The first explanation, and also the earliest, considers as preponderant the filler-filler interaction [170,173]. The formation of a network structure inside the rubber matrix is assumed (cf. Figure VI-1-5a). The rigidity of this structure depends on the rigidity of the filler-filler bonds. The deformation of the composite leads to its breakage and the loss of rigidity. During cycled deformation, as observed by DMA, there is alternately breakage and reformation of the filler bonds, which is a dissipative phenomenon at the origin of the peak of the loss modulus observed in Figure VI-1. Many experiments support this scheme. The decrease of the filler size down to the nanoscale leads to a statistically nanometric distance in between filler, which can favour their interaction, and their agglomeration in complex structure.

The formation of this structure has been followed by electrical conductivity measurement in the case of carbon black filled elastomer [174,175]. It was found a good correlation between the LAM value and the conductivity, suggesting that this modulus is directly the consequence of a mechanical percolation of the filler. And, as in other polymer composites, it has been shown (by conductivity measurement and mechanical characterization) the existence of an optimum mixing time to obtain the highest LAM, which allow a macroscopically uniform dispersion of the filler but also the existence of a filler network [174]. The "agglomeration-desagglomeration scheme" is also suggested by the analogy between viscoelastic behavior of filled elastomer and the rheology of nanofiller filled suspension. The latter shows a decrease of viscosity with shear rate similar to the decrease of modulus with shear in filled elastomer [176-178]. A decrease of shear modulus is also observed for suspension of carbon black particles in oil for which the role of polymer chains cannot be evoked. In that case, the only obvious mechanism is a modification of state of aggregation with shear rate[179].

Medalia[122] made the assumption of trapped matrix inside the cluster of filler agglomerates. This trapped matrix increases the apparent filler fraction, and its unshielding during the deagglomeration of the filler enhances the modulus decrease [180]. However, the preponderance of the surface of the filler over their structure suggest that the occluded volume theory is not a

key mechanisms in the Payne effect [181]. Moreover, some might object that a filler network has a too low modulus to explain the LAM measured in filled elastomer. And it has been shown that the Payne effect is also observable in Carbon Black composite even when they are non-conducting composite, i.e. without the presence of a percolating filler structure effect [181].

Many authors prefer to consider the mechanism of adhesion-desadhesion of polymer chains at the filler interface [182]. In that case, the adsorbed polymer might act as supplementary crosslinks in the elastomer. Its mobility is then decreased (cf. Figure VI-1-5b). Moreover, the distance in between crosslink being reduced, the chain might not act in the low deformation range as predicted by the Gaussian description but more like a chain at the limit of its extensibility [183].

Figure VI-1-5

Many studies have been devoted to the characterization of the assumed immobilised matrix. Dutta [184] has studied by NMR technique the mobility of adsorbed polymer (styrene-butadiene) at the surface of carbon black particles extracted (in solvent) from the composite. They conclude in the presence of three regions with different mobility, a bound rubber region, a loosely bound region, and the non-influenced polymer. This has been supported by other studies on similar or different systems [185-187]. The amount of adsorbed polymer depends on the chemical nature of the polymer and the particle surface, and also of the molecular weight of the polymer [188]. In the case of silica filled PDMS, Cohen-Addad has shown that the adsorbed polymer involves a multiple link structure. Numerous monomeric units are involved in a binding site which is a dynamic system consisting of bonds which form and dissociate permanently [189]. It is noteworthy that some studies by NMR indicate the presence of a region with an increase of mobility in nanoclay composites (cf. part VI). The authors [38] assume the effect of a confinement of polymer in between the filler. The contradiction with the assumed decrease of polymer mobility is just apparent. It is likely that the polymer of increased mobility is not different, or at worst less mobile, than polymer above T_g . In that case, this phenomenon becomes negligible compared to the effect of adsorbed polymer layer (shown by the same experiments). This is implicitly admitted by Van Es since he assumes the possible role of adsorbed polymer on the filler surface when he studies the rheology (i.e. above T_g) of his composites. Another argument for the presence of immobilised polymer chain is the recovery kinetic of the LAM after deformation, at large amplitude or

during the application of an offset since it is for some authors, similar to the physical ageing of polymer in the glassy state after stretching [190].

However, the estimation of the bound rubber thickness leads to very contradictory results. In the case of nanofiller, the thickness of few nanometers means an important volume fraction of immobilised matrix. But DSC measurement never revealed any modification of the glass transition of the material, either the presence of phase with different glass transition temperature. The absence of such evidence is often explained by the mobility gradient of the polymer near the surface (with no neat difference of glass transition temperatures), or by the assumed total lack of mobility (i.e. of glass transition) of the bound rubber. Some information might be deduced from the current attempt to model the molecular dynamic in the vicinity of the filler surface [1991].

To conclude, the mechanisms of the Payne effect probably involves the filler structure and the adsorbed chain. The viscoelastic nature of the mechanical coupling of the filler to the matrix , particularly shown by the recovery experiments of the LAM, strongly suggest the role of the filler elastomer structure in which filler-filler bonds are made via an adsorbed layer of polymer[192,193].

VI-1-2. Modeling of the Payne effect

Due to its complexity, the modeling of the Payne effect is still the topic of many publications. Some authors proposed the extension to the composite modeling of the phenomenological model used with unfilled elastomer (Ogden or Mooney type). However, there is no physical meaning of the parameters and the model does not account for the viscoelastic response of the material when submitted to a complex stress-strain history. They can be however improved with the introduction of a function accounting for the evolution of the material during deformation [194].

A more physical description such as the Krauss model [173], which is one of the earliest and most cited model, clearly refer to the breakage of the filler network. The contribution given by interaction forces between aggregates to the modulus is proportional to the number of contact whose rigidity is governed by the size and the form of the aggregates. Their separation occurs at a given strain corresponding to the maximum of restoring force. The model only accounts for strain dependence. This assumption is supported by the temperature independence of the strain at which the storage modulus decrease occurs [195]. However, this model does not predict the values of the high and low amplitude moduli, neither the strain necessary for the modulus decrease, nor the exponent of the power law dependence of this decrease with the strain amplitude. Moreover, it completely neglects the frequency

dependence of the LAM and HAM and the kinetic aspects of the phenomena. This model is similar to those developed in the case of nanoparticles suspension. Though the analogy between fluid mechanics and solid mechanics should be restricted to simple case (dilute system), it is noteworthy that the modeling of Non-Newtonian behavior of filled suspension such as that of Cross model leads to equation very similar to the Krauss equation. In both cases, the assumption used is that of a breaking of agglomerate under shear.

The estimation of the HAM can be performed from the Guth-Gold equation in the case of low filler content. For higher content, the occluded volume can be an explanation of the discrepancy with the predicted result, but its estimation is only empirical. Moreover, it seems difficult to estimate the amount of occluded volume before the filler network breakage. To estimate the LAM, some authors prefer to consider the filler structure from the percolation theory [196]. They make the assumption that it has a scale invariance of a fractal object [197]. The reinforcement is deduced from the calculation of the rigidity of the cluster objects forming the network. It is found a power law dependence of the modulus with the filler content. The composite deformation leads to the breakage of the cluster in smaller and smaller units which loose they effectiveness [198]. This description leads to the same Krauss formula in which the parameters are related to the description of the filler structure: its fractal dimension and its connectivity [196]. Gerspacher use a different formalism to describe the process of rupture and reformation of contact between aggregates. It is assumed a distribution of pair of aggregates in the material, alternatively going from a linked state to a separated state, during DMA measurements [199].

The model developed by Maier and Goritz [182] is based on a radically different vision of the Payne effect. The increase of the modulus at low deformation would be due only to adsorption of polymer chains on the filler surface. This increases the number of crosslinks in the elastomer network. The modulus expression of the composite is derived from the entropic elasticity theory; but is modified in that the total number of crosslinks is equal to the summation of those provided from the matrix, those permanently adsorbed to the filler surface and those which are unstable and destroyed with deformation. The adsorption rate of the chain is constant while the desorption rate is amplitude dependent. From this description and experiments at different temperature, the author deduces a reasonable energy of bonding between 0.15 and 0.18 eV. The dissipation is due to friction of chain on the filler surface, it is proportional to the number of unstable links and to their probability to slip on a neighbour site. This model is probably excessive in that the calculation of the modulus does not take at all into account the increase of rigidity due to the presence of the rigid inclusions (in the present case, filler with a complex geometry, aggregates and agglomerates) and the possibility of occluded volume).

To conclude, all the experimental evidences and theoretical calculations seems to indicate that both filler structure and adsorption of polymer chains are involved in the non-linear viscoelastic behavior of the nanoparticle filled rubber. The modulus measured is obviously the result of a viscous mechanical coupling of the matrix to a complex structure of more or less aggregated fillers. For this reason, a description of the Payne effect need a nanocomposite model based on a mechanical approach, such those described in Part IV-3. This mechanical modeling of the LAM must account for the occluded volume, the complex geometry of the filler, the filler structure which might percolate mechanically, and the probable presence, as revealed by many experiments, of a less mobile phase which influences this structure rigidity. For instance, this can be done through a self-consistent scheme with 3 steps, in which is introduced a bonding phase (cf. for more detail part IV). The evolution of the modulus with deformation is accounted by a thermo-mechanical activation of the debonding - or an increased mobility of the "bonding phase". The volume fraction of the latter decreases, and leads also to the decrease of the occluded volume, i.e. the effective filler fraction. This is taken into account in a new mechanical calculation of the modulus. Figure VI-1-6 presents the result of such modeling. A more detailed presentation of this work will be published soon [200].

Figure VI-1-6

The non-linear viscoelastic behavior might also be described from a discrete approach such as those presented in Part IV. This needs the knowledge of the microstructure of the filler network, made from direct or indirect (via the matrix) filler-filler contacts. The non-linearity is then simulated from an evolution of the mechanical properties of the links in between the filler, during the deformation (this evolution can be implemented incrementally).

VI-2. The Mullins effect and the ultimate behavior

VI-2-1. The Mullins effect

Another interesting properties of filled elastomers is to show a mechanical behavior modified after a pre-straining. This effect has been firstly shown by Holt [201] and studied by Mullins [202], whose name has been given to the phenomenon.

This so-called Mullins effect is illustrated in Figure VI-2-1. A sample is stretched at a maximum deformation ϵ_{\max} . Then it is unloaded during a time in between half an hour and several days. A new loading of the sample leads to a stress-strain curve which is below the curve obtained during the pre-stretching, for deformation level below ϵ_{\max} . For deformation above ϵ_{\max} , the second curve joins the first one. Some experiments suggest that this effect is partly recoverable [202,203] but for much longer time (in the scale of months) than that involved in the Payne effect (see above). However, a real recovery in the cited experiments is not obvious since it needs heating of the sample at temperature for which a post-crosslinking can occur in the matrix.

Figure VI-2-1

This Mullins effect is strongly dependent on the particle size. Like in the Payne effect, the origin of the phenomenon can be found in the filler structure or in the molecular mobility of the polymer chain, or in both. Mullins did not proposed any interpretation in the molecular mechanism involved. He modelled the experimental results with a phenomenological description of the material seen as the assembly of two phases, one soft and one rigid. Under deformation, a fraction of the rigid phase would be broken and softened [204].

The first molecular interpretation was promoted by Bueche [205,206]. He assumed the existence of adsorbed polymer chains linking two different filler particles. The distance between particles would be distributed, so for the linking segments of chains. An increasing deformation would lead the shortest segments to reach their maximum extensibility. In that case, they would break or they would be debonded from the filler surface (cf. Figure VI-2-2a). The key parameters in this model are the distance in between particle, related to their size, and the bonding surface. Dannenberg [207] and Boonstra [208] had a very similar interpretation except that they preferred to consider a slipping of the stretched polymer chain on the filler surface (cf. Figure VI-2-2b).

Figure VI-2-2

Wagner [209] has a more biased vision of the phenomenon since he considers that the Mullins effect would come from the immobilized polymer phase around the particles. Under deformation, this shell would deform quasi irreversibly (i.e. plastically) and would not contribute anymore to the reinforcement.

Recently, Killian et al.[210] made a synthesis of the different modeling. The filler structure results from direct filler -filler interaction and indirect, i.e. filler-matrix-filler, interaction. The first sub structure deforms irreversibly under stretching [211]. This would explain the often residual deformation after a first stretching. The second sub-structure follows the mechanism described by Boonstra.

Interesting features have been shown by Lapra [212]. He confirms by birefringence the presence of short or strongly stretched chains during the deformation, which do not obey to Gaussian statistic. A.F.M. experiments showed that there is strong heterogeneity of deformation. This confirms the important role of the distribution of local volume concentration of fillers.

Besides the physical description of the experiments, different mechanical approaches have been developed [213-215]. They are more or less phenomenological. They incorporate the physical description in a so-called "damage" function, which is introduced in a hyper-elastic model (Ogden or Mooney type). The main difficulty of such modeling lies in the correct description of the relaxation phenomena.

The mechanisms involved in the Mullins effect are probably very similar to those involved in the Payne effect, except that the characteristic times involved drastically differ. Because of this similarity, a correct study of the Payne effect especially recovery experiments, must be performed on "de-mullinised" samples: samples have to be pre-strained in the deformation range where the Payne effect is measured.

VI-2-2. Ultimate behavior

Besides properties previously discussed, filled elastomers with nanoscopic particles exhibit an increase of stress at break. In certain condition of testing, they also exhibit an increase of the strain at break. Figure VI-2-3 shows stress-strain-curve obtained at 298K with a strain rate of $4 \cdot 10^{-1} \text{ s}^{-1}$ with Styrene-Butadiene Rubber filled with untreated nanoscopic silica. It is also illustrated in the case of carbon nanofibers (Pyrograf III TM) in an rubbery epoxy ($T_g = -35^\circ\text{C}$) (Figure VI-2-4) [51]. The main difference between both examples concerns the amount of nanofiller (below 5wt.% in the case of carbon nanofibers , 25 vol. % in the case of silica).

Figure VI-2-3

Figure VI-2-4

The increase of stress can be explained by strain amplification effects [216], which are known to occur in such complex materials. However, this cannot account for the apparent increase of the ultimate strain. In fact, the total rupture envelope of such composites must be considered. The latter can be obtained by a logarithmic plot of the ultimate stress, corrected by a factor T_{ref}/T , as a function of the ultimate strain. T_{ref} is the chosen reference temperature for the curve, while T is the temperature of the test. The correction factor accounts for the temperature dependence of the entropic elasticity. All the tests made at different strain rate and temperature lead to a unique curve (cf. Figure VI-2-5). The variation of temperature or strain rate only moves the representative point along the envelope, anticlockwise for a decrease of temperature or an increase of strain rate. At high temperature and low strain rate, the reinforcement is limited (low ultimate stress and strain). At low temperature and high strain rate, the ultimate stress increases but the ultimate strain reaches a maximum and then decreases. The rupture properties are optimal in an intermediary region. A maximum ultimate strain can be determined from the envelope curve and will be hereafter call ϵ_{ultm} .

Figure VI-2-5

As shown on figure VI-2-5, the addition of filler in the elastomer decreases ϵ_{ultm} . However, the zone of optimal behavior is shifted toward higher temperature. For instance, Lapra [212] showed that unfilled SBR exhibits, when stretched at a strain rate of 0.1 s^{-1} , a maximum ultimate strain at 273K when the latter is observed at ambient temperature with the same SBR filled with 20 vol.% of untreated silica. The same observation was made with different surface treatments: in all cases, the decrease of the properties for temperature above the ambient is much slower than for unfilled SBR. This lead to an ultimate strain systematically higher in the filled samples than in the unfilled ones at 333K.

The increase of the ultimate strain for untreated silica filled SBR when compared to treated silica filled SBR (with a coupling agent), strongly suggests the role of a cavitation around particles. The latter might dissipate energy and retard the material rupture. The existence of a polymer phase with a reduced mobility in the vicinity of the nanofiller might be an explanation of the temperature shift on the envelope curve. Bueche and Halpin[217] gave another explanation. Like for the Mullins effect, some chains linking aggregates have a low limit of extensibility : a higher temperature is needed to allow the relaxation of the high stress they support. This might be the reason for an increase of the ultimate stress at high

temperature with filler content but such reason for the increase of the ultimate strain at ambient temperature is less obvious.

The same authors showed a link in between the creep behavior of elastomer and the rupture envelop. They consider the rupture process as the propagation of a fissure. During deformation, small tears are initiated and begin to grow. Their growth is controlled by the viscoelastic response of the material and is describable in terms of the creep curve. As shown in figure VI-2-5 the description of SBR filled with Carbon Blacks is satisfactory. However, in the model, the creep behavior is supposed to be independent of the stress, which is known not to be the case. Moreover, the model needs three adjustable parameters.

The role of the dissipated energy in the rupture mechanism has been studied to determine some kind of rupture criteria. Hardwood and Payne[216] proposed a law which relates the rupture energy, calculated as the whole surface under the stress strain curve, to the hysteresis H_b , measured during the first cycle of deformation at a strain level close to the ultimate strain. However this criteria is not efficient in the case of silica filled polymer. The main contribution of such analysis is to recall that the rupture of the material is essentially dependent on the Mullins effect, which, as said previously- involves damage (i.e. irreversible modification) of the material. For filled elastomer, H_b mainly represents the Mullins hysteresis.

To conclude, the ultimate properties of filled elastomer appear like a consequence of the behavior previously described. This involves the filler structure, the filler-filler interaction, the filler - matrix interaction for which the nanoscopic nature of the filler is a key parameter.

General conclusion

All along this chapter, different aspects of nanocomposites have been listed. For sake of simplicity, we decided to restrict the review to the case where such composites are made of polymeric matrix, reinforced by fillers stiffer than the matrix. This excluded in particular, polymers reinforced against impact or rupture, by the addition of soft domains having size between 10 to 1000 nm.

First of all, as for all heterogeneous materials, the nanocomposite macroscopic behavior depends on the behavior of each phase, on their topological arrangement and their volume fraction, and on interfacial properties. In fact, all studies confirm that interfacial properties become of first importance when the typical dimensions of domains decrease down to nanometers. At least two reasons may explain this particular feature, (i) the small size leads to

a high interface/volume ratio, and moreover (ii), in the case of polymeric matrix, the average distance between domains, i.e. between filler surface becomes of the order of the macromolecule coils. This is the main reason to pay a specific attention on nanocomposite polymer based materials. Though lots experimental data are still difficult to really understand, several features can be pointed out.

The existence of filler network, which is never discussed for classical, i.e. micrometer scale composites, is evidenced for most of the nanocomposites already studied. This is the case where direct bonding between neighboring fillers can exist within the matrix, i.e. for fillers with high tension surface, such as silica particles, or cellulose whiskers, etc... But this is also the case where macromolecules may adsorb or may be chemically linked onto the filler surface during the composite processing. In fact, one macromolecule can link together two (or more) fillers. This results in a large scale network, and can be analyzed through the percolation concept, but whatever the analyze, such network provides very specific behavior. For small stress, i.e. within the linear stress-strain domain, and mainly when the matrix is soft, the reinforcement is most of the time higher than for micronic fillers, and the difference can be attributed to the contribution of such a network. But the situation is often more complicated if the apparent volume fraction of stiff domains is increased by a volume of immobilised macromolecules (interphase). It is thus difficult to determine the exact contribution of each of these two effects, (i) more or less flexible of fillers network, and (ii) increase of rigid phase volume fraction (immobilised interphase). This later contribution may play a large role for very small fillers, as the interphase volume may become large.

The existence of a filler network could be also at the origin of a specific behavior of semicrystalline polymer like polyamide reinforced by platelet fillers (nanoclay like montmorillonite). Here again, the stiffness of the composite material is much higher than expected with a few percent of fillers, and a recent hypothesis proposes that the fillers act as nucleation agent. The crystallites could grow more or less perpendicularly to the surface platelets, and link them together, especially if the process (like injection) has already oriented them parallel to each other.

On the other hand, the presence of such network is clearly evidenced under large deformation, especially in the case of rubbery matrix. It is well established that carbon black or silica as well, act as crosslinking nodes which increase drastically the stiffness of the rubber (particularly important for automotive application). This indicates that the fillers together with some macromolecular segments form flexible network, but also that the properties of this network strongly depend on the interfacial properties between fillers and macromolecules. These properties are at the origin of well-known behaviors in rubbery materials, like the Payne and the Mullins effects. They result in an energy loss under cyclic conditions for the

first one, and in non-recoverable deformations for the later.

Below their glass rubber transition temperature, for amorphous polymers, or between the glass rubber transition temperature and the melting temperature of semi-crystalline polymers, i.e. for rather stiff matrix, nanofillers here again act in a specific way. For reasons not so well established, nanocomposites often exhibit favorable behaviors, i.e., an increase of their rigidity, as expected from the above recalled arguments, but also a much larger ductility than for corresponding micronic composites. This ductility results mainly from both a plastic deformation induced by local stress concentration, and a distributed damage, consisting in cavitations, decohesion and probably local crack propagation. This propagation is limited by the average distance between fillers, and as for high impact polymers, typical distance are in the range of tens of nm. About the ultimate properties (rupture, tear), the situation is even more complicated. The already mentioned arguments for the behavior under high strain and ductility still apply, but the rupture itself and its propagation are not well understood.

One of the key point necessary to study more deeply the incidence of the various parameters already mentioned (size, shape, interfacial energy, topological distribution, etc.) should consist in processing model materials by just modifying one of these parameters. Unfortunately, it is impossible to produce fillers having the same chemical structure with different shapes (rod, platelet, sphere), or even with different size and identical surface properties. This results in various materials for which the behavior analysis requires to account for several parameters, and each conclusion must be announced with care. Moreover, all studies need the combination of several techniques, including microstructural observations at various scales, physico-chemical measurements for interfacial characterization, mechanical tests are very different scales and stress-strain ranges (from AFM to standard tests up to tear or rupture), and *in situ* mechanical tests (i.e. where observations are performed during the tests).

Concerning the modeling of nanocomposite behaviors, classical mean field approaches, which have been shown to work well for micronic composites, underestimate experimental modulus. The reason probably comes from the fact that such approaches do not account for interactions between fillers. As an alternative way, numerical calculations based on discrete descriptions of the heterogeneous medium seem to give solid basis for a good prediction of both elastic or viscoelastic behavior, but also for taking into account the material damage which occurs for large deformation. The drawback of such modeling technique is that it is extremely computer time consuming. The convenient solution should be a combination of both discrete description of as realistic as possible representative elementary volume, and its use as the basis for a mean field calculation. However, it seems difficult to account for percolation phenomenon as it involves a distribution of correlation length ranging from nanoscale up to

macroscopic scale. It is clear that the modeling of nanocomposite materials, able to predict their behavior as function of temperature and strain rate is one of the challenges to be wined for the next years.

Acknowledgments

The authors are very grateful to all the colleagues whose works, done during PhD studies, have been cited and sometimes reprinted in this review : Dr. E. Chabert, Dr. E. Reynaud, Dr. V. Favier, Dr. P. Hajji, Dr. M. Hidalgo, Dr. J. Ramier, Dr. M. Shaterzadeh, Dr. T. Prasse.

REFERENCES

- 1 S.A. Wainwright, W.D. Biggs, J.D. Currey, J.M. Gosline, Mechanical Deign in Organisms, Princeton University Press, New Jersey (1976)
- 2 R. A. Dikie, M. F. Cheung, S. Newman, J.Appl. Polym. Sci. 17, 65 (1973)
- 3 R. A. Dikie, J.Appl. Polym. Sci. 17, 45 (1973)
- 4 R. A. Dikie, M. F. Cheung, J.Appl. Polym. Sci. 17, 79 (1973)
- 5 E. Herve, A. Zaoui, Int. J. Engin. Sci. 31, 1, 1 (1993)
- 6 J. Perez, Physics and Mechanics of Amorphous polymer , Ed. A.A. Balkema, Rotterdam/Broohfield (1998)
- 7 P.G. De Gennes, Scaling concepts in polymer physics, Cornell Univeristy Press, Ithaca (1979)
- 8 L. R. G. Treloar, The physics of rubber elasticity, Clarendon press, Oxford (1976)
- 9 L. David, R. Quinson, C. Gauthier, J. Perez, Polymer Engineering and Science vol.37, N°10, 1633-1640 (1997)
- 10 C. Gauthier, J.M. Pelletier, L. David, J. Perez, G. Vigier, J. of Non Cryst. Sol. 274, 181(2000)
- 11 J.A. Roetling, Polymer 6, 311 (1965)
- 12 R.E. Robertson, J. Chem. Phys. 6, 3950 (1966)
- 13 A.S. Argon, Phil. Mag. 28, 839 (1973)
- 14 P.B. Bowden, S. Raha, Phil. Mag. 21, 149 (1975)
- 15 P.B. Bowden, S. Raha, J. Mater. Sci. 7, 52 (1972)
- 16 C. G'Sell, J.J; Jonas, J. Mat. Sci. 16, 19,56 (1981)
- 17 J.M. Lefebvre, B. Escaig, J. Mat. Sci. 20, 438 (1985)
- 18 J.M.C. Li and J.J. Gilman, J. Appl. Phys. 11, 42,48 (1970)

- 19 M.B.M.Mangion, J.Y.Cavaillé, J.Perez, *Phil. Mag.* 66, 773 (1992)
- 20 E. Van Der Giessen and P.D. Wu, *Mech. Res. Comm.* 19, 427 (1992).
- 21 E.M. Arruda, M.C. Boyce, *J. Mech. Phys. Solids* 41,389 (1993)
- 22 M. Mooney, *Phil. Trans. Of the Royal Society A*240, 459 (1948).
- 23 R.W. Ogden, *Proc. Roy. Soc. Of London A*328, 567 (1972)
- 24 T.L.Smith, J.E.Frederick, *J. Appl. Phys.* 36, 2996 (1965)
- 25 A. Peterlin, *J. Mat. Sci.* Vol.6, 490 (1971)
- 26 I.M. Ward, *J. Mater. Sci.* Vol.6, 1397 (1971)
- 27 P.B. Bowden, R.J. Young, *J. Mat. Sci.* Vol.9, 2034 (1974)
- 28 J.M. Haudin, *Plastic Deformation of amorphous and semi-crystalline materials*, Ed. B. Escaig&C. G'ssell, Les Ulis (France), Les Editions de Physique (1982)
- 29 L. Lin, A.S. Argon, *J. Mat. Sci.*, Vol.29, 294-323 (1994)
- 30 J.M. Shultz, "Polymer Materials Science" Prentice Hall Inc. (1974)
- 31 M.J. Wang, S. Wolff, *Carbon Black*, 2nd Edition, Donnet, Bansel and Wang, Dekker (1993)
- 32 W.A. Ladd, W.B. Wiegand, *Rubber Age* 57,299 (1945)
- 33 H. Barthel, *Coll. And Surf. A: Physicochemical and Engeneering aspects* 101, 217 (1995)
- 34 A. Damour D. Salvetat, *Ann. Chim. Phys. Ser.* 21,376 (1847)
- 35 M. Zanetti, G. Camino, R. Thomann, R. Mulhaupt, *Polymer* 42,4501 (2001)
- 36 U. Hoffman, K. Endell, D. Wilm, *Z. Krist.* 86, 340 (1933)
- 37 K.A. Carrado, *Appl. Clay. Sci.* 17,1,1 (2000)
- 38 S. Van Es, *Polymer - Clay Nanocomposites : the Importance of particle dimensions*, PhD Thesis, Technische Universiteit Delft (2001)
- 39 D. Maldas, B.V. Kokta, *Trends Polym.* , 1, 174-148 (1993)
- 40 P. Flodin, P. Zadorecki, "Composite systems from natural and synthetic polymers" L. Salmen, A. de Ruvo, J.C. Seferis, E.B. Stark Eds., Elsevier Science Publishers, pp59-83 (1986)
- 41 S. Yano, S. Hirose, H. Hatakeyama *J. Appl. Polym. Sci.* , 40, 657 (1990)
- 42 S. Varghese, B. Kuriakose, S. Thomas, *J. Appl. Polym. Sci.* , 53, 1051 (1994)
- 43 J.F. Sassi , *Etude ultrastructurale de l'acétylation de la cellulose : application à la préparation de nanocomposites*, P.H.D Thesis, Grenoble (1995)
- 44 V. Favier , *Etude de nouveaux matériaux composites obtenus à partir de latex filmogènes et de whiskers de cellulose : effets de percolation mécanique*, P.H.D Thesis, INPG, Grenoble (1995)
- 45 V. Favier, R. Dendievel, G. Canova, J.Y.Cavaillé, P. Gilormini, *Acta Mater.* 45, 4, 1557 (1997)

- 46 S. Ijima, Nature 354, 56 (1991)
- 47 T. Ebbesen, Carbon nanotubes: Preparation and properties , CRC Press, Boca Raton, Florida (1997)
- 48 E. Dujardin, T. W. Ebbesen, A. Krishnan, P. N. Yianilos, M. M. J. Treacy, Physical Review B 58, 20, 1401 (1998)
- 49 E.T. Thostenson, Z. Ren, T.W. Chou, Composites Science and Technology, 61, 13, 1899 (2001)
- 50 M.F. Yu, B. S. Files, S. Arepalli, R. S. Ruoff, Phys. Rev. Lett. 84, 5552 (2000).
- 51 P. Richard, T. Prasse, J.Y. Cavaille, L. Chazeau, C. Gauthier, Polymer, submitted (2002)
- 52 L.E. Nielsen, R.F. Landel, Mechanical properties of polymers and composites, 2nd edition, Marcel Dekker, (1994)
- 53 A. Einstein, Annalen der Physik 19, 289 (1906)
- 54 A. Okada, M. Kawasumi, A. Usuki, Y. Kojima, T. Kurauchi, O. Kamigaito, Mater. Res. Soc. Proc., 171, 45 (1990)
- 55 P. Hajji, L. David, J.F. Gerard, J.P. Pascault, G. Vigier, J. Polym. Sci., part B : Polym. Phys., 37, 3172 (1999)
- 56 T.J. Pinnavaia, G.W. Beall, eds, Polymer-Clay Nanocomposites, Wiley, Chichester (2000)
- 57 J.R. Harbour, M.J. Walzak, W. Limburg, J. Yanus, Carbon, 24, p725 (1986)
- 58 C. Bonini, L. Heux, J.Y. Cavaillé, proc. MRS Meeting, San Fransisco, April (2002)
- 59 J.C. Daniel, Macromol. Chem Symp. 10/11, 359 (1985)
- 60 J. Y. Cavaillé, R. Vassoille, G. Thollet, L. Rios and C. Pichot, Colloid. Polym. Sci. 269, 248 (1991)
- 61 L. Rios, M. Hidalgo, J. Y. Cavaillé, J. Guillot, A. Guyot, C. Pichot, Colloid Polym. Sci. 269, 812 (1991)
- 62 M. Hidalgo, J. Y. Cavaillé, J. Guillot, A. Guyot, C. Pichot, L. Rios., R. Vassoile, Colloid Polym. Sci. 270, 1208 (1992)
- 63 E.P. Giannelis R. Krishnamoorti, E. Manias, Ad. Polym. Sci. vol 138, 107 (1999)
- 64 P.C. LeBaron, Z. Wang , T. J. Pinnavaia, Aplied Clay Science 15, Issues 1-2, 11 (1999)
- 65 M. Alexandre, P. Dubois, Materials Science and Engineering: Reports, 28, Issues 1-2, 15, p 1-63, (2000)
- 66 A. Okada, M. Kawasumi, A. Usuki, Y. Kojima, T. Kurauchi, O. Kamigaito, Mater. Res. Soc. Proc., 171, 45-54 (1990)
- 67 E.P. Giannelis , Adv. Mater., 8 , n°1 p.29-35, (1996)

- 68 T.J. Pinnavaia, G.W. Beall, Polymer-Clay Nanocomposites, Wiley, Chichester (2000)
- 69 G. Lagaly, Appl. Clay. Sci., 15, 1-9, (1999)
- 70 A. Guinier, Théorie et technique de la radiocristallographie, Dunod Paris, (1964)
- 71 R.H. Atalla, D.L. VanderHart, Science, 223,283-284,(1984)
- 72 T. Labour, C. Gauthier, R. Seguela, G. Vigier, Y. Bomal, G. Orange, Polymer 42, 7127 (2001)
- 73 K. Varlot, E. Reynaud, M.H. Kloppfer, G. Vigier, J. Varlet, J. Polym. Sci., Part B, Vol.39, 1360, (2001)
- 74 O. Glatter, Small Angle X-ray Scattering, Ed. O. Glatter and O. Kratky, Academic Press, (1982)
- 75 J.T. Koberstein, B. Morra, R.S. Stein, J. Appl. Crys., Vol.13, 34-43, (1980)
- 76 G. Porod, Small Angle X-ray Scattering, Ed. O. Glatter and O. Kratky, Academic Press, (1982)
- 77 O. Glatter, J. Appl. Crys., Vol.10, 415-421, (1977)
- 78 C. Mai, F. Livet, G. Vigier, Scripta Met., Vol.15, 1179-1184, (1981)
- 79 R. Baur, V. Gerold, Acta Metall., Vol.12, 1449-1457, (1964)
- 80 P.W. Schmidt, « Modern aspects of Small-Angle Scattering », Ed. H. Brumberger, Kluwer Academic Publishers, (1985)
- 81 L.C. Sawyer, D.T. Grubb, « Polymer Microscopy », Ed. Chapman&Hall, 2nd edition, (1997)
- 82 C. Maertens, G. Raes, C. Vandermeerssche, Proc. of the Stockholm Conf., 292, (1956)
- 83 G. Binnig, C.F. Quate and C. Gerber, Phys. Rev. Lett., 12,930 (1986)
- 84 S.M. Hues, R.J. Colton, E.Meyer, H-J. Güntherodt, MRS Bulletin,41-48, January (1993)
- 85 D. Stauffer, Introduction to percolation theory, Taylor and Francis, London and Philadelphia (1985)
- 86 I. Balberg, N. Binenbaum and N. Wagner, Phys. Rev. Letters 52, 1465 (1984)
- 87 I. Balberg and N. Binenbaum, Phys. Rev B. 28, 3799 (1983)
- 88 V.Favier, G. R. Canova, J. Y. Cavailié, H. Chanzy, A. Dufresne, C. Gauthier, Polym. Adv. Technol. 6, 351 (1995)
- 89 K. Tashiro, M. Kobayashi, Polymer 32, 1516 (1991)
- 90 T. Nishino, K. Takano, K. Nakamae, J. Polym. Sci. : B Polym. Phys. 33, 1647 (1995)
- 91 V.Favier, H. Chanzy, J.Y. Cavailié, Macromolecules 28, 6365 (1995)
- 92 Z. Hashin, J. App. Mech. 50, 481 (1983)

- 93 D. Hull, an introduction to composite materials, Cambridge, Cambridge University Press (1981)
- 94 S.Ahmed, F. R. Jones, *J. Mater. Sci.* 25, 4933 (1990)
- 95 J. Aboudi, *Mechanics of Composite Materials: a unified Micromechanical Approach.*, Elsevier, Amsterdam (1991)
- 96 Z. Hashin, *Int. J. Solids Structures* 6, 797 (1970)
- 97 R. M. Christensen, *Theory of viscoelasticity*, Academic Press, New York (1971)
- 98 J. M. Whitney and R. L. McCullough, *Micromechanical Materials Modeling*, Technomic Publishing Co., Lancaster USA (1990)
- 99 J. D. Eshelby, *Proc. Roy. Soc. London A* 241, 376 (1957)
- 100 Z. Hashin, S. J. Shtrickman, *Mech. Phys. Solids* 11, 127 (1963)
- 101 Z. Hashin, *J. Appl. Mech.* 29, 143 (1962)
- 102 E. H. Kerner, *Proc. Phys. Soc. London* 69 B, 808 (1956)
- 103 R. M. Christensen, K. H. Lo, *J. Mech. Phys. Solids* 27, 315 (1979)
- 104 G. K. Batchelor., J.T. Green, *J. Fluid. Mech.* 56, 375 (1972)
- 105 H. -S. Chen, A. Acrivos, *Int. J. Solids. Structures* 14, 331 (1978)
- 106 E. Guth, *J. Appl. Mech.* 16, 20-25 (1945)
- 107 N. A. Frankel, A. Acrivos, *Chem. Eng. Sci.* 22, 847, (1967)
- 108 A. V. Hershey A.V., *J. Appl. Mech.* 21, 236 (1954)
- 109 E. Kroner, *Z. Phys.* 151, 504, (1958)
- 110 R. Hill, *J. Mech. Phys. Solids* 13, 213, (1965)
- 111 B. Budiansky, *J. Mech. Phys. Solids* 13,223 (1965)
- 112 T. Mori, K. Tanaka, *Acta Metall. Mater.* 21, 597 (1973)
- 113 E. Reynaud, T. Jouen, C. Gauthier, G. Vigier, J. Varlet, *Polymer* 42,8759 (2001)
- 114 Z. Hashin, B. W. Rosen, *J. Appl. Mech.* 31, 223, (1964)
- 115 W. B. Russel, *Z. Angewandte Math. Phys.* 24, 581 (1973)
- 116 G. P. Tandon, G. J. Weng, *Polymer Composites* 5,4, 327 (1984)
- 117 S. W. Tsai, N. J. Pagano, Technomic Publishing Co., N.Y., 233 (1968)
- 118 J. C. Halpin, J. L. Kardos, *J. Appl. Phys.* 43, 2235 (1972)
- 119 J. C. Halpin, S. W. Tsai, AFML-TR 67, 423 (1969)
- 120 J. E. Ashton , J. C. Halpin, P. H. Petit, *Primer on Composite Materials: Analysis*, Technomic Publishing Co., Chapter 5 (1969).
- 121 L. Chazeau, M. Paillet, J.Y. Cavailié, *J. Polym Sci. Polym. Phys*, 37 2151(1999)
- 122 A. I. Medalia, *J. Colloid Interface Sci.* 32, 115 (1970)
- 123 J. G. Broodnyan, *Trans. Soc. Rheology* 3, 61 (1959)

- 124 M. Shaterzadeh-Yazdi, Etude et Modélisation physique et mécanique du comportement viscoélastique et plastique de composites particuliers à matrice polymère, Thèse de doctorat, INSA-Lyon (1997)
- 125 P. Hajji, C. Gauhtier, proc. Eurofillers'99, Lyon, France, sept (1999)
- 126 N. Alberola, P. Mele, Polym. Compos. 17,5,751 (1996)
- 127 P. Hajji, J. Y. Cavallé, V. Favier, C. Gauthier, G. Vigier, Polymer Composites 17, 612 (1996)
- 128 C. Stoltz, A. Zaoui, C. R. Acad. Sci., Paris, Série II, 312, 143 (1991)
- 129 M. Bornert, E. Hervé, C. Stoltz, A. Zaoui, Appl. Mech. Rev. 47, 1, Pt.2 (1994)
- 130 M. Bornert, C. Stoltz, A. Zaoui, J. Mech. Phys. Solids 44, 307 (1996)
- 131 Burr A., Monnerie L., Polymer 41, 5909, (2000)
- 132 P. S. Theocaris, G. C. Papanicolaou, Colloid Polym. Sci. 258, 9, 1044 (1980)
- 133 G. C. Papanicolaou, P. S. Theocaris, G. D. Spathis, Colloid and Polym. Sci. 258, 11, 1231 (1980)
- 134 E. Sideredis, J. Appl. Polym. Sci., 48, 243 (1993)
- 135 H. Eklind, F. Maurer, Polymer, 37, n° 13, 2641-2651 (1996)
- 136 M. Takayanagi, S. Uemura, S. Minami, J. Polym. Sci : C5, 113 (1964)
- 137 N. Ouali, J. -Y. Cavallé, J. Perez, Plast., Rubber and Compos. Process. Appl. 16, 55 (1991)
- 138 J. -F. Gouyet, Physique et Structures fractales, Masson, 234 (1992)
- 139 P. G. De Gennes, J. Phys. Lett. (Paris) 37, L1.(1976)
- 140 A. Jagota, G. W. Scherer, J. Amer. Ceram. Soc. 78, 521 (1995)
- 141 A. Okada and A. Usuki, Mater.Sci. Eng. C3,109 (1995)
- 142 K. Masenelli-Varlot, E. Reynaud, G. Vigier, J. Varlet, J.of Polym. Sci., part B : polym. Phys., 40,2072 (2002)
- 143 X. Korman, Doctoral thesis, Lulea University of Technology, 2001 : 14
- 144 D.A. Brune, J. Bicerano, Polym. 43 , 369 (2002)
- 145 G.M. Kim, D.H. Lee, B. Hoffmann, J. Kressler, G. Stoppelmann, Polymer,42,3,1095 (2001)
- 146 H. Shi, T. Lan, T.J. Pinnaviaa, Chem. Mater. , 8, 1584 (1996)
- 147 Y.Kojima, A. Usuki, M. Kawasumi, A. Okada, Y. Fukushima, T. Kurauchi, O. Kamigaito, J.Mater. Res., 8, 1185 (1993)
- 148 A. Usuki, A. Koiwai, Y.Kojima, M. Kawasumi, A. Okada, T. Kurauchi, O. Kamigaito, J.Appl. Polym. Sci., 55, 119 (1995)
- 149 J.M. Gloaguen, JM Lefebvre proc. 11th Int. Conf. On Deformation, Yield and Fracture of polymers, Cambridge, Ap. (2000)

- 150 D.B. Zax, D.K. Yang, R.A. Santhos, H. Hegemann, E.P. Giannelis, E. Manias, J. Chem. Physics, 112(6), 2945 (2000)
- 151 P. Gilormini, C.R. Acad. Sci. Série II, 320 115 (1995)
- 152 M. Bornert, T. Bretheau, P. Gilormini, in 'Homogénéisation en mécanique des matériaux 2, Comportements non linéaires et problèmes ouverts', Hermes Science Publications, Paris (2001)
- 153 A. Zaoui and R. Masson, in IUTAM Symposium on Transformations Problems in Composite and Active Materials (Cairo, 1997), edited by E. Dvorak, G.J. Bahei-El-Din and Y.A. Dordrecht, Kluwer Academic Publishers, (1998)
- 154 M. Berveiller, A. Zaoui, J. Mech. Phys. Solids, 26 213 (1979)
- 155 L. Chazeau, J.Y. Cavaille, P. Terech, Polymer, 40,19,5333 (1999)
- 156 L. Chazeau, J. Perez, J.Y. Cavaille, J. Polym Sci. Polym. Phys, 38, 383 (2000)
- 157 P. Terech, L Chazeau., J.Y. Cavaille, Macromolecules 32, 1872 (1999)
- 158 Sumita M, Shizuma T, Miyasaka K, Ishikawa K. J. Macromol. Sci.- Phys.; B22(4), 601 (1983)
- 159 D.C. Lee, L.W. Jang, J.Appl. Polym.Sci., 61, 1117 (1996)
- 160 J. Massam, T.J. Pinnavaia, Mat. Res. Soc. Symp. Proc., 520, 223 (1998)
- 161 N. Hasega, M. Kawasumi, M. Kato, A. Usuki, A. Okada, J. Appl. Polym. Sci., 66, 1781 (1997)
- 162 J.P. Harcup and AF Yee, proc. 11th Int. Conf. On Deformation, Yields and Fracture of polymers, Cambridge, Ap. (2000)
- 163 AS. Zerda, AJ Lesser, J. Polym. Sci., B Polym. Phys., 39 (11) : 1137 (2001)
- 164 T. Lan, T.J. Pinnavaia, Chem. Mater. 6, 2216 (1994)
- 165 Z. Wang, T.J. Pinnavaia, Chem. Mater, 10, 3769 (1998)
- 166 K. Arai, J. D. Ferry, Rubber Chem. Technol. 59, 605, (1986)
- 167 C. M. Roland, J. Rheol, 34, 1, (1990)
- 168 L. Chazeau, J. D. Brown, L. C. Yanyo, and S. S. Sternstein, Polymer Composites 21, 2, 202 (2000)
- 169 Y. Isono, J. D. Ferry, Rubber Chem. Technol. 57, 925, (1984).
- 170 A. R. Payne, J. Appl. Polym. Sci. 19,57 (1962)
- 171 Zaborski M., A kormalska, L. Slusarski, J.B. Donnet, SILICA 2001, Conf. Proc., Mulhouse, 3 - 6 September, (2001)
- 172 J. Ramier, C. Gauthier, L. Chazeau, L. Ladouce, L. David, R. Vassoille, Euro-Fillers 01 Conference, Lodz, Poland, 9-12 July (2001)
- 173 G. Krauss, J. Appl. Polym. Sci. : Appl. Polym. Symp. 39, 75 (1984)

- 174 W. M. Hess, *Rubber Chem. Technol.* 64, 386 (1991)
- 175 T. M. Aminabhavi, P. E. Cassidy, *Rubber Chem. Technol.* 63, 451 (1991)
- 176 D. J. Jeffrey, A. Acrivos, *AIChE J.* 22, 3 (1976)
- 177 I. M. Krieger, T. J. A. Dougherty, *Trans. Soc. Rheol.* 3, 137 (1959)
- 178 M. M. Cross, *J. Colloid Interface Sci.* 33, 1 (1970)
- 179 A.R. Payne, *J. Colloid Sci.* 19, 744 (1964)
- 180 M. J. Wang, *Rubber Chem. Technol.* 72, 4, 657 (1999)
- 181 J. M. Funt, *Rubber Chem. Technol.* 61, 842 (1988)
- 182 P. G. Maier, D. Goritz, *Kautsch. Gummi Kunstst.* 49,1, 18 (1996)
- 183 A. Zhu, S. S. Sternstein, *Filled and nanocomposite polymer materials*, Res. Soc. Proc. 661 Warrendale, Pa, Ed. A. Khakatani, R. P. Hjelm, M. Gerspacher, R. Krishnamoorti (2001)
- 184 N. K. Dutta, N. R., Choudhury, B. Haidar, A. Vidal, J. B. Donnet, L. Delmotte, J. M. Chezeau, *Polymer* 35, 20, 4293, (1994)
- 185 S. Asai, H. Kaneki, M. Sumita, K. Miyasaka, *J. Appl. Poly. Sci.* 43, 7, 1253, (1991)
- 186 A. Vidal, B. Haidar, L. Delmotte, 8th Int. Sem. on Elastomers, 8-11 May, le Mans, Conf Proc. (2001). See also A. Vidal and B. Haidar, *elastomery* 3, 4, 28 (1999)
- 187 W. Y. Lin, F. D. Blum, *J. Am. Chem. Soc.* 123, 2032 (2001)
- 188 B. Meissner, *J. Appl. Polym. Sci.* 18, 2483 (1974)
- 189 J. P. Cohen-Addad, C. Roby, M. Sauviat, *Polymer* 26, 8, 1231 (1985)
- 190 B. Haidar, H. Salah Deradji, A. Vidal, E. Papirer, in "Polymers and surface: a versatile combination" (Ed. H. Hommel) *Research signpost*, Trivandrum p. 103. (1998)
- 191 D. Brown, S. Marceau, P. Mele, N. Alberola, *SILICA 2001*, Conf. Proc., Mulhouse, 3 - 6 September, (2001)
- 192 M. I. Aranguren, E. Mora, V. J. De Groot, C. W. Macosko, *J. of rheology* 36, 1165 (1992)
- 193 J. L. Leblanc, *J. Appl. Polym. Sci.* 78, 1541 (2000)
- 194 A. Lion, *Rubber Chem. Technol.* 72, 410 (1998)
- 195 C. M. Roland, *J. Rheol.* 34, 1 (1990)
- 196 G. Huber, T. A. Vilgis, G. Heinrich, *J. Phys. Condens. Matter* 8, L409 (1996)
- 197 T. A. Witten, M. Rubinstein, R. H. Colby, *J. Phys II France* 3, 367, (1993)
- 198 R. H. Schuster, M. Klüppel, J. Schramm, G. Heinrich, paper 56, ACS Rubber Division Meeting, Indianapolis, USA (May 1998).
- 199 M. Gerspacher, C. P. O'Farrel, H. H. Yang, C. Tricot, *Rubber World* 214, 27 (1996)
- 200 C. Gauthier, E. Reynaud, K. Mourier, R. Vassoille, L. Ladouce, *Rubber Chem. Technol.*, submitted.

- 201 W. L. Holt, Rubber Chem. Technol. 5, 79 (1932)
- 202 L. Mullins, J. Rubber Research 16, 275 (1947)
- 203 F. Bueche, J. Appl. Polym. Sci. 4, 10, 107 (1960)
- 204 L. Mullins, N. R. Tobin, Rubber Chem. Technol. 30, 555 (1957)
- 205 F. Bueche, J. Appl. Polym. Sci. 4, 10, 107 (1960)
- 206 F. Bueche, J. Appl. Polym. Sci. 5,15,271 (1961)
- 207 E. M. Dannenberg, Rubber Chem. Technol. 48, 410 (1975)
- 208 B. B. Boonstra, in Reinforcement of elastomers, G. Kraus Ed., Interscience Publishers, John Wiley and Sons, NY p529-561 (1965)
- 209 M.P. Wagner, Rubber Chem. And Technol. 49 , 703 (1976)
- 210 H. Ambacher, M. Strauss, H. G. Kilian, S. Wolff, Kautsch. Gummi Kunstst. 12, 1111 (1991)
- 211 J. Oberdisse, G. Carrot, F. Boué, SILICA 2001, Conf. Proc., Mulhouse, 3 - 6 September (2001)
- 212 A. Lapra, Ph-D Thesis, Université Pierre et Marie Curie, Paris IV (1999)
- 213 A. V. Tobolsky, Structure and Properties of Polymers, Interscience, NY (1965)
- 214 G. Chagnon, E. Verron, L. Gornet, G. Marckmann, P. Charrier, P. Fort , 8th int seminar on elastomers, Le Mans, conf. Proceeding, 34, may (2001)
- 215 E. G. Septanika, L. J. Ernst, Mechanics of materials 30, 253 (1998)
- 216 J. A. C. Hardwood, A. R. Payne, J. Appl. Polym. Sci. 12, 889 (1968)
- 217 F. Bueche, J. C. Halpin, J. Appl. Polym. Sci 35, 36 (1964)

FIGURES

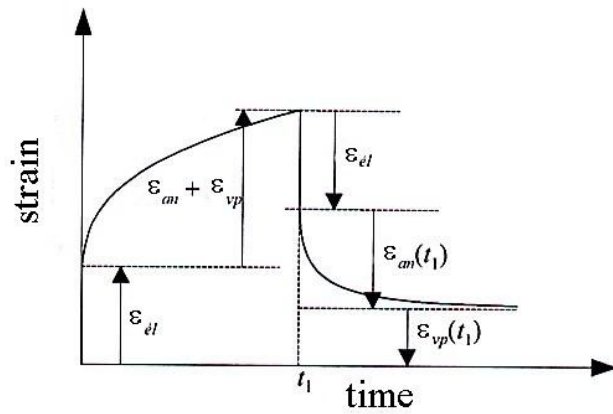


Figure I.1 Various components of deformation during a creep experiment

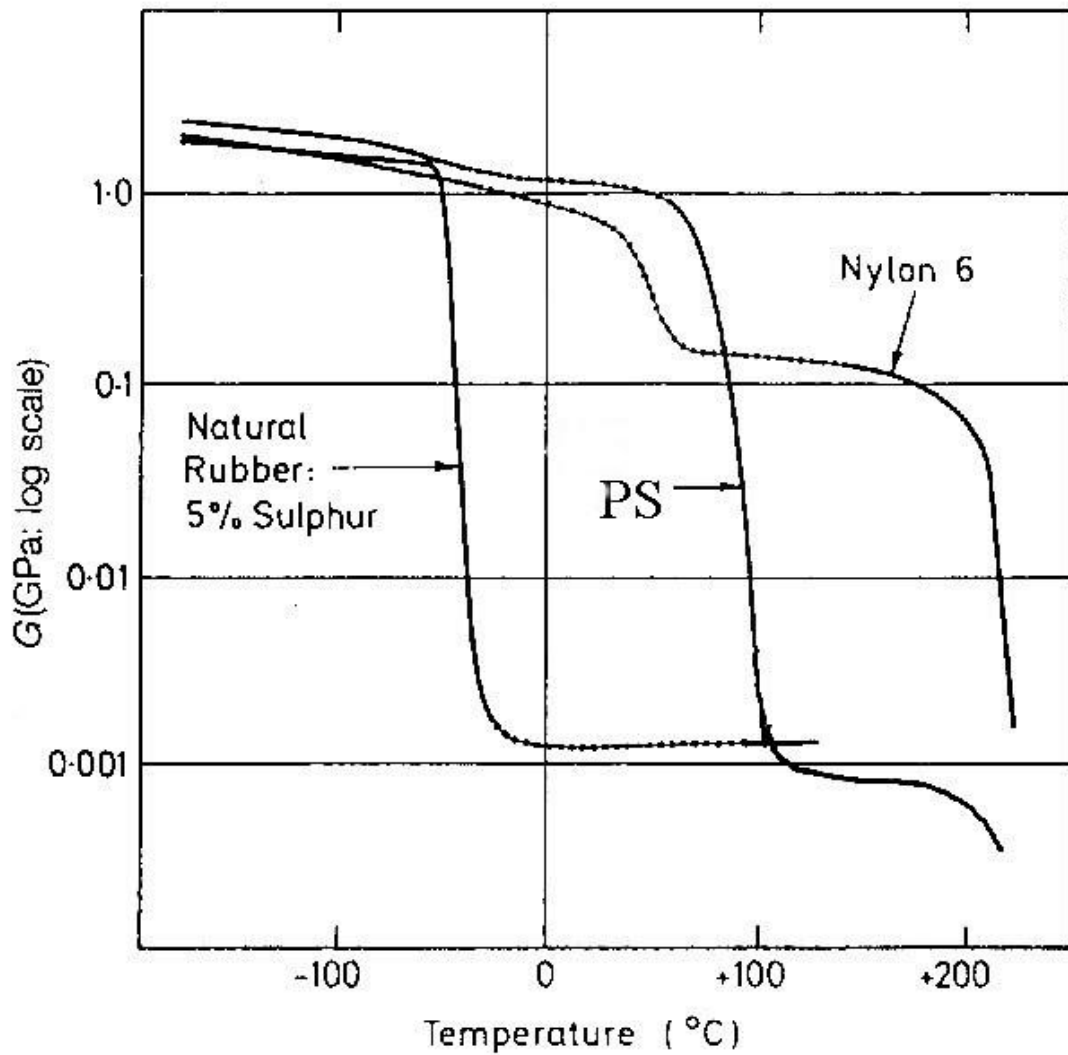


Figure I-2: Evolution of the real part of the dynamic modulus (G') and the loss factor ($\tan\Phi = G'/G''$) as a function of temperature.

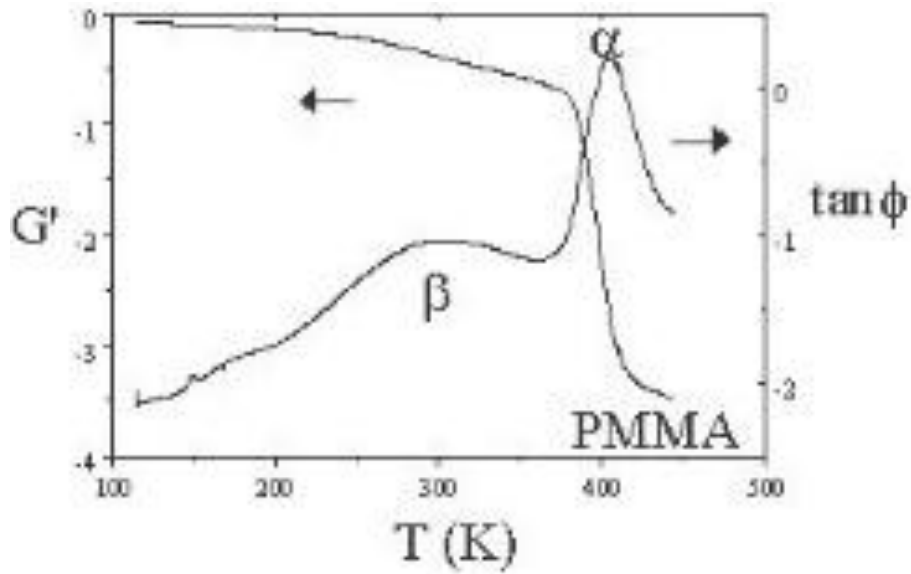


Figure I-3: Evolution of the storage modulus as a function of temperature for different types of polymers.

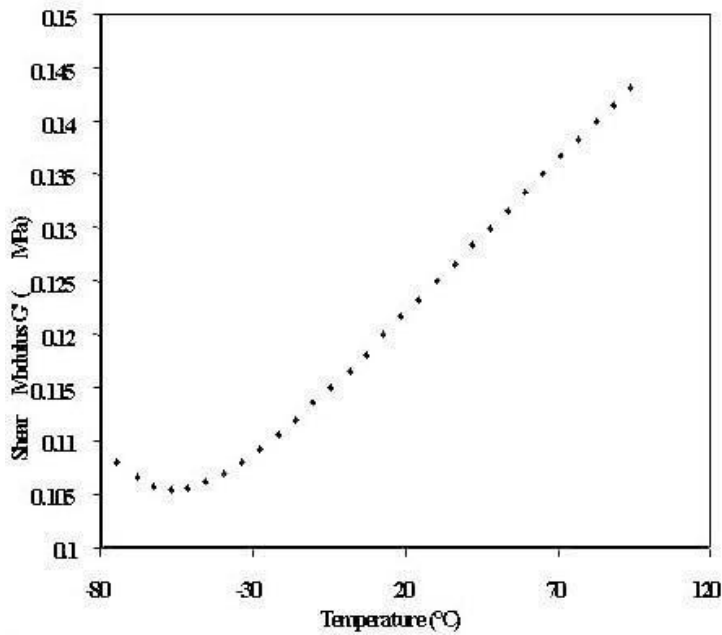


Figure I-4: Typical behavior of unfilled elastomer : increase of the storage modulus with temperature measured by dynamic mechanical analysis.

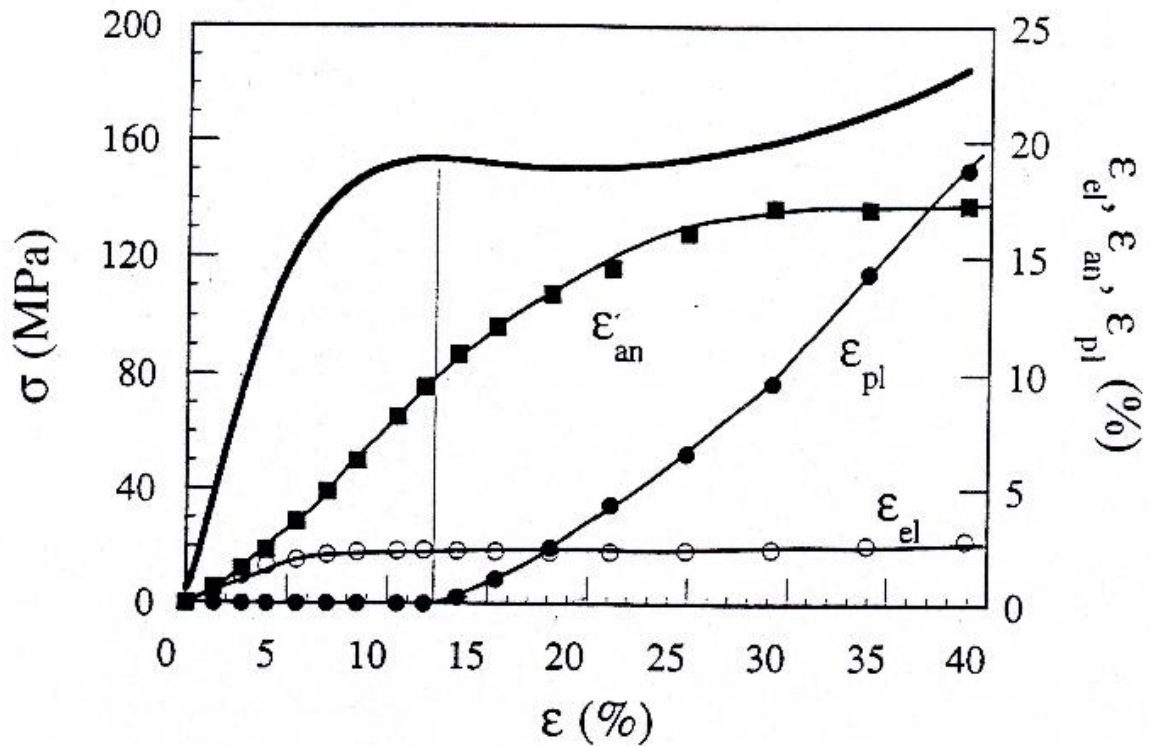


Figure I.5: Variation of ϵ_{el} , ϵ_{an} and ϵ_{pl} during deformation of PMMA under plane strain compression, $T_{def}=20^{\circ}C$, $d\epsilon/dt=2.10^{-3}s^{-1}$. Reprinted from Ref. 9 : L. David, R. Quinson, C. Gauthier and J. Perez, Polym.Eng. Sci. , 37,10 (1997) with permission from the Society of Plastics Engineers.

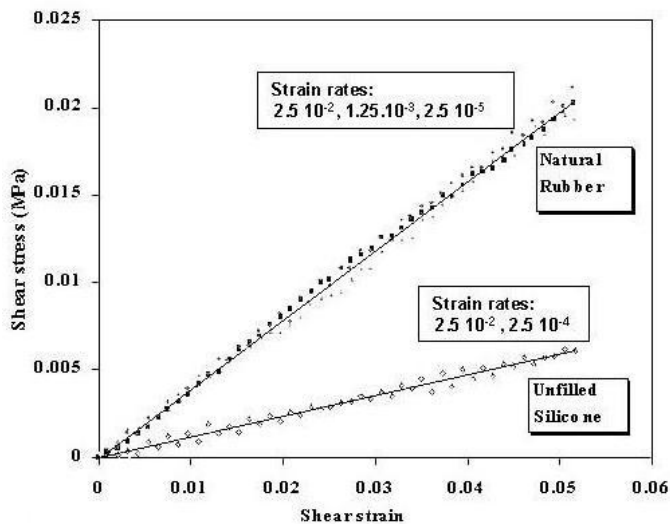


Figure I-6: Quasi linearity observed in shear test in a low deformation range. Reprinted from Ref. 168 L. Chazeau, J.D. Brown, L.C. Yanyo and S.S. Sternstein, Polymer composites 21, 2, 202 (2000) with permission from Society of Plastics Engineers.

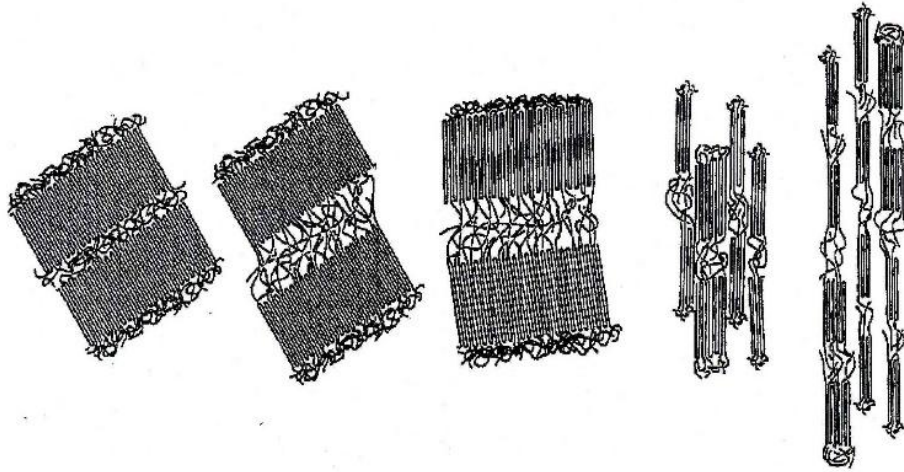


Figure I.7: Transformation of a lamellar structure into a fibrillar structure. Reprinted from. Ref. 30 : "Polymer Materials Science", J. Schultz, 1974, Prentice Hall Inc., Englewood Cliffs, New Jersey, 551p with permission from publishers.

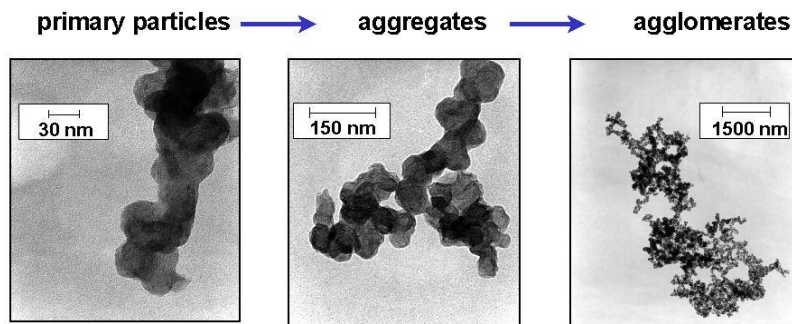


Figure II-1-1 : T.E.M. micrography of primary carbon black particles coalesced into primary aggregates and further associated in agglomerates.

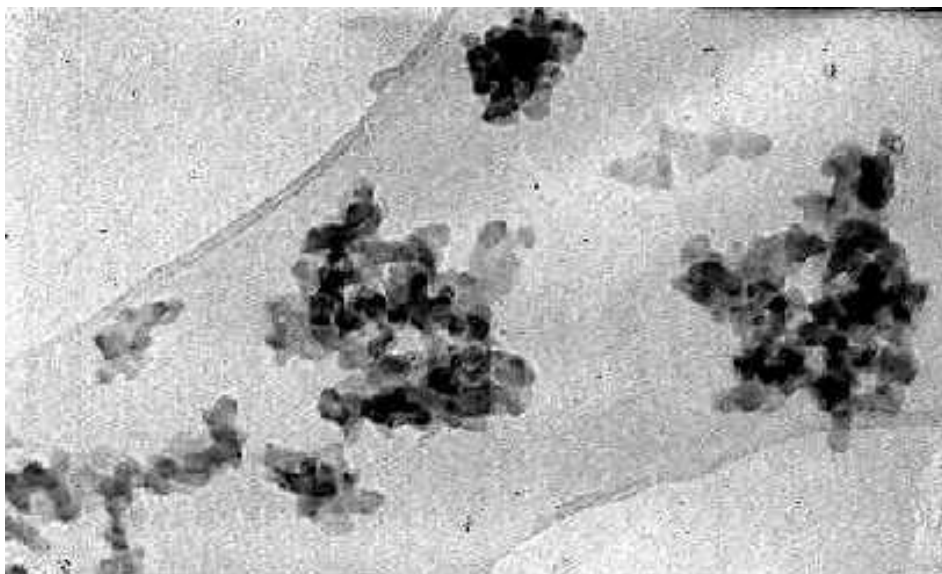


Figure II-1-2 : Silica particles observed by transmission electron microscopy.

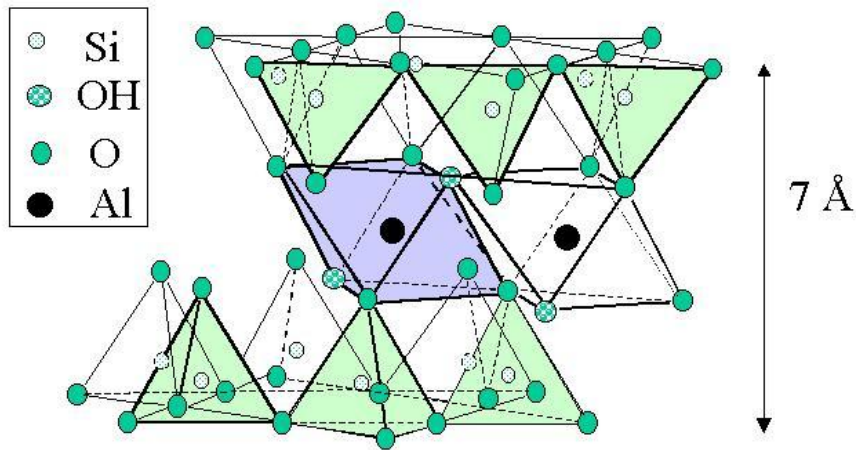


Figure II-2-1 : Crystalline structure of a 2:1 layered silicate. Reprinted from ref. 38 : M. A. Van Es, Ph-D thesis, Technische Universiteit Delft, 2001, 215p. with permission from the author.

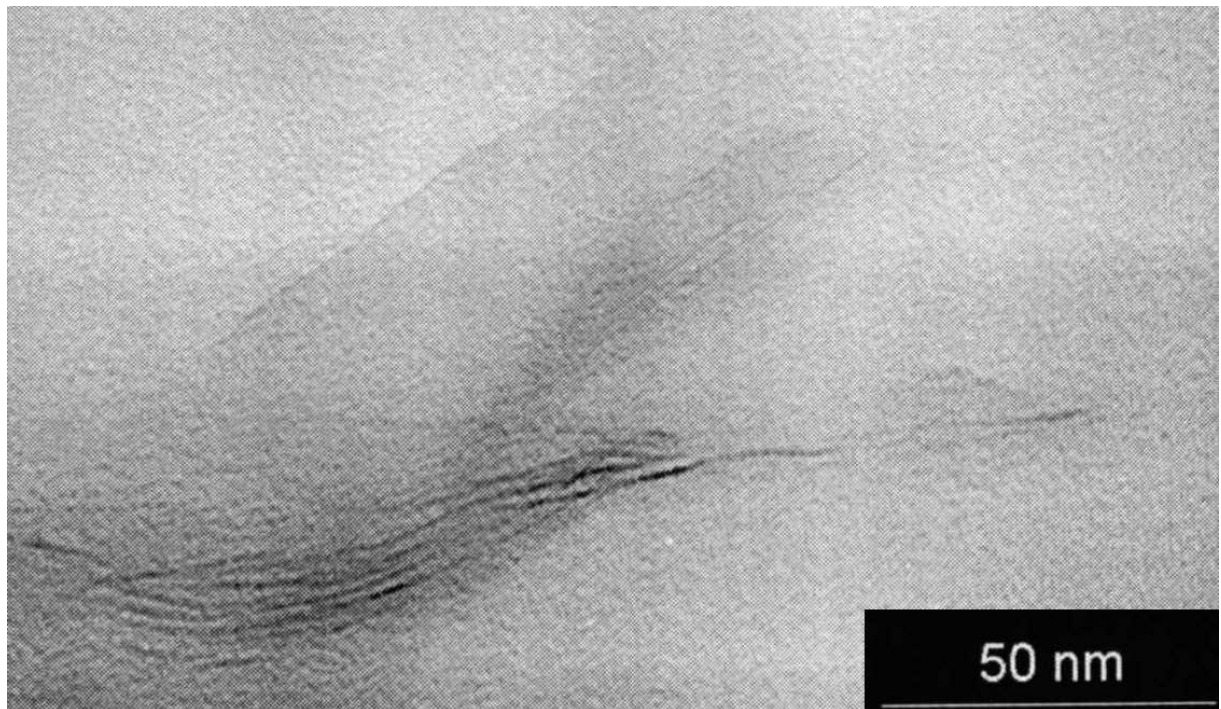


Figure II-2-2 : Montmorillonite platelets in nylon matrix observed by transmission electron microscopy.

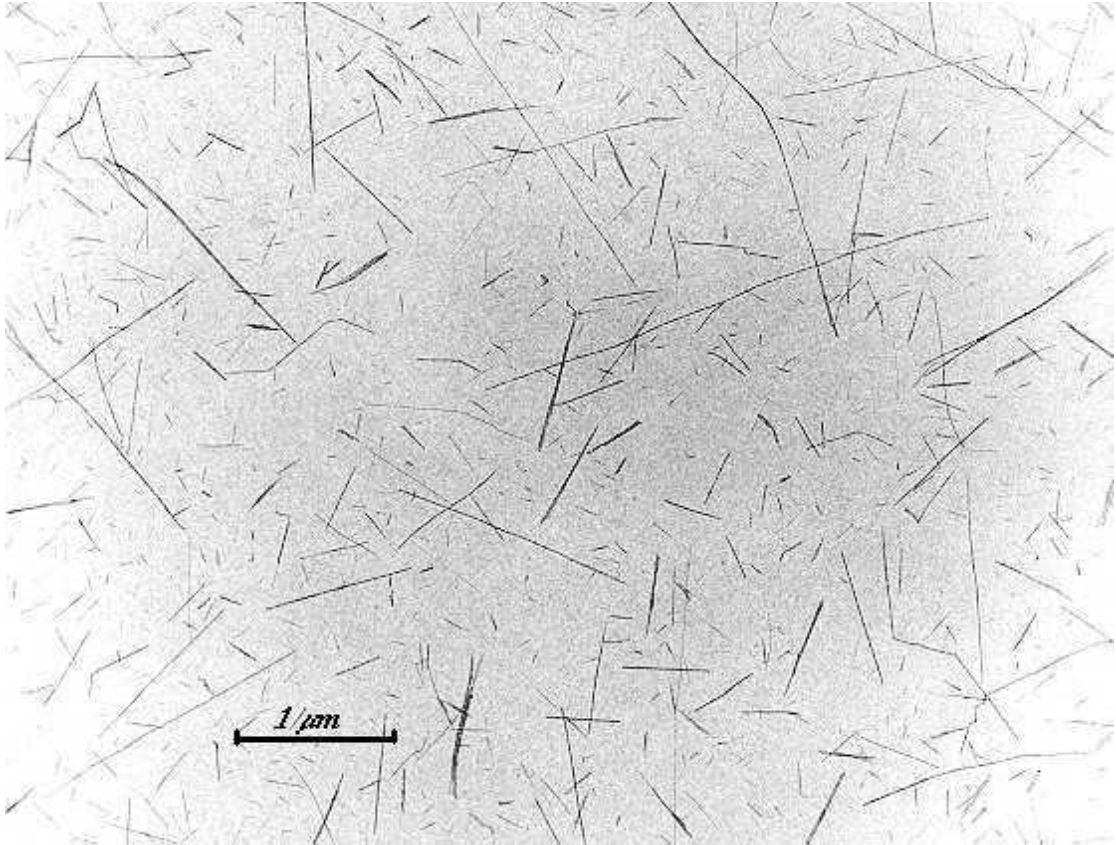


Figure II-3-1: Cellulose whiskers from tunicates observed by transmission electron microscopy.

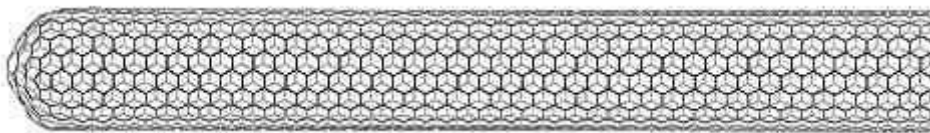


Figure II-3-2 : Crystallographic structure of a single wall carbon nanotube (SWNT).

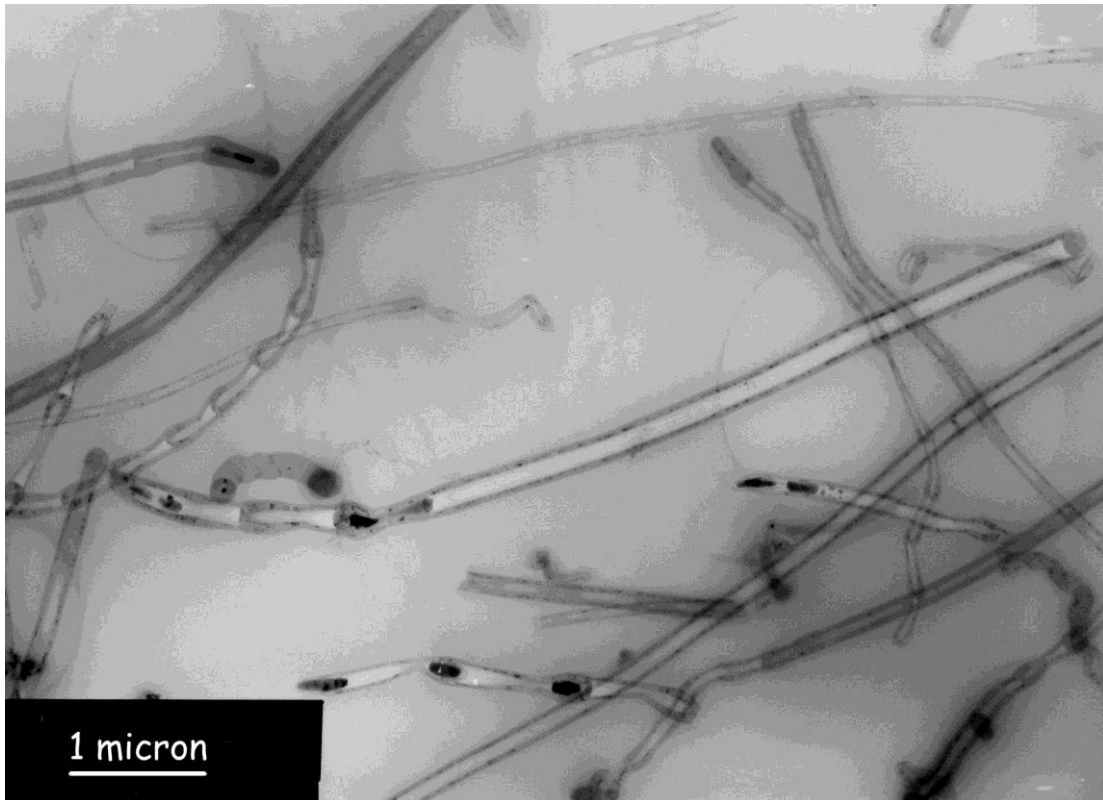


Figure II-3-3: T.E.M. micrograph of nanofibres (pyrograph III from Applied Science Inc.).

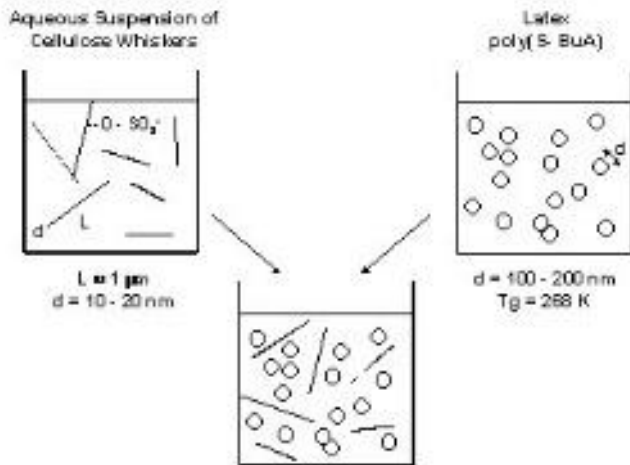


Figure III-1-1 : Schematic protocol leading to the dispersion of cellulose whiskers within a thermoplastic matrix using latex and whisker aqueous suspension. The acid hydrolysis (by H_2SO_4) leads to the grafting of negative ions, which ensure the colloidal stability. The composite material is obtained by water evaporation.

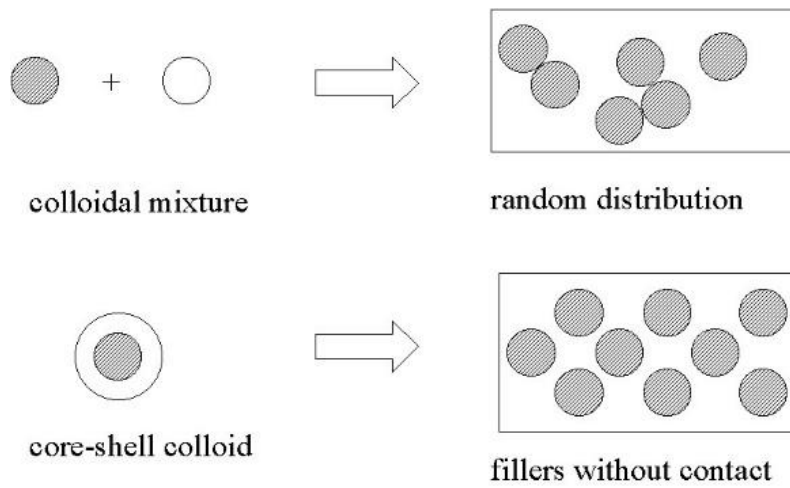


Figure. III-1-2: Schematic representation of the expected morphology of films resulting from the coalescence of mixture of a soft latex (white domains) with a stiff latex (hatched)

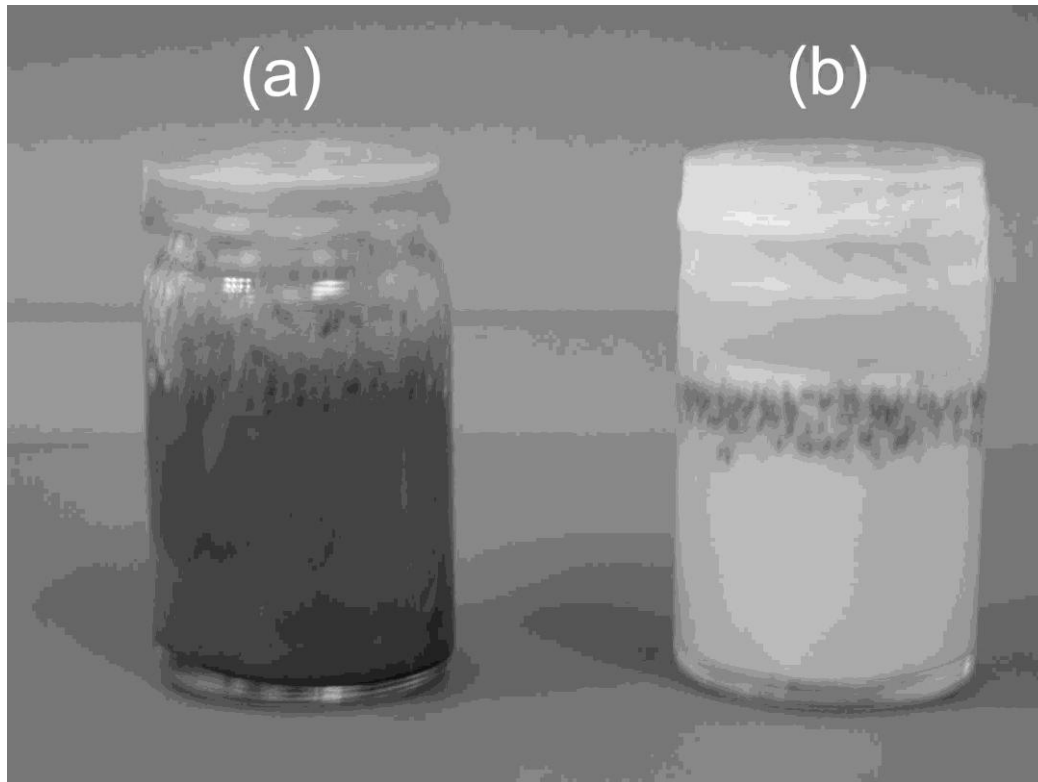


Figure III-1-3 : SB-latex with 1 wt% CNF with (A) and without (B) addition of a surfactant.

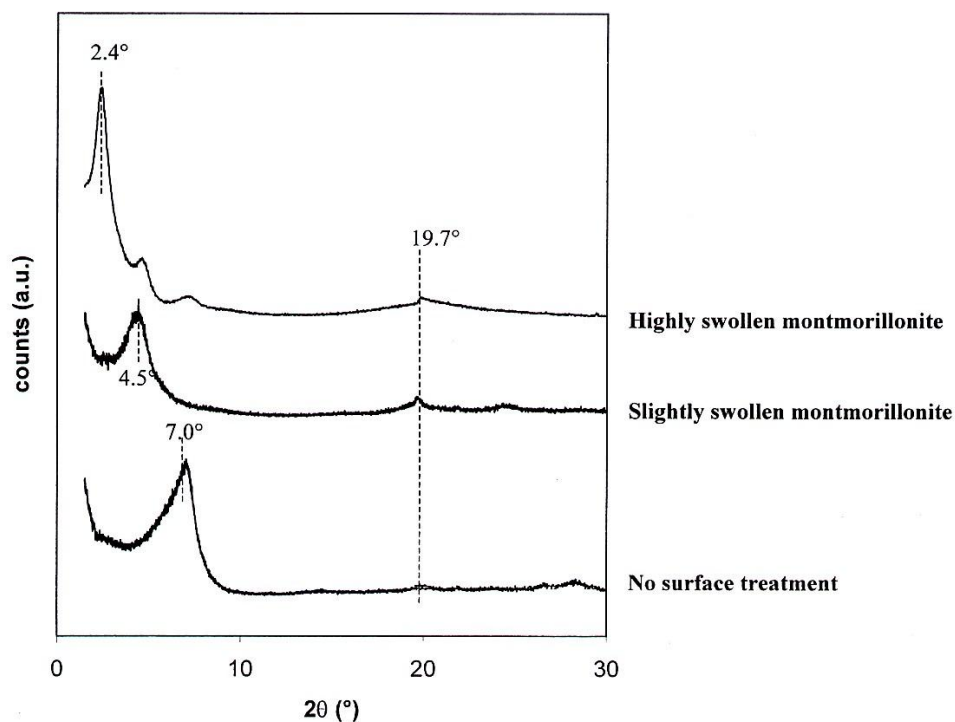


Figure III-2-1: WAXS spectra of non-treated, slightly swollen and highly swollen montmorillonite. The shift of the peak at 7° (non-treated montmorillonite) toward low angles is characteristic of an increase of interlaminar d_{001} during the swelling procedure. Reprinted from ref. 73 : K. Varlot, E. Reynaud, M.H. Kloppfler, G. Vigier, J. Varlet, J. Polym. Sci. PtB: Polym. Phys., 39, 1360 (2001), with permission from John Wiley&Sons, Inc.

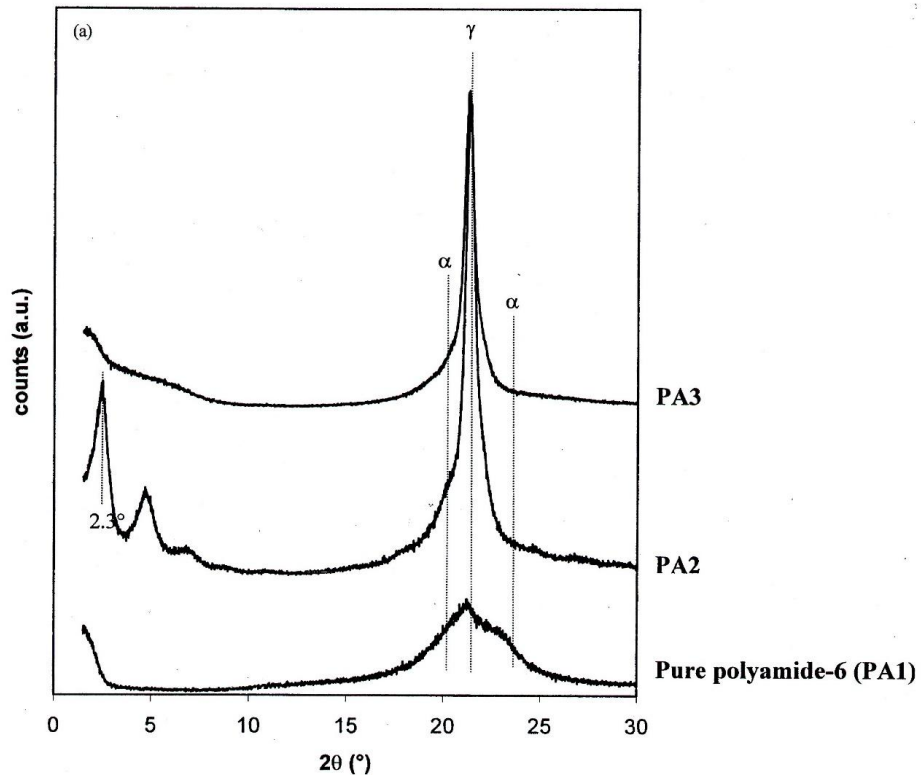


Figure III-2-2: WAXS spectra of exfoliated (PA3) and intercalated (PA2) montmorillonite in PA-6. Reprinted from ref. 73 : K. Varlot, E. Reynaud, M.H. Kloppfer, G. Vigier, J. Varlet, *J. Polym. Sci. PtB: Polym. Phys.*, 39, 1360 (2001), with permission from John Wiley&Sons, Inc.

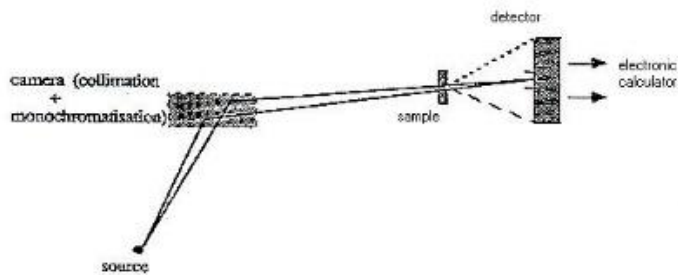


Figure III-2-3: Small Angle Scattering set up.

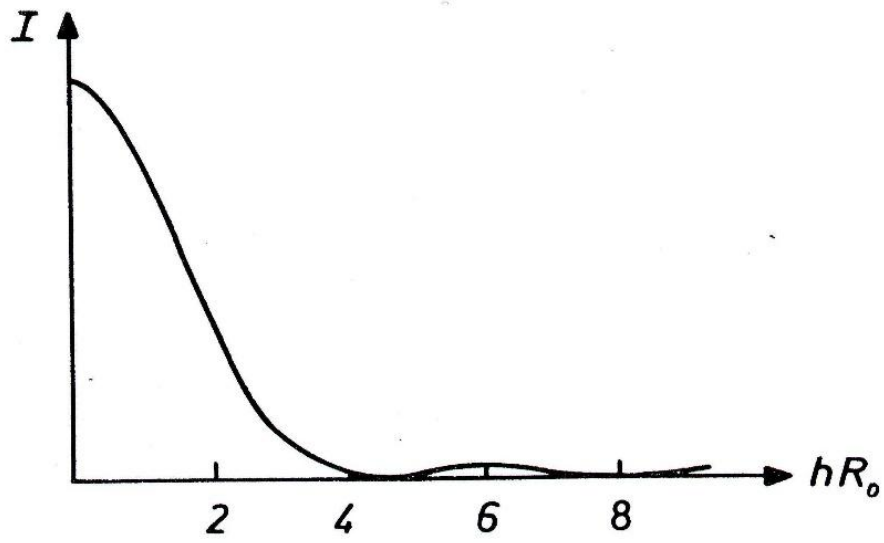


Figure III-2-4: Scattering intensity of a sphere

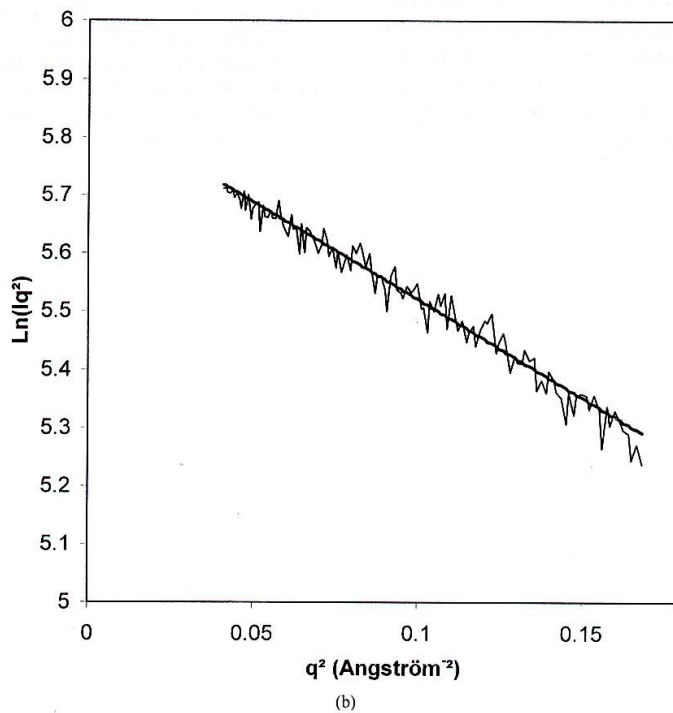
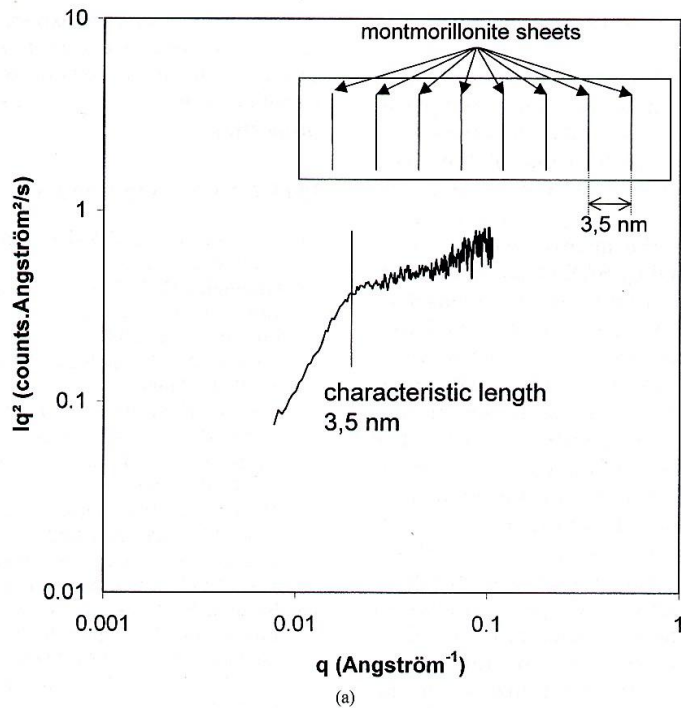


Figure III-2-5: Correlation bump (a) and Guinier Plot (b) of Polyamide-6 with exfoliated montmorillonite. A characteristic length of about 35 nm was deduced from the correlation bump. The guinier plot shows the length of the diffusing unit (6-7 Angstrom). The Guinier. Reprinted from ref. 73 K. Varlot, E. Reynaud, M.H. Kloppfler, G. Vigier, J. Varlet, J. Polym. Sci. PtB: Polym. Phys., 39, 1360 (2001), with permission from John Wiley&Sons, Inc.

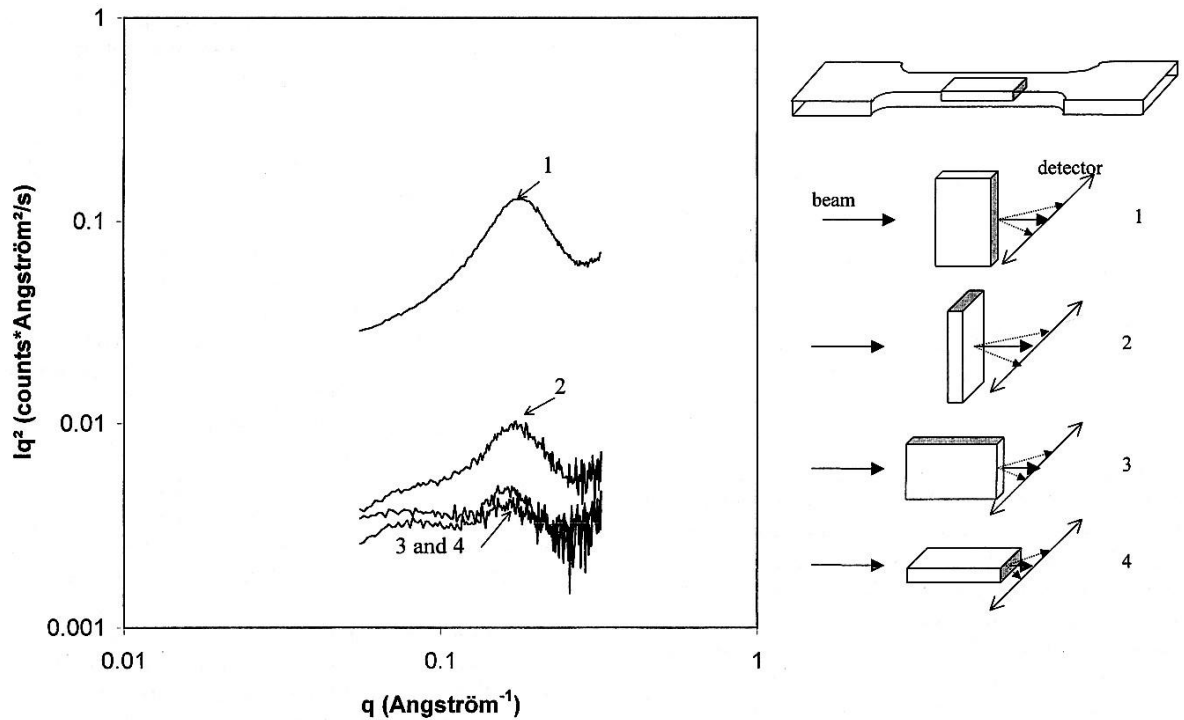


Figure III-2-6 : SAXS Spectra of intercalated montmorillonite in Polyamide-6. The intensity of the correlation peak shows that montmorillonite is preferentially oriented in the injection direction. Reprinted from ref. 73 K. Varlot, E. Reynaud, M.H. Kloppfler, G. Vigier, J. Varlet, J. Polym. Sci. PtB: Polym. Phys., 39, 1360 (2001), with permission from John Wiley&Sons, Inc.

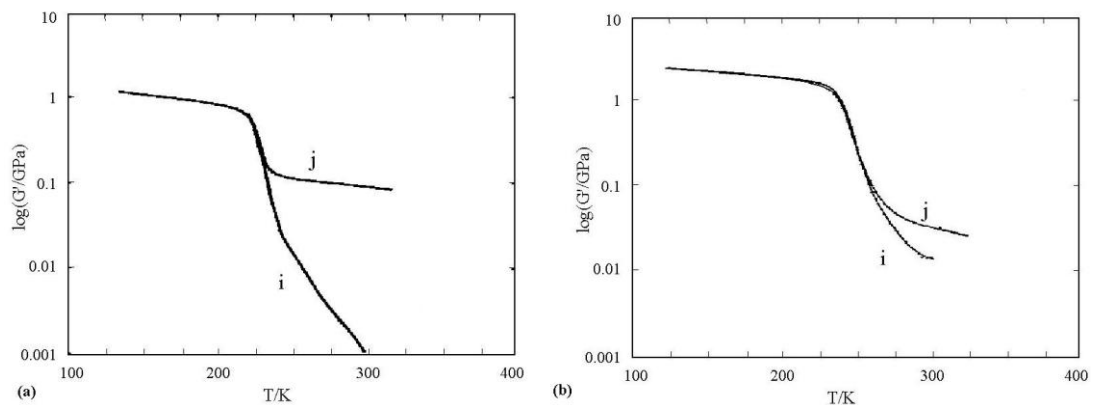


Figure IV-1-1: Dynamic mechanical behavior of film obtained after water evaporation of an aqueous suspension: a), of a mixture of PS and P(BuA) latexes, (i) as obtained, (j) after a heat treatment at 140°C (i.e. $T_g + 40^\circ\text{C}$); b) of an aqueous suspension of core (PS) shell (PBuA) particles (i) as obtained, and (j) after a heat treatment at 140°C. After M. Hidalgo, Ph-D thesis, Université Claude Bernard Lyon I, (1992).

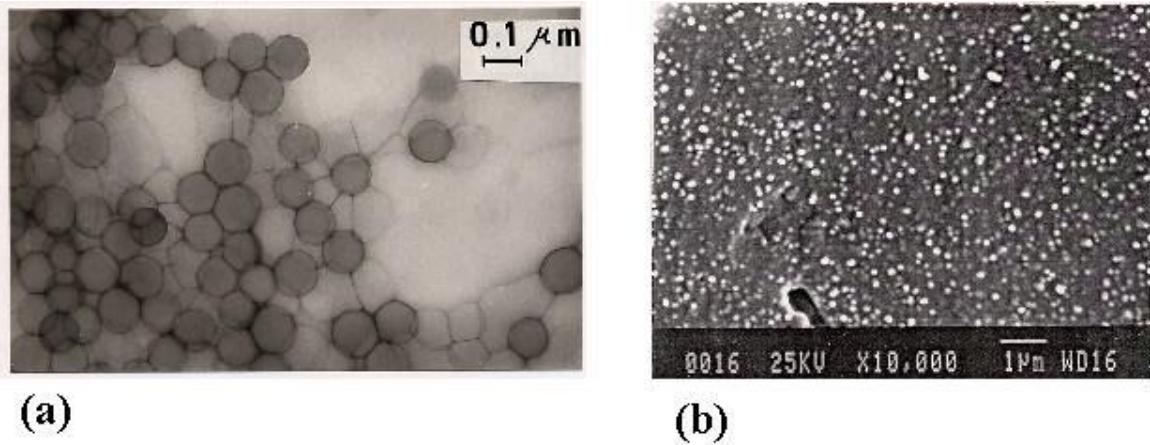


Figure IV-1-2: a) Transmission electron micrography obtained on a mixture of PS and PBuA latex particles deposited on a grid and dried; b) Scanning electron micrography performed on a fracture surface of a core (PS) shell (PBuA) film. White dots correspond to isolated PS domains (stiffer than the matrix). Reprinted from ref 60 : J.-Y. Cavail , R. Vassoille, G. Thollet, L. Rios, C. Pichot, Colloid Polym. Sci. 269 :248 (1991) with permission from Springer Verlag.

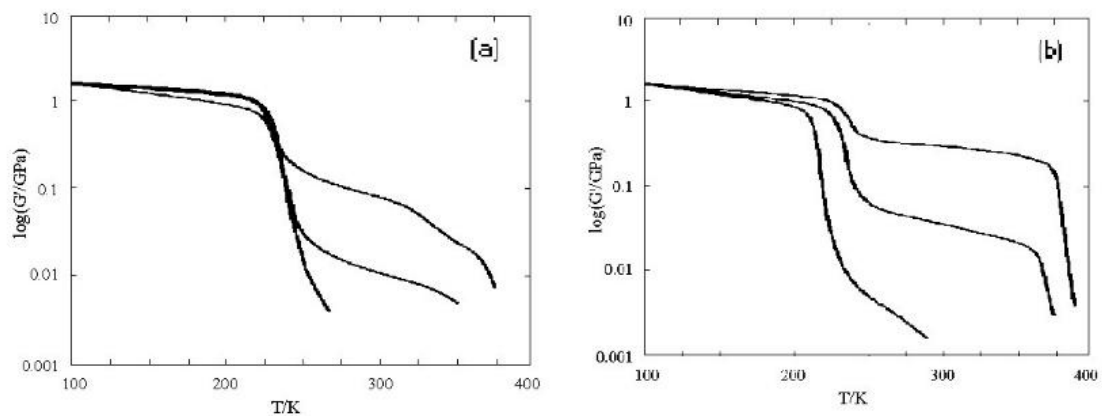


Figure IV-1-3: Dynamic mechanical behavior of films obtained after water evaporation of an aqueous suspension of a mixture of PS and PBuA latexes: a) before any heat treatment above the film forming temperature for 30 vol. %, 40 vol. % and 50 vol. % PS, b) after a heat treatment at 140°C (i.e. $T_g + 40^\circ\text{C}$). After M. Hidalgo, Ph-D thesis, Universit  Claude Bernard Lyon I, (1992).

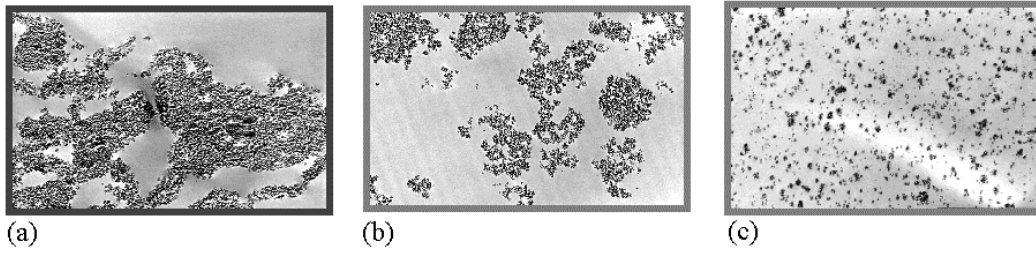


Figure IV-1-4: Transmission Electron Microscopy of silica filled PMMA made by a) ball-milling, b) dry-casting, c) and extrusion.). After E. Reynaud, Ph-D thesis, Université Claude Bernard Lyon I, (2000).

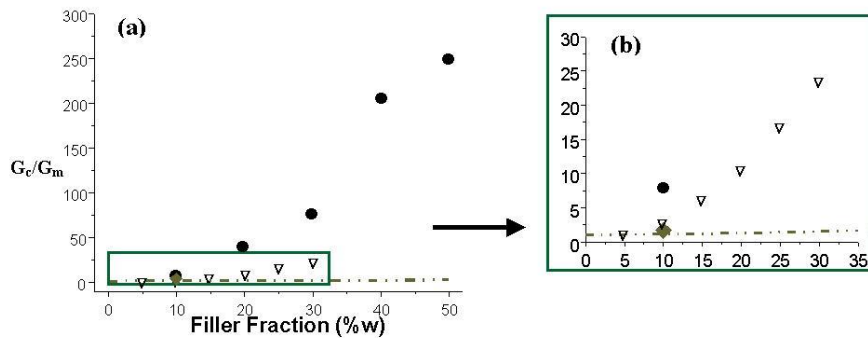


Figure IV-1-5: Storage modulus of silica filled PMMA in the rubbery domain ($T=1.03T_g$, $f=1\text{Hz}$). Composite made by ball-milling (λ), dry-casting (∇) and extrusion (\blacklozenge). Comparison with the 3-phase model (dotted line). After E. Reynaud, Ph-D thesis, Université Claude Bernard Lyon I, (2000).

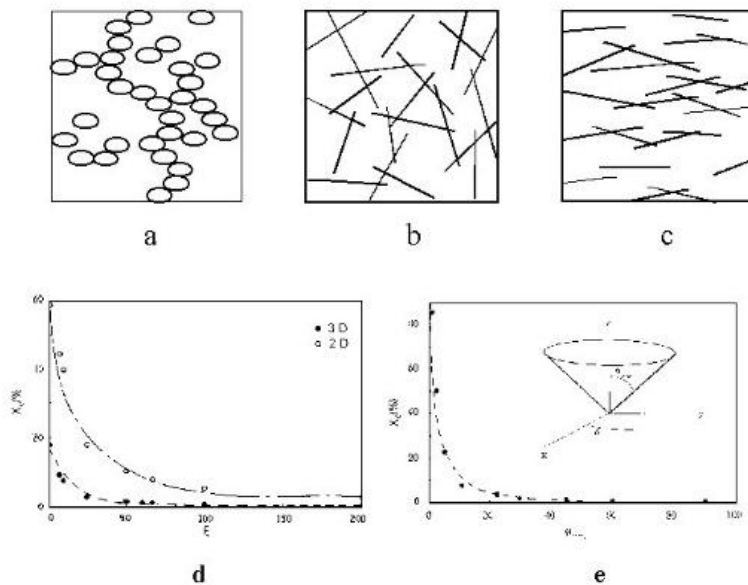


Figure IV-1-6: Effect of the shape and of the orientation of particles on the percolation threshold: a) shape factor ξ close to 1, b) $\xi \gg 1$ and random orientation, c) $\xi \gg 1$ and preferentially oriented in horizontal plane, d) percolation threshold versus ξ , e) idem versus orientation. After V. Favier, Ph-D thesis, Institut National Polytechnique de Grenoble, (1996).

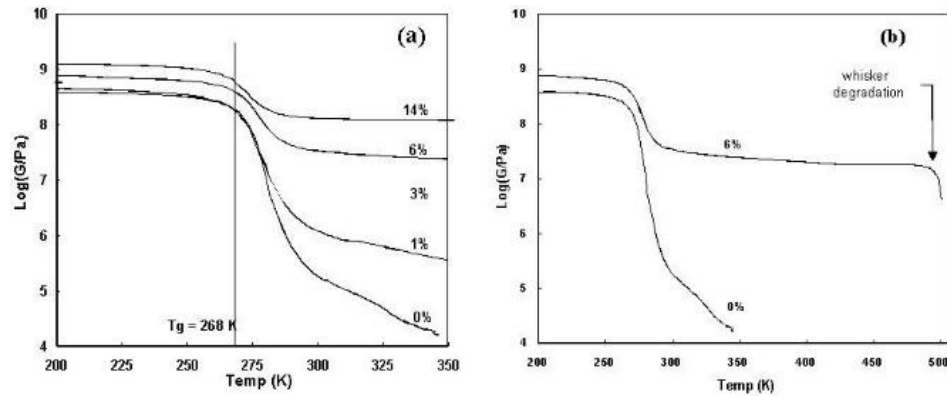


Figure IV-1-7: Linear viscoelastic behavior of cellulose whiskers / p(BuA-S) nanocomposites a) for various whisker contents (vol. %), b) for 6 vol. % in a larger temperature range. After V. Favier, Ph-D thesis, Institut National Polytechnique de Grenoble, (1996).

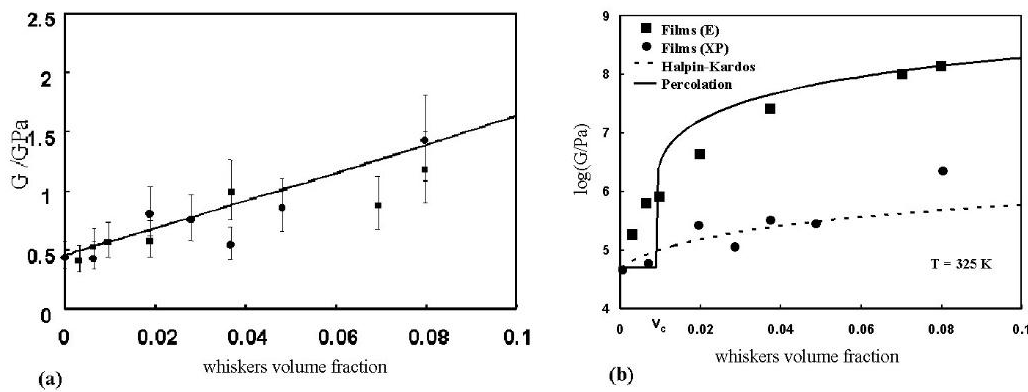


Figure IV-1-8: Shear modulus of nanocomposites obtained from styrene – butyl acrylate copolymer / cellulose whiskers, versus the whisker content; a) below T_g , $T=200$ K, dots corresponding to two types of process (dry casting (v), or extrusion and hot pressing (λ)). The full line corresponds to the Halpin Kardos equation; b) above T_g , $T=350$ K, for the same two processes. Full line corresponds to the Takayanagi model combined with percolation equation, dash line corresponds to a mean field type calculation. After V. Favier, Ph-D thesis, Institut National Polytechnique de Grenoble, (1996).

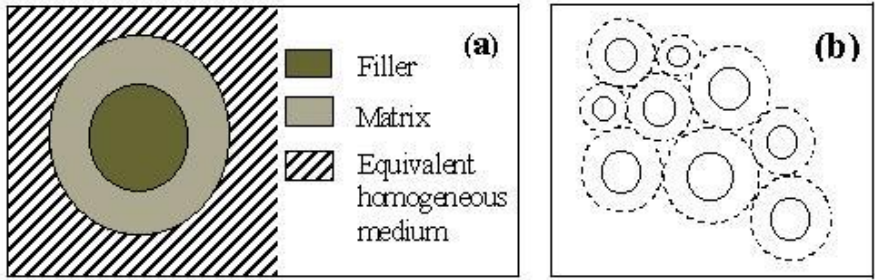


Figure IV-2-1: (a) 3-phase model or generalized self-consistent model, (b) Composite sphere model of Hashin.

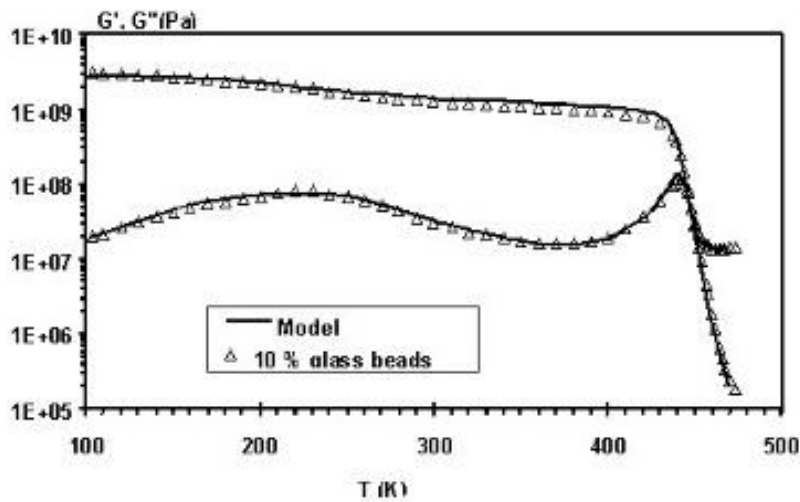
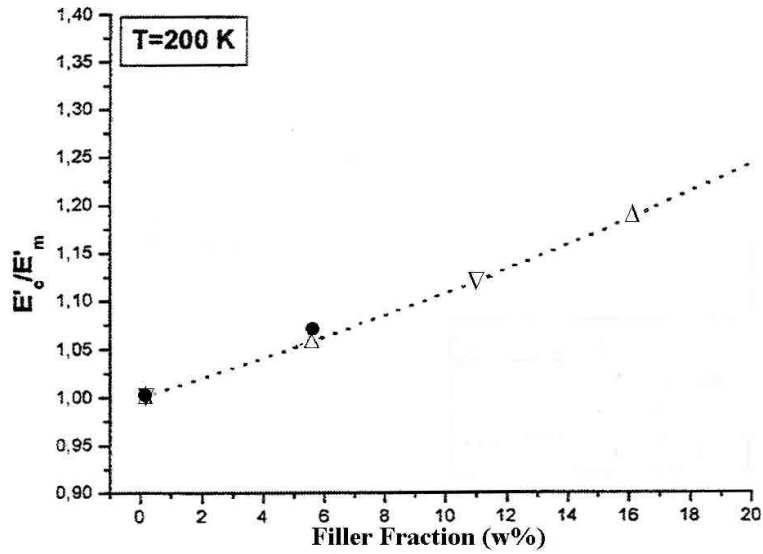
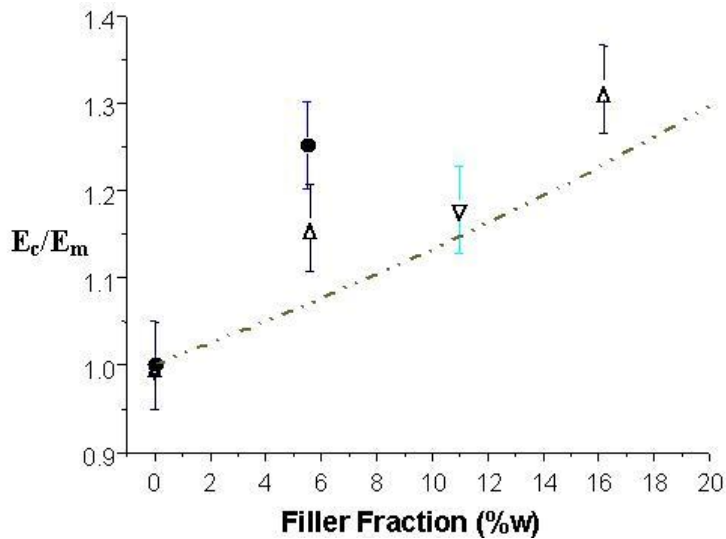


Figure IV-2-2: Experimental storage modulus for epoxy-glass beads composite ($\phi=10\%$ vol.) - Comparison with the 3 phase self-consistent model. After M. Shaterzadeh, Ph-D Thesis, Institut National des Sciences Appliquées, (1997).



a)

bàbbb



b)

Figure IV-2-3: Elastic modulus of silica filled PA6 ($f=1\text{Hz}$). Particle diameter of 17nm (λ), 30 nm (∇) and 80 nm (Δ). Comparison with theory (dotted line): (a) in the glassy domain and (b) in the rubbery domain. Reprinted from Ref. 113 , E . Reynaud, J. Jouen, C. Gauthier, C. Vigier, J. Varlot, Polymer,42, 8759 (2001) with permission from Elsevier.

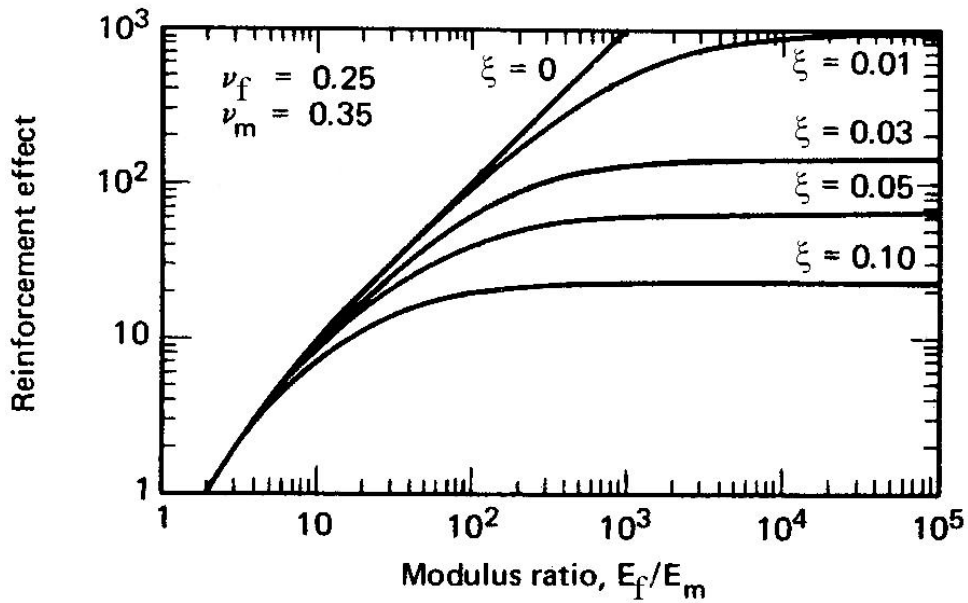


Fig IV-2-4: Influence of the Fiber length on the reinforcing factor A ($E_{11}/E_m=1+\phi A$, E_{11} being the longitudinal in plane modulus, E_m the matrix modulus and ϕ the filler volume fraction) as a function of the filler to matrix modulus ratio. After R.M. Christensen, Mechanics of Composite Materials Chichester, UK: Wiley, 348p. 1979.

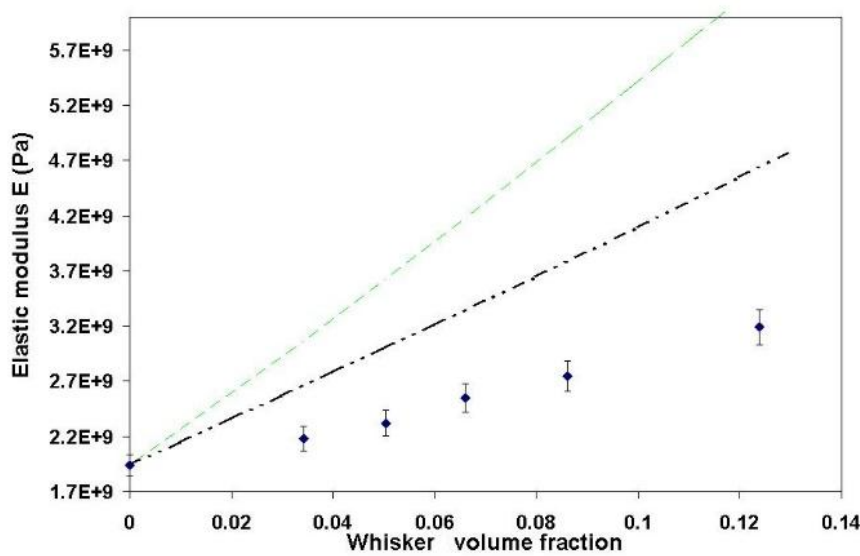


Figure IV-2-5: Elastic modulus of whisker filled plasticised PVC matrix (ν) in the glassy domain ($T=333$ K, $f=0.1$ Hz), comparison with Halpin Kardos model (---) and 3D average laminate model (- · · -)

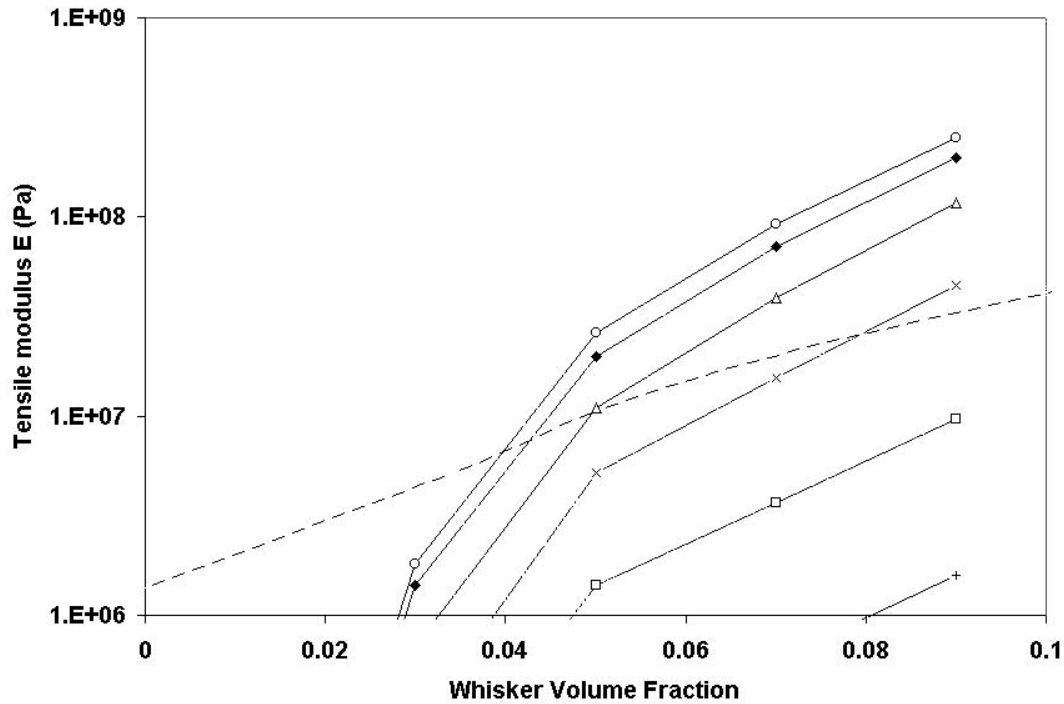


Figure IV-2-6: Experimental modulus of plasticised PVC filled with cellulose whiskers above T_g ($T=60^\circ\text{C}$) (dotted line) and comparison with theoretical modulus of a whisker network calculated by a discrete approach, with different link beam modulus: 1.5MPa (-+-), 15MPa (-□-), 150MPa (-x-), 1.5GPa (-Δ-), 15GPa (-◆-), 150GPa (-o-).

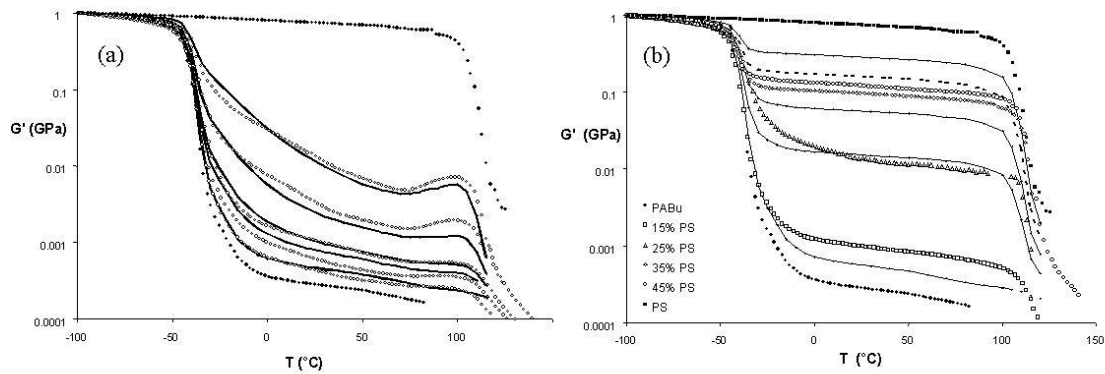
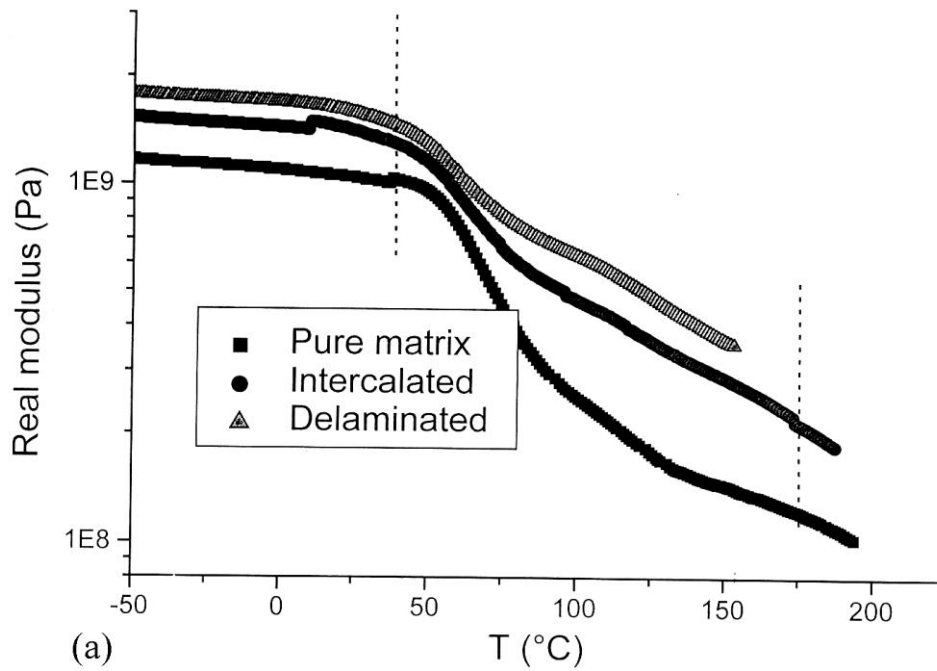
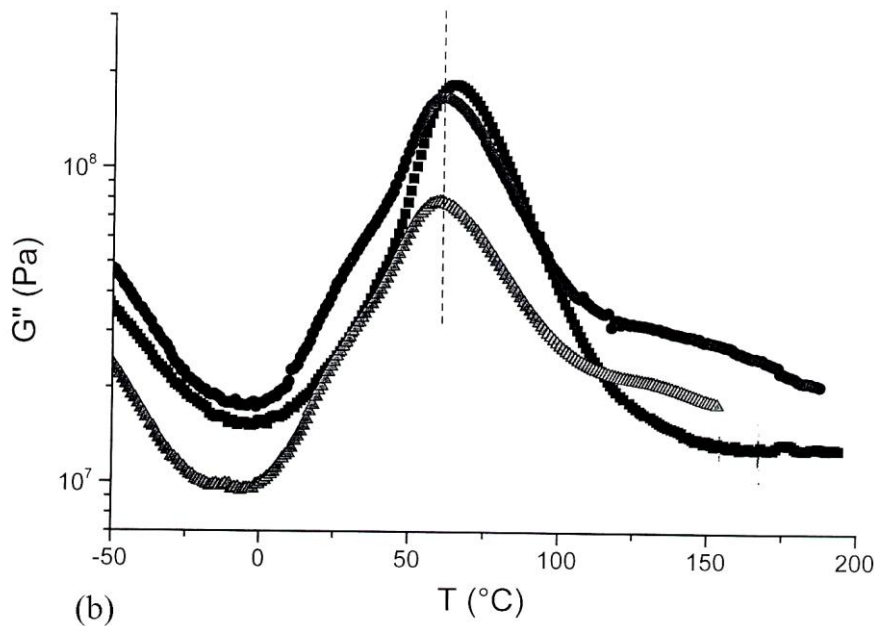


Figure IV-2-7: (a) Shear storage modulus as a function of temperature for P(BuA) latex films filled with different volume fraction of PS particles (symbols) and comparison with theoretical calculation from discrete approach (bold line) (b) shear storage modulus as a function of temperature for P(BuA) latex films filled with different volume fractions of PS particles (symbols), annealed above the glass transition temperature of PS, and comparison with theoretical calculation from

discrete approach (bold line). After E. Chabert, Ph-D thesis, Institut National Science Appliqué, (2002).



a)



b)

Figure IV-3-1 : a) Storage modulus of pure polyamide-6, PA2 (intercalated) and PA3 (exfoliated) b) loss modulus of pure polyamide-6, PA2 (intercalated) and PA3 (exfoliated). After E. Reynaud, Ph-D thesis, Institut National Science Appliqué, (2002).

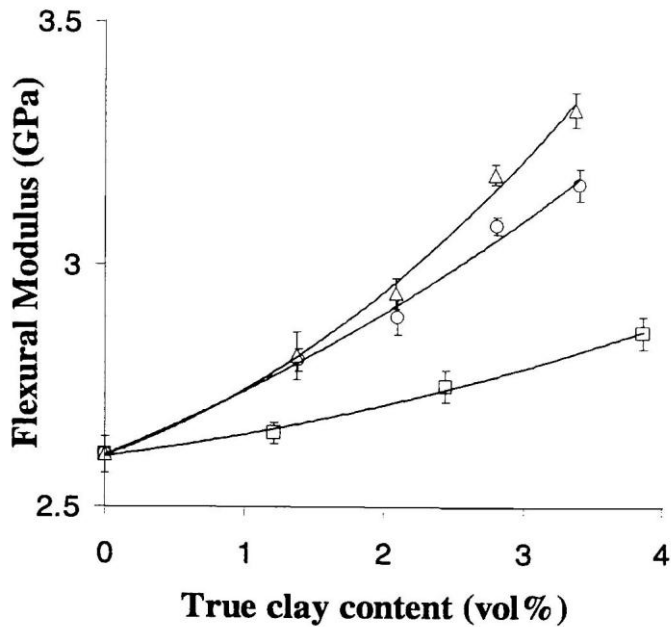


Figure IV-3-2 : Evolution of the flexural modulus of a conventional composite (square), an intercalated (circle) and an exfoliated nanocomposite (triangle) with the true clay content. The epoxy system used is EPON 828/3DCM. Reprinted from Ref. , X. Kornmann, Doctoral thesis, Lulea University of Technology with permission from the author.

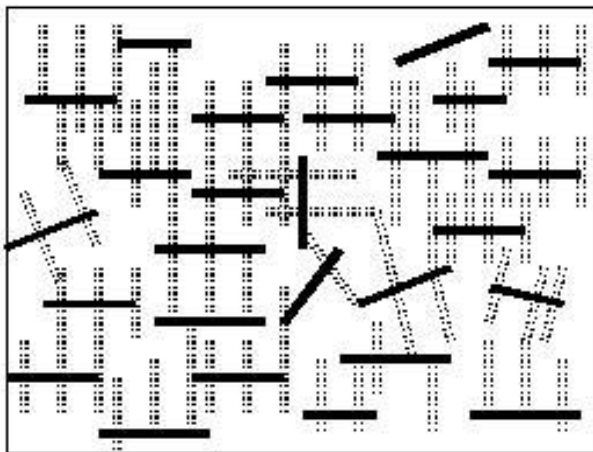


Figure IV-3-3 . Proposal for a nanostructured network in inorganic-organic nanocomposite. Bold lines for silicate layers, dashed lines for semi-crystalline lamellae.

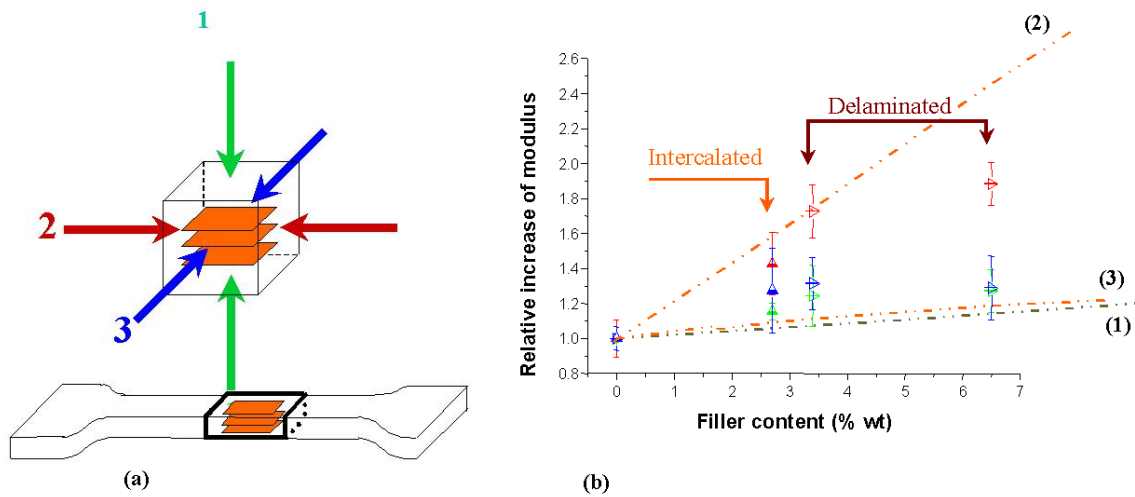


Figure IV-3-4: (a) schematic view of the deformation axis compared to the preferential orientation of the montmorillonite sheets ; (b) values of modulus relative to the deformation axis. Comparison with the calculations from Tandon and Weng, (1), (2), and (3) refers to the directions. After E. Reynaud, Ph-D thesis, Institut National Science Appliqué, 2002.

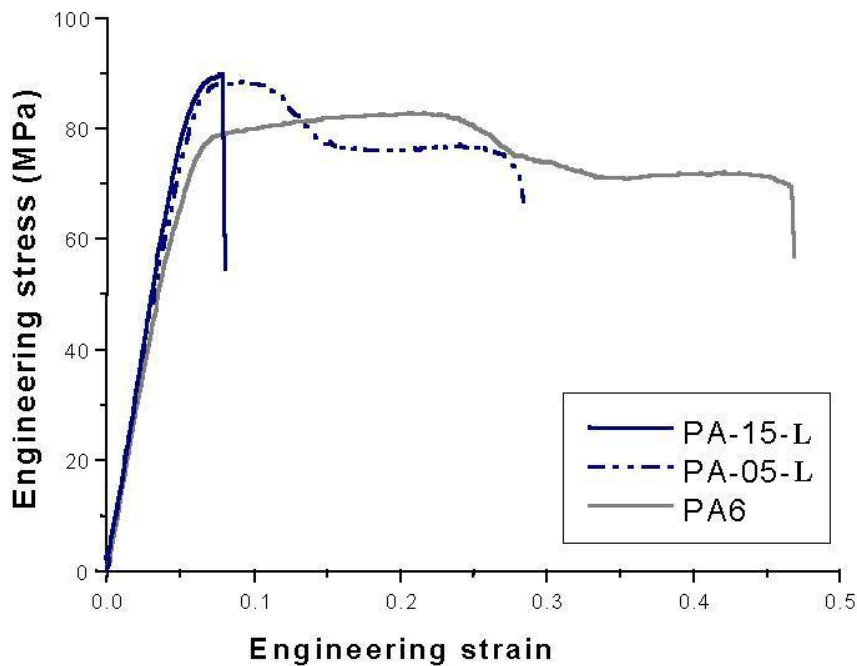


Figure V-1-1 : Filler amount effect on the mechanical behavior in tension for the nanocomposites PA6-silica (80 nm). Reprinted from Ref. 113 , E ; Reynaud, J. Jouen, C. Gauthier, C. Vigier, J. Varlot, Polymer,42, 8759 (2001) with permission from Elsevier.

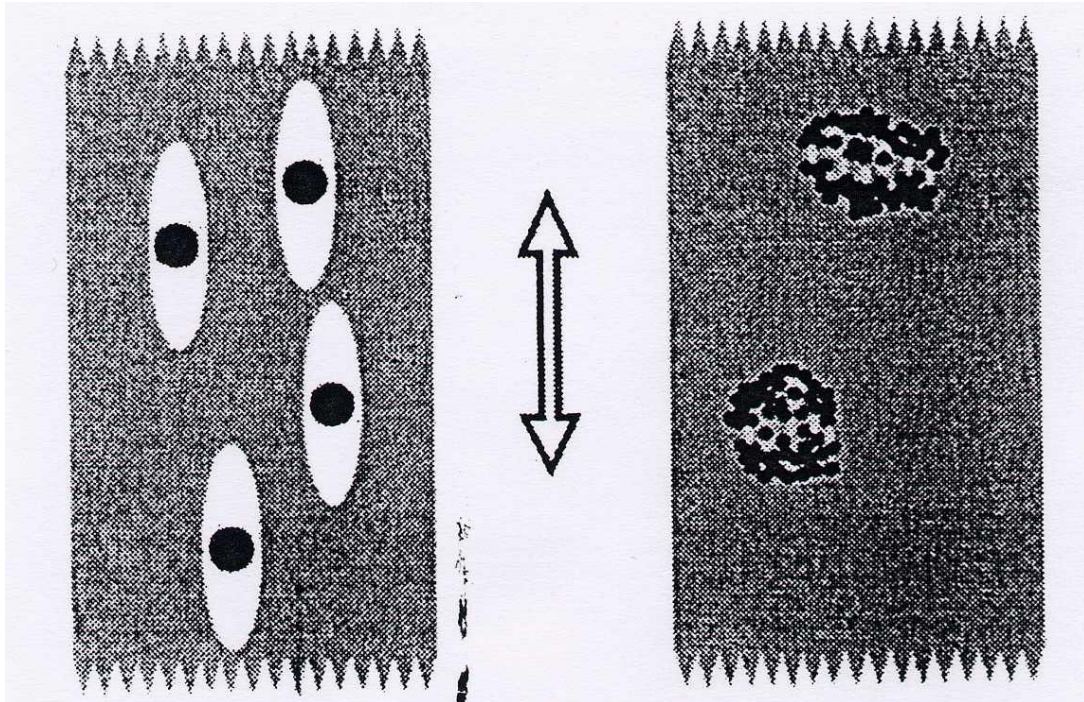


Figure V-1-2 : Schematic representation of the suggested deformation process occurring on the systems containing respectively the 80 nm diameter particles (left) and the 17 nm diameter particles (right). Reprinted from Ref. 113 , E ; Reynaud, J. Jouen, C. Gauthier, C. Vigier, J. Varlot, Polymer,42, 8759 (2001) with permission from Elsevier.

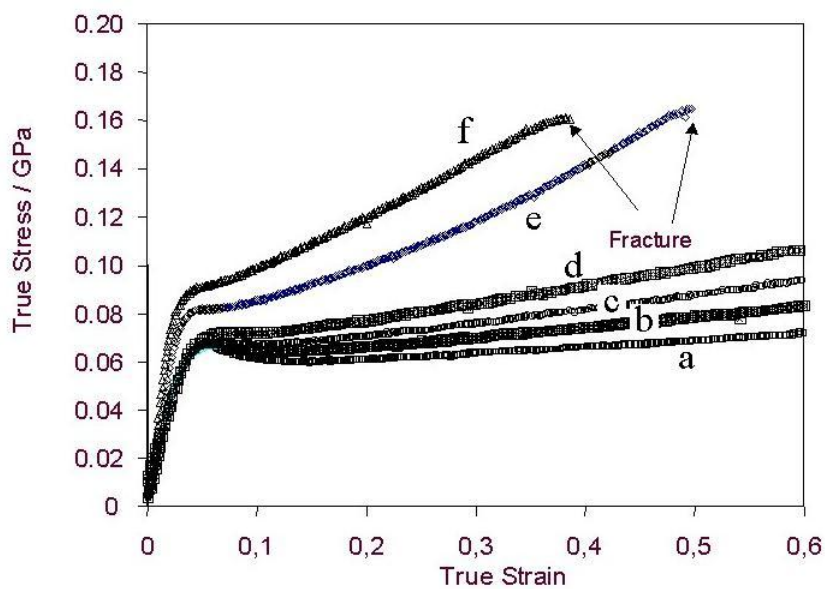


Figure V-1-3: Stress –strain curves at constant strain rate $\dot{\epsilon} = 10^{-2} \text{ s}^{-1}$; a) pure pPVC, b) 3.4 vol.%, c) 5 vol.%, d) 6.6 vol.%, e) 8.4 vol.% and f) 12.4 vol.%

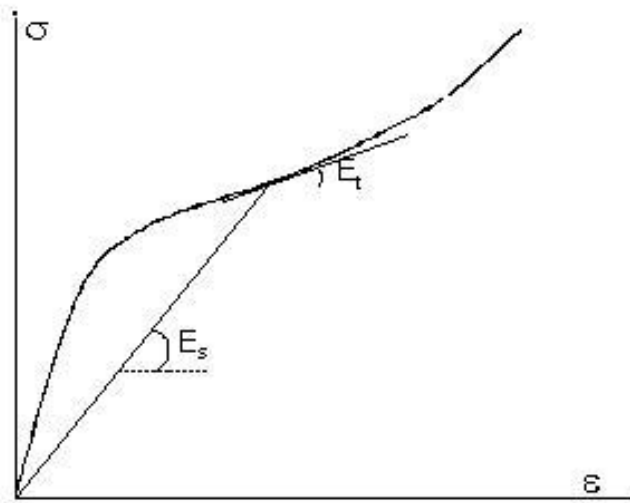


Figure V-2-1: schematic determination of both secant modulus (E_s) and tangent modulus (E_t) from non linear stress – strain curves

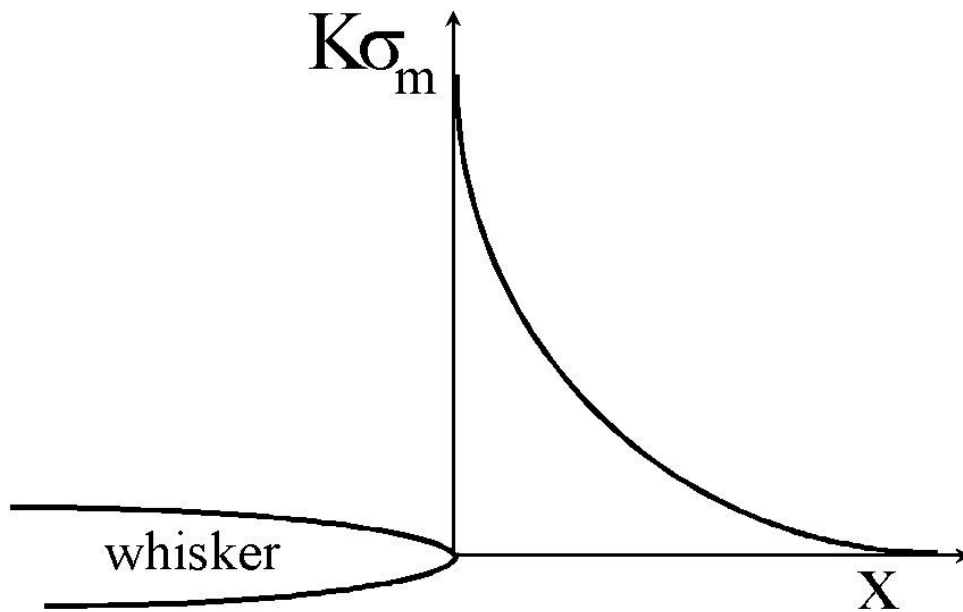


Figure V-2-2: schematic expected variation of local stress within the matrix of a composite, versus the distance x from the surface of a reinforcing particle. K is the stress concentration factor.

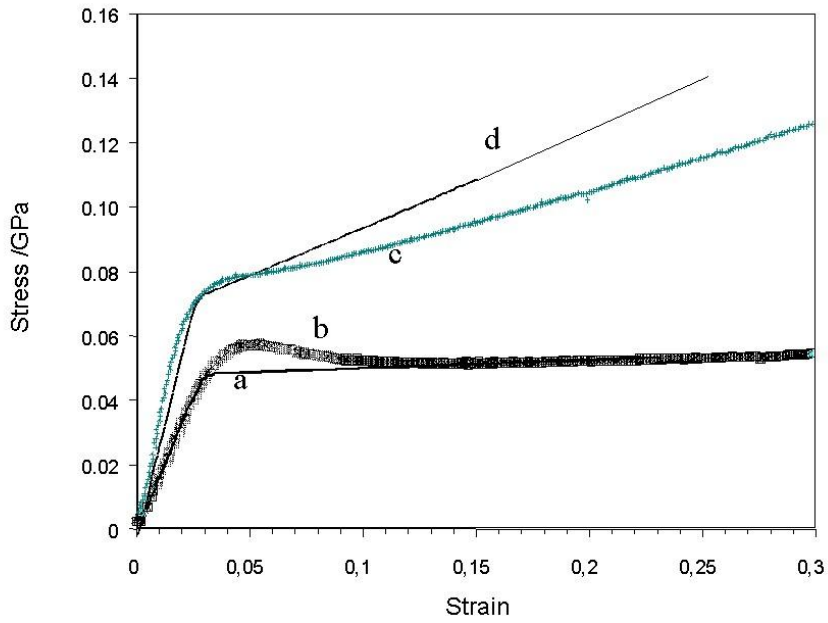


Figure V-2-3: modeling of the σ - ε curves of pPVC reinforced with 8.4 vol.% of whiskers: (a) is the linearisation of the experimental curve of pPVC (b); (c) is the experimental curve of the nanocomposite material and (d) is the prediction of the composite behavior

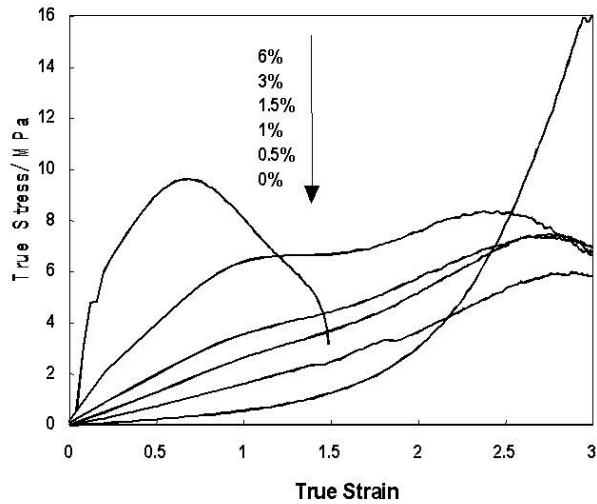


Figure V-2-4: tensile behavior of cellulose whiskers / p(BuA-S) nanocomposites processed following Figure IV-6, for various whiskers contents (v/v).

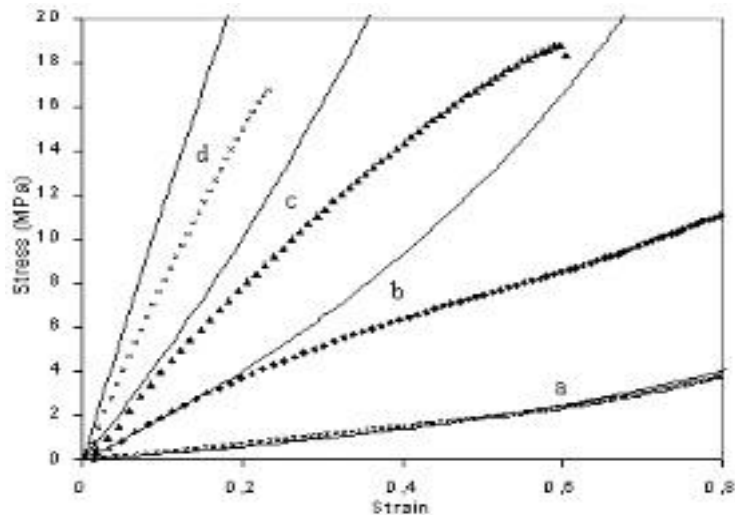


Figure V-2-5: tensile curves for pPVC reinforced by cellulose whiskers, in which only weak interactions between whiskers were allowed. Dotted curves are experimental data, lines are corresponds to the theoretical rubbery elasticity. Divergences are mainly attributed to damage at the matrix-filler interface. Reprinted from Ref. 155 L. Chazeau, J.-Y. Cavallé, P. Terech, *Polymer*, 40, 19 (1999) with permission from Elsevier.

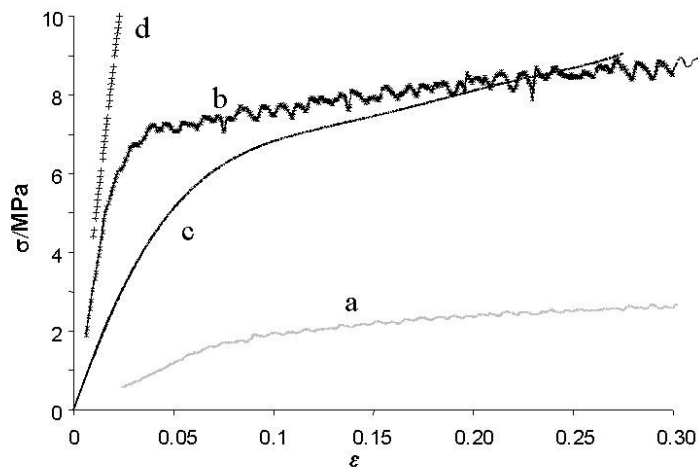


Figure V-2-6: tensile behavior of silica reinforced p(BuA-S), at $T = -5^{\circ}\text{C}$; a) pure matrix; b) experimental data for 45 wt.% silica fillers; c) calculation based on a 3 phase mean field model; d) numerical simulation. After E. Chabert, Ph-D thesis, Institut National Science Appliqué, 2002.

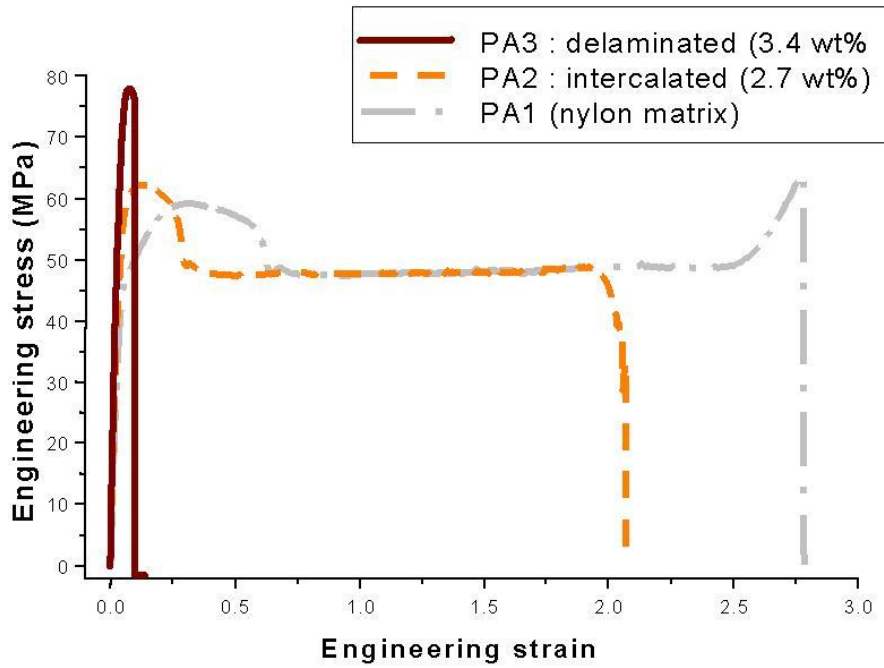


Figure V-3-1: mechanical behavior in tension for the nanocomposites PA6-montmorillonite containing 2.7 (intercalated) and 3.4 wt.% (exfoliated).

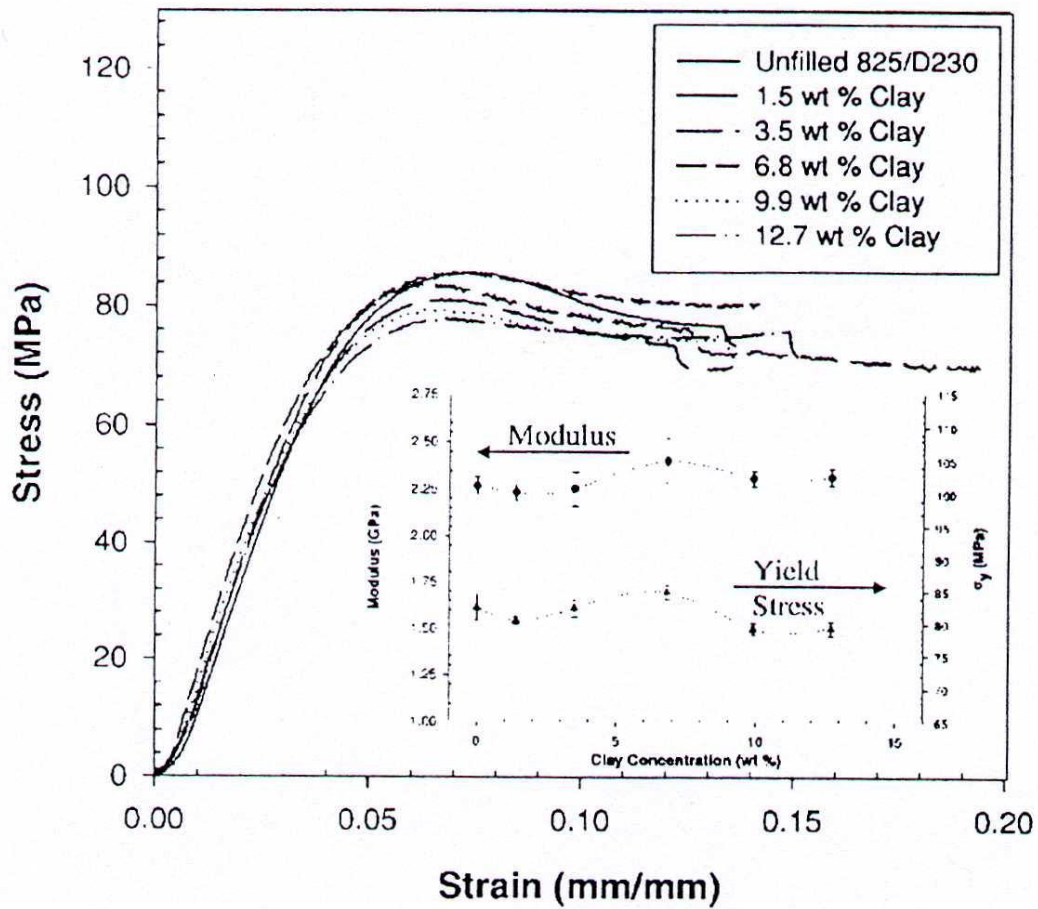


Figure V-3-2 : Compressive behavior of intercalated nanocomposites based on epoxy matrix and nano layered silicates. Reprinted from Ref. 163 : AS. Zerda, AJ Lesser, J. Polym. Sci., B Polym. Phys., 39 (11) : 1137-1146 (2001) with permission from John Wiley&Sons, Inc.

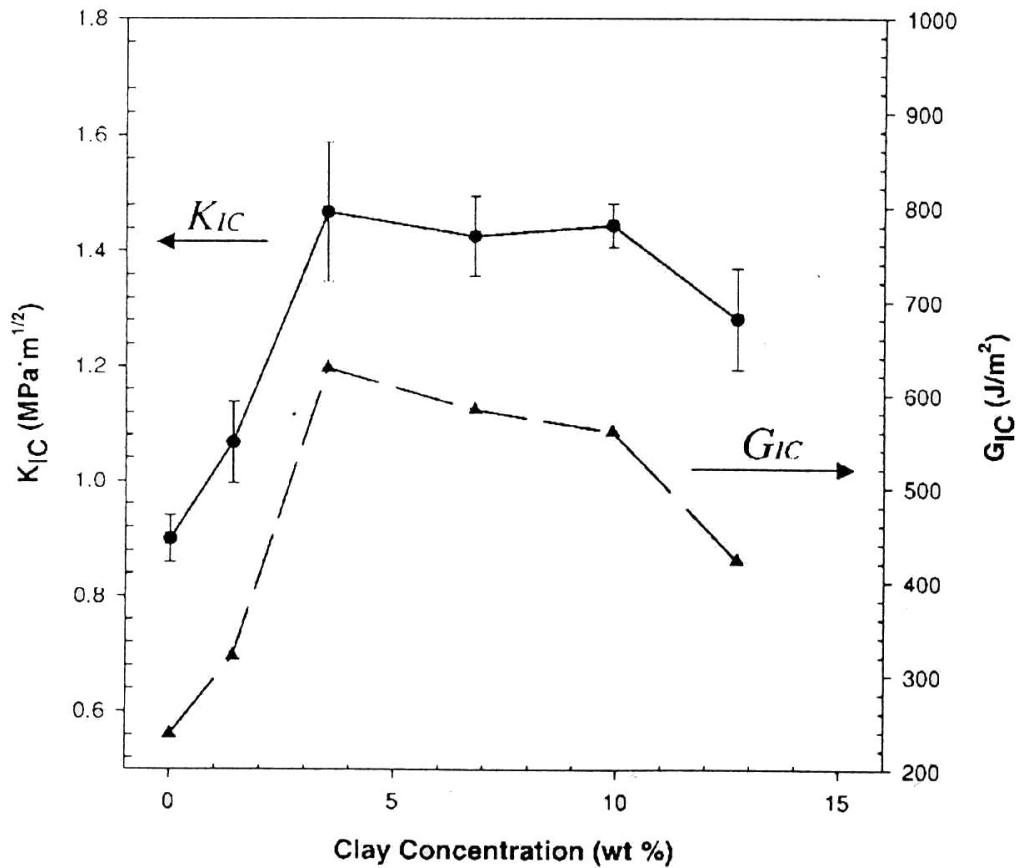


Figure V-3-3 : Changes in fracture toughness with increasing clay content. Both the stress-intensity factor (K_{IC}) and energy-release rate (G_{IC}) are reported. Reprinted from Ref. 163 : AS. Zerda, AJ Lesser, , J. Polym. Sci., B Polym. Phys., 39 (11) : 1137-1146 (2001) with permission from John Wiley&Sons, Inc.

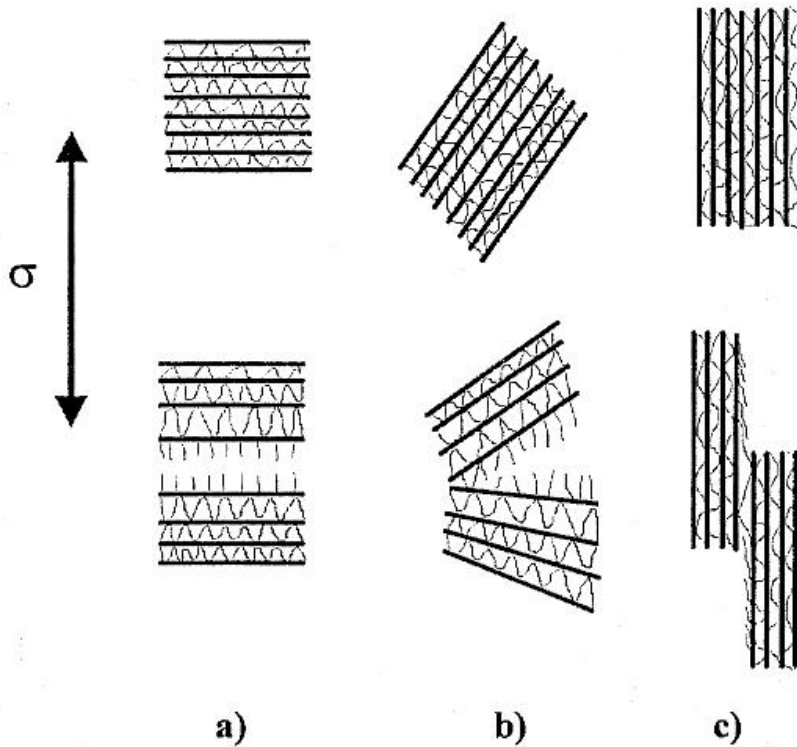


Figure V-3-4 : Schematic models of micromechanical deformation processes of the stacked silicate layer depending on their orientation (arrow indicates the load direction): (a) splitting mode, (b) opening mode and (c) sliding mode. Reprinted from Ref. 145 , Kim G.-M.; Lee D.-H.; Hoffmann B.; Kressler J.; Stoppelmann G., Polymer, 42, no. 3, pp. 1095-1100(6)

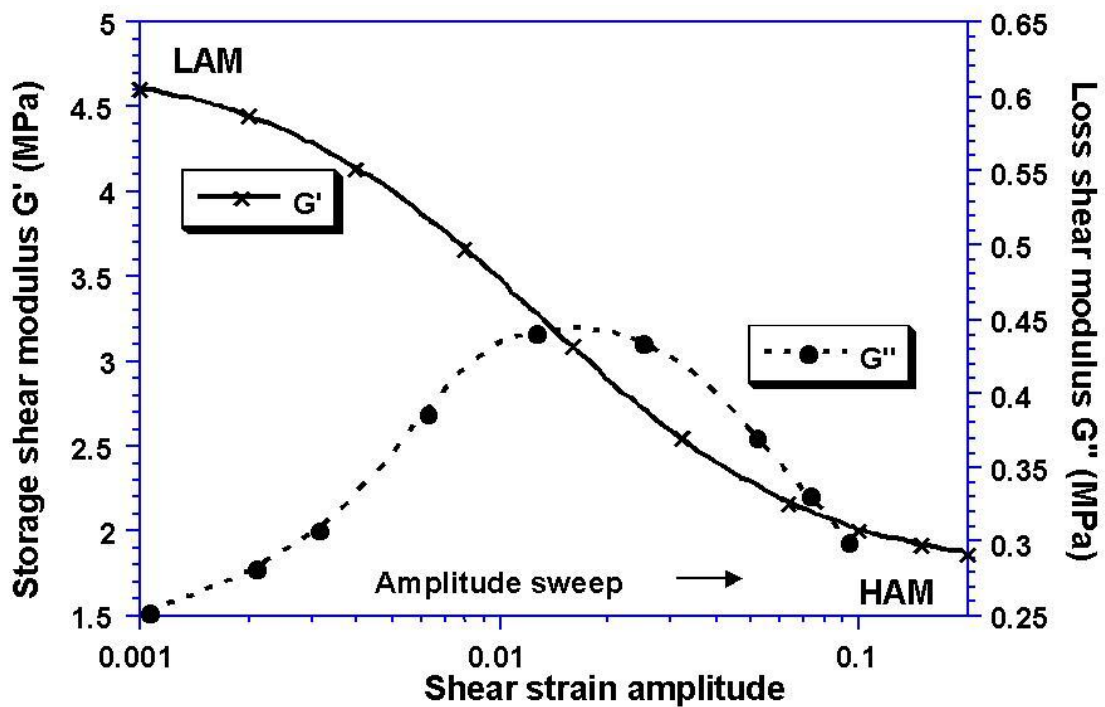


Figure VI-1-1: Storage and loss shear moduli versus dynamic shear strain amplitude for CB filled elastomer ($f=1\text{Hz}$ and $T=25^\circ\text{C}$). Reprinted from L. Chazeau, J.D. Brown, L.C. Yanyo, and S.S. Sternstein, *Polymer Composites*, 21, 2, 202-222, 2000 with permission from Society of Plastics Engineers.

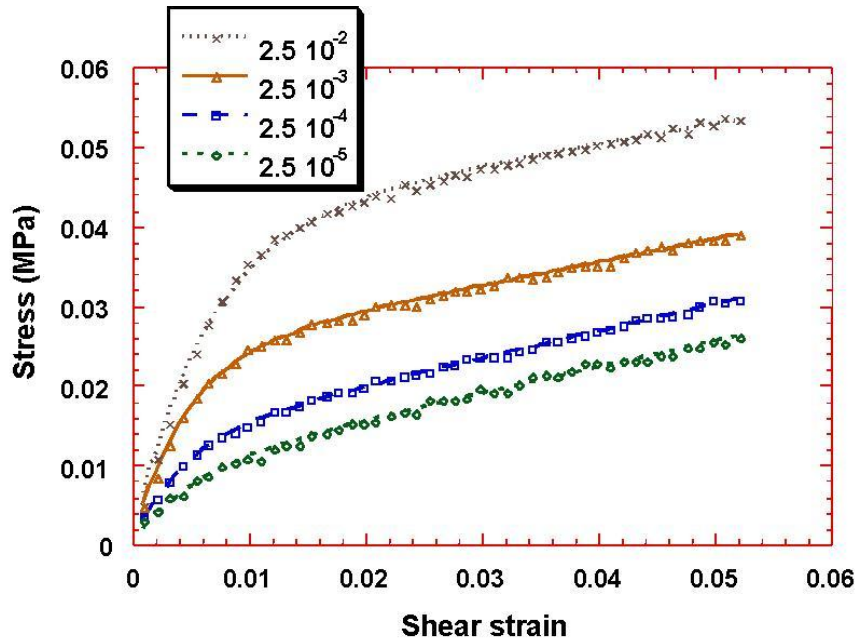


Figure VI-1-2: Constant shear strain rate, stress-strain behavior of a silica filled silicone at several strain rates (units of per second); $T=25^\circ\text{C}$. Reprinted from Ref. 168 :L. Chazeau, J.D. Brown, L.C. Yanyo, and S.S. Sternstein, *Polymer Composites*, 21, 2, 202-222, 2000 with permission from Society of Plastics Engineers.

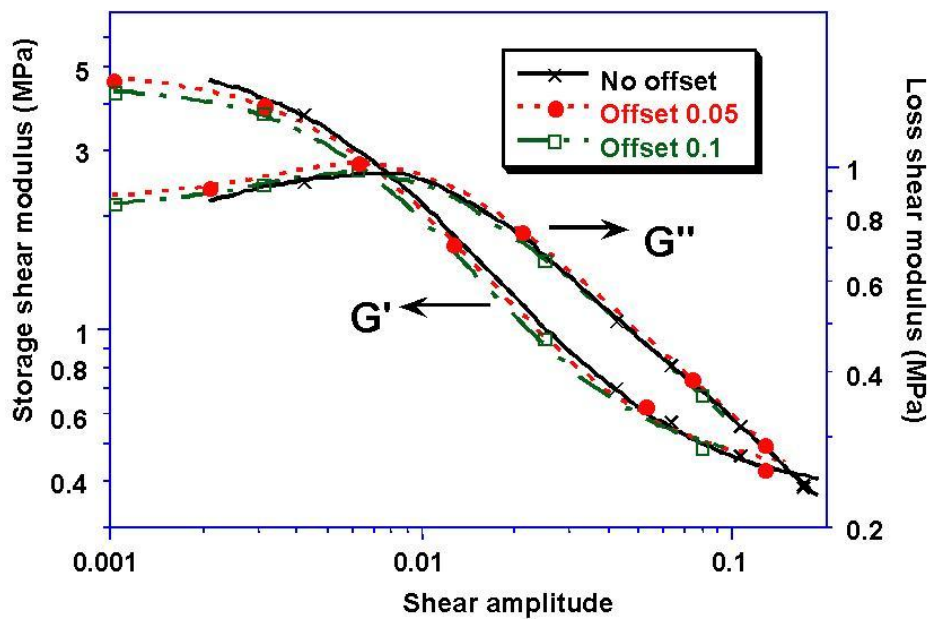


Figure VI-1-3: Effect of static strain offsets on the fully equilibrated dynamic storage and loss shear moduli versus strain amplitude relationship for a filled silicone

elastomer at 25°C and 1Hz. Reprinted from Ref. 168 : L. Chazeau, J.D. Brown, L.C. Yanyo, and S.S. Sternstein, *Polymer Composites*, 21, 2, 202-222, 2000 with permission from Society of Plastics Engineers.

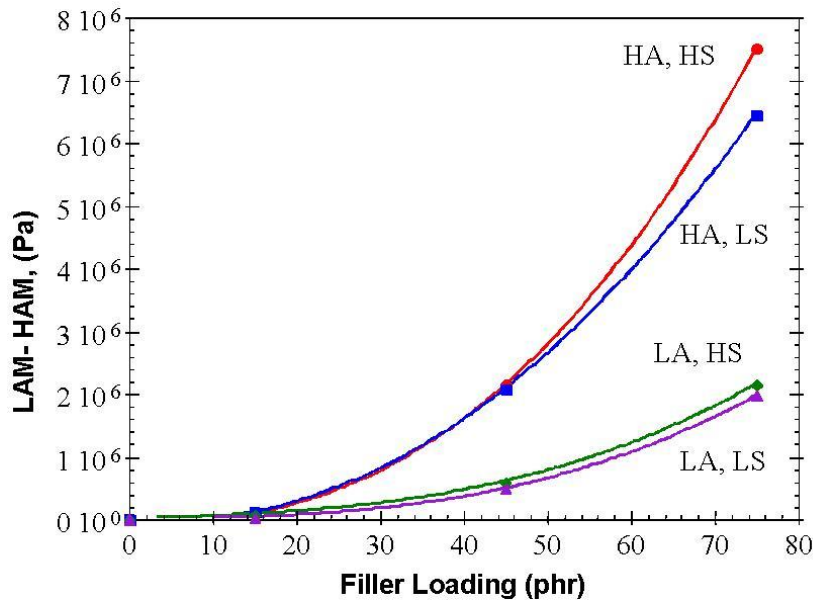


Figure VI-1-4: Filler effectiveness curves showing fully equilibrated change in storage shear modulus versus filler loading for CB filled rubber (T=25°C): effect of surface area and of structure. Reprinted from Ref. 168 : L. Chazeau, J.D. Brown, L.C. Yanyo, and S.S. Sternstein, *Polymer Composites*, 21, 2, 202-222, 2000 with permission from Society of Plastics Engineers.

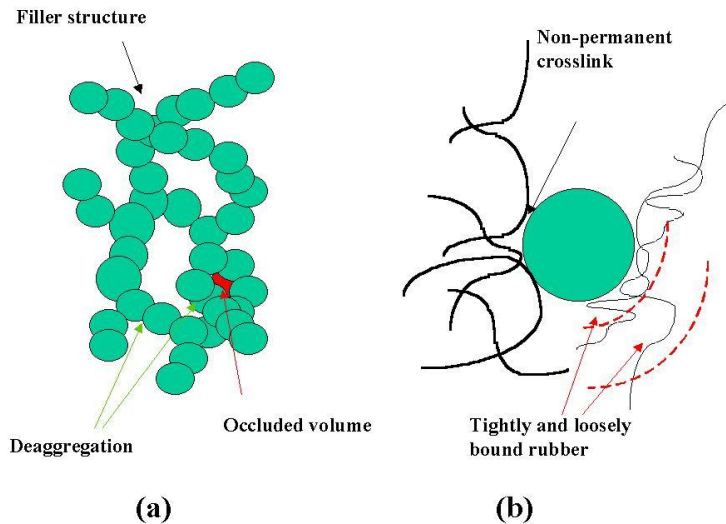


Figure VI-1-5: Schematic representation of the mechanism involved in the Payne effect. (a) network interpretation, (b) physical interpretation with bound rubber.

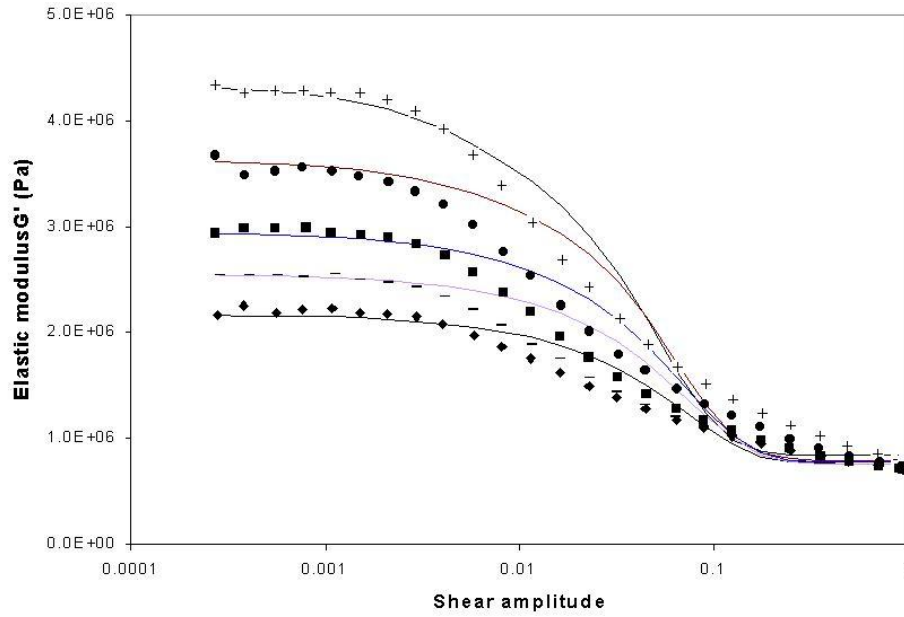


Figure VI-1-6: Experimental shear moduli measured at 5Hz as a function of the shear amplitude in a filled elastomer at different temperature: 23°C (9), 40°C (λ), 60 °C (ν), 80 °C (σ), 100 °C (ν) and theoretical calculation (bold line).

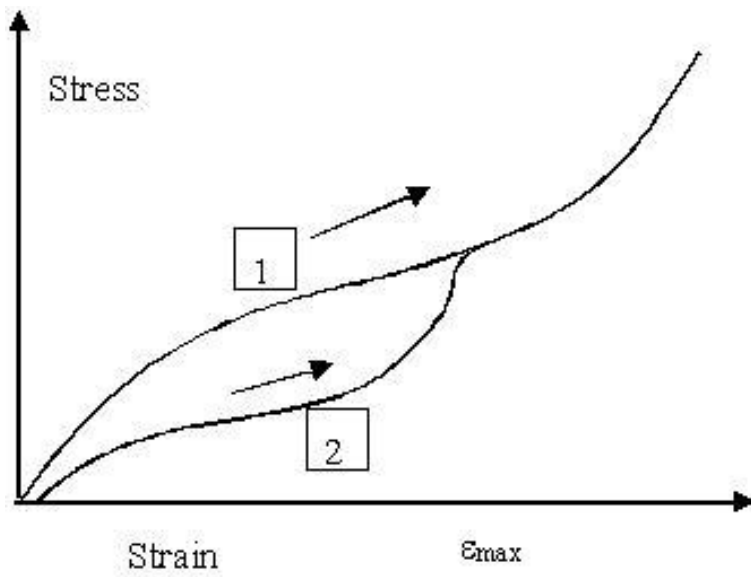


Figure VI-2-1: Typical Mullins effect measured with a filled elastomer.

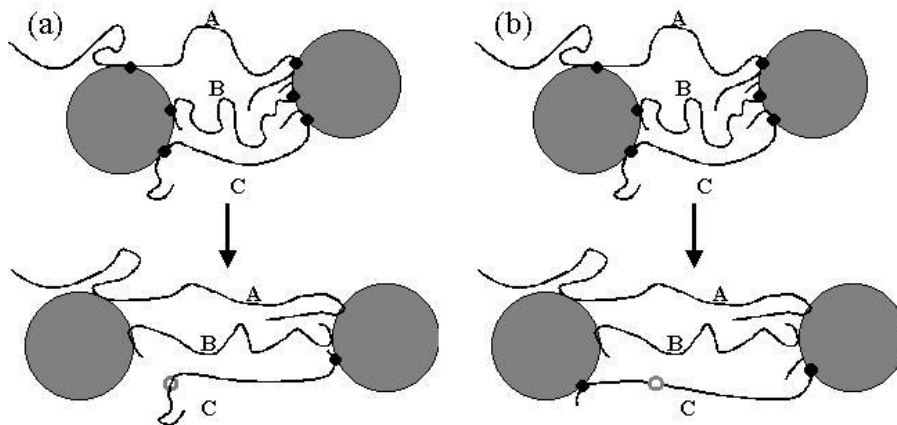


Figure VI-2-2: Physical interpretation of the Mullins effect as described by Bueche (a) or by Dannenberg (b).

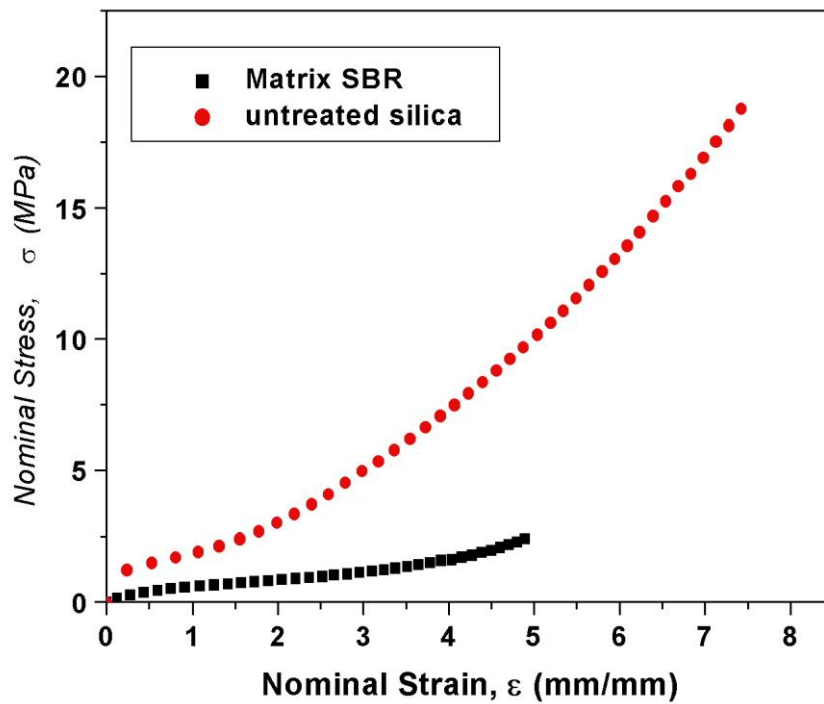


Figure VI-2-3: Tensile stress strain curve of unfilled SBR and SBR filled with untreated silica (25 vol.%, T=298K).

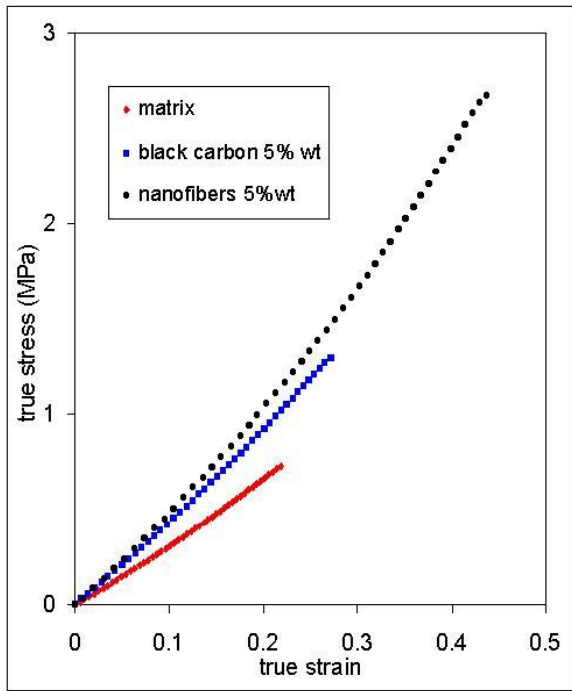


Figure VI-2-4: Tensile stress-strain curve if unfilled rubbery epoxy and rubbery epoxy filled with 1 wt. % and 5 wt.% of Carbon Nanofibers.

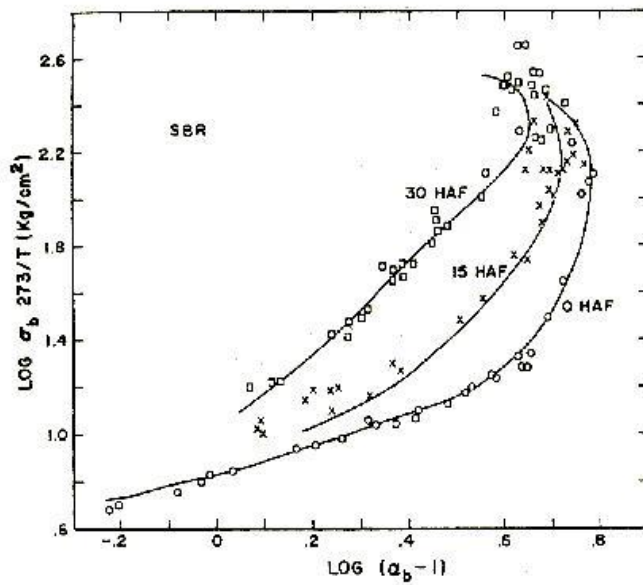


Figure VI-2-5: Rupture envelope for an SBR elastomer filled with different concentration of Carbon Blacks Ref (x). Theoretical curve (full lines) deduced from the combination of creep curves and the Bueche and Halpin theory. Reprinted from Ref. 217 : F. Bueche, J.C. Halpin, J. appl. Phys., 35, 36, (1964) with permission from the Institute of Physics.